Pure- and Mixed-Gas Transport Study of Nafion® and Its Fe^{3+}-Substituted Derivative for Membrane-Based Natural Gas Applications

Dissertation by

Mohsin Ahmed Mukaddam

In Partial Fulfillment of the Requirements

For the Degree of

Doctor of Philosophy

King Abdullah University of Science and Technology

Thuwal, Kingdom of Saudi Arabia

The dissertation of Mohsin Ahmed Mukaddam is approved by the examination committee:

Committee Chair: Ingo Pinnau

Committee Member: Zhiping Lai

Committee Member: Udo Schwingenschlögl

Committee Member: Giulio Cesare Sarti

ABSTRACT

Pure- and Mixed-Gas Transport Study of Nafion® and Its Fe^{3+}-Substituted Derivative for Membrane-Based Natural Gas Applications

Mohsin Ahmed Mukaddam

The focus of this research project was to develop a fundamental understanding of the structure-gas transport property relationship in Nafion® to investigate its potential use as a gas separation membrane material for natural gas (NG) applications including carbon dioxide removal from NG, helium recovery, higher-hydrocarbon removal, and nitrogen separation from methane.

Separation processes account for ~45% of all energy used in chemical plants and petroleum refineries. As the drive for energy savings and sustainability intensifies, more efficient separation technology becomes increasingly important. Saudi Arabia ranks among the world's top 5 NG producers. Commercial hydrocarbon-based glassy polymers often lose their gas separation properties in the presence of condensable, highly sorbing NG components such as CO_2, ethane, propane, *n*-butane, and C_{5+} hydrocarbons. This deterioration in gas separation performance results from penetrant-induced dilation and plasticization of the polymer matrix, leading to significant methane and higher hydrocarbon losses. Polymers that have intrinsically low affinity to high-solubility NG components may be less susceptible to plasticization and therefore offer better performance under actual field conditions. By virtue of their strong carbon-fluorine bonds and chemical inertness, perfluoropolymers exhibit very low affinity for hydrocarbon gases. Nafion®, the prototypical perfluoro-sulfonated ionomer, comprising hydrophilic sulfonate groups phase-separated from a hydrophobic perfluorocarbon matrix, has

demonstrated interesting permeability and selectivity relationships for gas pairs relevant to NG applications.

Gas transport properties of Nafion® indicated gas solubility behavior similar to rubbery polymers but with sieving properties more commonly observed in low free volume glassy polymers. Nafion® demonstrated very low solubility for CO_2 and hydrocarbon gases; the trend-line slope of solubility versus penetrant condensability in Nafion® was almost 2.5 times lower than that of typical hydrocarbon polymers, highlighting Nafion's® effectiveness in resisting high-solubility induced plasticization. Additionally, Nafion® showed *extraordinarily* high permselectivities between small gases (He, H_2, CO_2) and large hydrocarbon gases (C_{1+}): He/CH_4 = 445, He/C_3H_8 = 7400, CO_2/CH_4 = 28, CO_2/C_3H_8 = 460, H_2/CH_4 = 84 and H_2/C_3H_8 = 1400 owing to its tightly packed chain domains. These high selectivities could potentially be harnessed for helium recovery and CO_2 removal in natural gas applications, and hydrogen recovery from refinery gas streams.

Pressure-dependent pure- and mixed-gas permeabilities in Nafion® were determined at 35 °C. Nafion® demonstrated two divergent pressure-dependent permeability phenomena: gas compression and plasticization. In pure-gas experiments, the permeability of the permanent gases H_2, O_2, N_2 and CH_4 decreased with increasing pressure due to polymer compression, whereas the permeability of the more condensable gases CO_2, C_2H_6 and C_3H_8 increased dramatically due to solubility-induced plasticization. Binary CO_2/CH_4 (50:50) mixed-gas experiments showed reduced performance with up to 2-fold increases in CH_4 permeability from 0.075 to 0.127 Barrer,

and a 45% drop in selectivity (from 26 to 14), between 2 and 36 atm total pressure as a result of CO_2-induced plasticization. At a typical NG CO_2 partial pressure of 10 atm, Nafion® exhibited 24% lower CO_2/CH_4 selectivity of 19, with a 4-fold lower CO_2 permeability of 1.8 Barrer relative to a commercial cellulose acetate (CA) membrane. Ternary $CO_2/CH_4/C_3H_8$ (30:50:20) experiments quantified the effect of CO_2 and C_3H_8 plasticization. The presence of C_3H_8 reduced CO_2 permeability further due to a competitive sorption effect causing a 31% reduction in CO_2/CH_4 selectivity, relative to its pure-gas value of 29, at 16 atm total feed pressure.

The strong cation-exchanging sulfonate groups in Nafion® provided an opportunity to tailor the material properties by incorporating metal ions through a simple ion-exchange process. Nafion® neutralized with Fe^{3+} was investigated as a potential approach to mitigate CO_2-plasticization. XRD results demonstrated an increase in crystallinity from 9% in Nafion H^+ to 23% in Nafion Fe^{3+}; however, no significant changes in the average inter chain spacing was observed. Raman and FT-IR technique qualitatively measured the strength of the ionic bond between Fe^{3+} cation and sulfonate anion. The strong crosslinking effect in Fe^{3+}-cation-exchanged membrane demonstrated substantial increase in permselectivity: N_2/CH_4 selectivity increased by 39% (from 2.9 to 4.0) and CO_2/CH_4 selectivity increased by 25% (from 28 to 35). Binary CO_2/CH_4 (50:50) mixed-gas experiments at total feed pressures up to 30 atm quantified the effect of CO_2 plasticization on the CO_2/CH_4 separation performance. Nafion® Fe^{3+} demonstrated better resistivity to plasticization enduring approximately 30% CH_4 permeability increases from 0.033 Barrer at 2 atm to 0.043 Barrer at 15 atm CO_2 partial pressure. At 10 atm CO_2

partial pressure, CO_2/CH_4 selectivity in Nafion® Fe^{3+} decreased by 28% to 28 from its pure-gas value of 39, which was a significant improvement compared to Nafion® H^+ membrane that decreased by 42% to 19 from its pure-gas value of 32.

ACKNOWLEDGEMENTS

I would like to thank Allah for giving me this opportunity, as well as the strength, ability and patience to overcome numerous difficulties in successfully completing my journey as a Ph.D. student.

This Ph.D. was a true test of my capabilities as a student and researcher, and one of the more challenging tasks that I have undertaken. This work would not have been possible without the support and guidance of many people whom I would like to genuinely thank and acknowledge.

First and foremost, I would like to express my deepest gratitude and appreciation to my advisor, Dr. Ingo Pinnau, without whose persistent advice, guidance and support this dissertation would not have been possible. I have always been enthralled by his knowledge and experience in the field that inspired my interest and love for science. His very generous attitude in helping above and beyond his ability is something that I will always be grateful for. He believed in me despite my non-chemical engineering background, and successfully and patiently guided me from the naïve undergraduate researcher that I was, to the qualified Ph.D. student that I have become. I can never forget the amount of time and effort that he has spent in editing and shaping my work to the highest standards.

I would also like to thank a man who is the true substance of genius, Dr. Eric Litwiller, for his assistance throughout my research. He has been incredibly helpful and kind in sharing his knowledge and expertise in how to use the mechanical tools and

electronics that helped in building the state-of-the-art permeation and sorption apparatus on which I have conducted many of my research experiments. I sincerely appreciate the time and effort he spent in analyzing and criticizing my data that helped me structure my thoughts and ideas into what turned out to be excellent published manuscripts.

I am also grateful to have collaborated with great chemists including Dr. Yingge Wang, Dr. Xiaohua Ma and Dr. Bader Ghanem. They were always willing to help and answer any of my questions related to chemistry. I would also like to thank my group members Octavio, Raja, Jintang, Bander, Nasser, Fahd, Rakan, Federico, Zain, Ramy, Mahmoud, Dalila, Sherry, Melinda and Nigel who were always available to discuss research problems, lab issues, and assist with certain concepts I was unfamiliar with. In addition, I would like to dedicate my special thanks to my closest friends Adnan, Shifa, Areeb, Faraz, Faizan, Talal, Khadija, Ibad, Sayeed, Muyeed, Zakir, Unnat, Supriya, Mohannad, Ahmed, Mahmoud, Muhannad, Samer, Jamaliah, Alsaadi, Asem, Waseem, Fatima, Aditya, Afaque, Abid, Zahid, Sajid, Luay, and Ali, who have gone to great lengths in supporting me emotionally and morally during my difficult times. They always took a keen interest in listening to my issues and suggested to me possibilities to overcome them.

I am deeply honored to have my dissertation reviewed by top scientists Dr. Zhiping Lai, Dr. Udo Schwingenschlögl, and Dr. Giulio Sarti whose contributions to science have been remarkable.

Finally and most importantly, I would like to dedicate this Ph.D. to my family: my father Ahmed, my mother Shamshad, my lovely sister Shaista, and my brother Ashfaq,

my uncles Yaseen, Naseer, Nasrullah, my aunts Hameeda and Zubeida, for their emotional and moral support throughout my academic career and for their love, care and prayers.

TABLE OF CONTENTS

LIST OF FIGURES

LIST OF TABLES

Chapter 1. Overview of Natural Gas and Membrane Technology

The first part of this chapter provides a comprehensive overview of natural gas, from its discovery to its industrial commercialization, which led to significant technological advances. At present, natural gas meets 23.7% of the world's energy demand, and this value is continuously increasing. To satisfy the growing demand for natural gas, the limitations of existing technologies must be overcome. The next part of this chapter reviews two competing technologies: membrane and conventional technologies, focusing primarily on the use of polymer based membrane technology for natural gas purification. Further development of membrane technology necessitates application-specific materials assessment. Thus, the end of this chapter discusses some of the materials selection criteria and challenges of currently available polymeric membranes.

1.1. A Closer Look at Natural Gas

1.1.1. History of Natural Gas

Like coal, oil, and nuclear energy, natural gas (NG) is a non-renewable energy source. It is considered one of the cleanest, safest, and most hydrogen-rich fossil fuels worldwide [1, 2]. Currently, the global NG reserve is estimated to be 6610 trillion cubic feet (tcf) – sufficient to meet 54 years of global production [3]. **Table 1.1** lists major countries with known NG reserves. According to the BP Statistical Review of World Energy 2015, one-fifth of the world's energy demand is supplied by NG in public and private sectors [3]. Its global consumption is projected to triple between 1990 and 2040, as shown in **Fig. 1.1** [4]. It is believed that NG will be the next-generation fuel, overtaking oil in 2030 [1].

Table 1.1. Top holders of natural gas proven reserves as of 2014 [5].

Rank	Country	Gas reserves (tcf)
1	Russia	1688
2	Iran	1193
3	Qatar	885
4	United States	338
5	Saudi Arabia	291
6	Turkmenistan	265

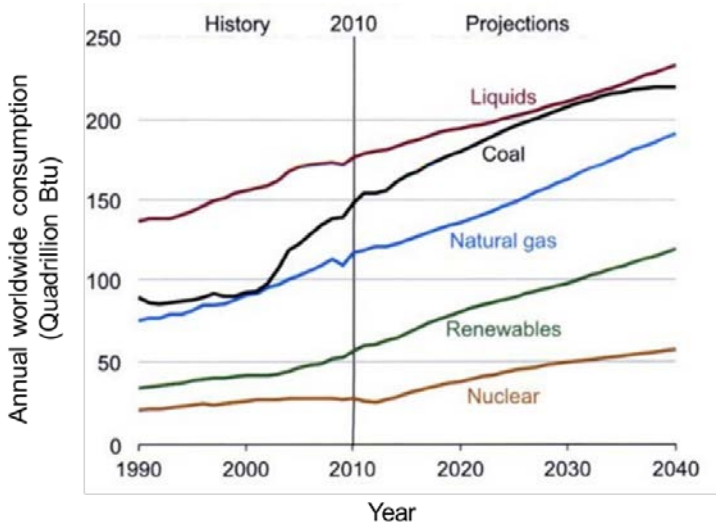

Fig. 1.1. Global energy consumption by fuel type between 1990 and 2040 [4].

The discovery of NG can be dated back to 500 BC, when the Chinese used NG to boil seawater for drinking purposes [6]. In the 18th century, NG was predominantly used to

light houses and streets. Later, in the 19th century, Robert Bunsen designed the famous *Bunsen burner* using NG to produce a hot, sootless, non-luminous flame [7]. Bunsen burners are still commonly used in laboratories [8]. Today, NG is utilized in a wide range of applications. For example, it is widely used as fuel for road vehicles in the form of compressed and liquefied natural gases (CNG and LNG, respectively) [1]. Currently, approximately 16.7 million natural gas vehicles (NGV) are in operation worldwide [9]. NG is also often used as a feedstock material in the petrochemical industry for the production of hydrogen, ammonia (fertilizers), ethylene, plastics, pharmaceuticals, fibers, and sulfur [1]. Additionally, it is used for domestic purposes, such as home heating and lighting, water heaters, cooking stoves, and gas grills [1].

The combustion of fossil fuels produces harmful greenhouse gases, such as carbon dioxide (CO_2), methane (CH_4), and nitrous oxide (N_2O). Indeed, these three gases account for two-thirds of global greenhouse gas emission, with carbon dioxide being the major contributor [10]. Carbon emissions are expected to increase from 32.2 billion metric tons in 2013 to 34.8 billion metric tons in 2030; worryingly, this increase in emissions is predicted to increase the global temperature by 3.5 °C by 2200 [10]. **Fig. 1.2** illustrates the increases in CO_2 emissions by fuel type [4]. Coal has been the major source of CO_2 emissions since 1990, and its use is projected to double by 2040. In contrast, NG has a low carbon footprint, and carbon emissions from NG are projected to be half those from coal in 2040. This benefit of NG opens an enormous market for its use as the primary fuel source to meet the goal of limiting global warming to 2 °C set during the recent 2015 UN climate summit in Paris [10]. Additionally, NG can facilitate the much-needed transition to carbon-free fuel in the form of hydrogen [1]. Based on the

above facts and current advances in efficient extraction and production technologies, NG consumption is expected to rise steadily over the next several decades.

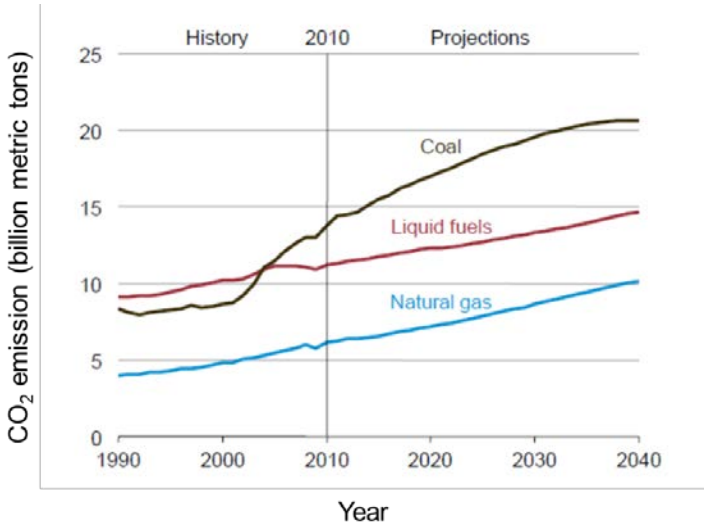

Fig. 1.2. Global energy-related CO_2 emissions (in billion metric tons) by energy source between 1990 and 2040 [4].

1.1.2. Natural Gas Composition

NG is obtained directly from gas wells at high pressures (typically 20-60 bar) as *associated* (gas produced with oil) or *non-associated* gas [11, 12]. The composition of NG varies substantially by source. **Table 1.2** shows the typical compositions of NG extracted in the U.S. [2] and Saudi Arabia [13]. CH_4 is the principal constituent of NG [2, 14]; other valuable components include ethane (C_2H_6), propane (C_3H_8), *n*-butane (*n*-C_4H_{10}), *iso*-butane (*i*-C_4H_{10}), and pentane (C_5H_{12}) [2]. NG also contains impurities, such as CO_2; hydrogen sulfide (H_2S); nitrogen (N_2); water vapor (H_2O); benzene, toluene, ethylbenzene, and xylene (BTEX) aromatics; and mercaptans (methanethiol, CH_3SH, and ethanethiol, C_2H_5SH). Before transportation through the pipeline for production, the gas

must be processed to remove these impurities and satisfy certain pipeline specifications, as presented in **Table 1.3** [14].

Table 1.2. Natural gas well compositions in the U.S. and Saudi Arabia.

Component	**U.S. [2]**	**Saudi Arabia [13] (associated gas)**
Methane	70 – 90%	63%
Ethane		15%
Propane	0 – 20%	7%
n-Butane		3%
C_{5+} hydrocarbons	-	1%
Hydrogen sulfide	0 – 5%	3%
Carbon dioxide	0 – 8%	9%
Nitrogen	0 – 5%	-

Table 1.3. U.S. natural gas pipeline specifications [14].

Component	**U.S. [2]**
CO_2	< 2%
H_2S	< 4 ppm
C_{3+} hydrocarbons	950 – 1050 Btu/scf; Dew point < -20 ^oC
Water vapor	< 120 ppm
Total inert gases (N_2, He, CO_2, etc.)	< 4%

CO_2 and H_2S categorized as acid gases, are known to cause severe pipeline damage. These gases are corrosive, and in the presence of water, CO_2 forms an acid, which can cause pipeline corrosion and compressor breakdown [15, 16]. H_2S is highly toxic and poses severe health and environment issues, especially during NG combustion, which releases harmful gases, such as SO_2. In addition, CO_2 reduces the heating value of NG and wastes pipeline capacity [17]. Thus, acid gas removal is the most important step in NG processing and is by far the largest industrial gas separation process.

The removal of hydrocarbons from NG is crucial for several reasons. For example, offshore platforms rely exclusively on raw and untreated gas to run compressors and engines [14], but the presence of heavy hydrocarbons causes coking problems in engines. In many other environments, gas is produced as a byproduct of oil production (associated gas) [18]. The hydrocarbon content in the associated gas, although small in proportion, can increase the amount of transportable hydrocarbon liquids produced. Finally, the hydrocarbons in gas transmission lines can condense and, in the presence of water, form freezable compounds as the temperature drops below the dew point of hydrocarbons [14, 19]. This phenomenon causes compressor breakdown and reduces pipeline capacity (blocking) [19].

N_2 and He are categorized as inert gases. NG with more than 4% N_2 is considered to be of low quality [20, 21], and the removal of N_2 is important because it reduces the heating value of NG. NG is also the largest source of He. Although it is only present in NG in trace amounts, the recovery of He is desirable because of its high industrial value for a variety of applications [22, 23].

1.2. Separation Technology

1.2.1. Membrane and Conventional Technology

Separation processes account for ~45% of all process energy used in chemical and petroleum refining industries [24]. As the push for energy savings and sustainability intensifies, more efficient separation technology will become increasingly important. Conventional technologies, such as amine absorption, cryogenic distillation, and pressure-swing adsorption, have been implemented for industrial NG separation [14, 25]. The typical stages involved in the treatment of an NG stream are shown in **Fig. 1.3.** These methods have been successfully applied to satisfy pipeline specifications. However, their high capital cost, complexity, energy-intensive operation, large size, and high environmental impact often make them unattractive [7]. For instance, many small producing wells in the U.S. deploying these traditional technologies have been shut down due to their high cost [26]. Considering these problems, membrane technology is considered a viable alternative to conventional methods.

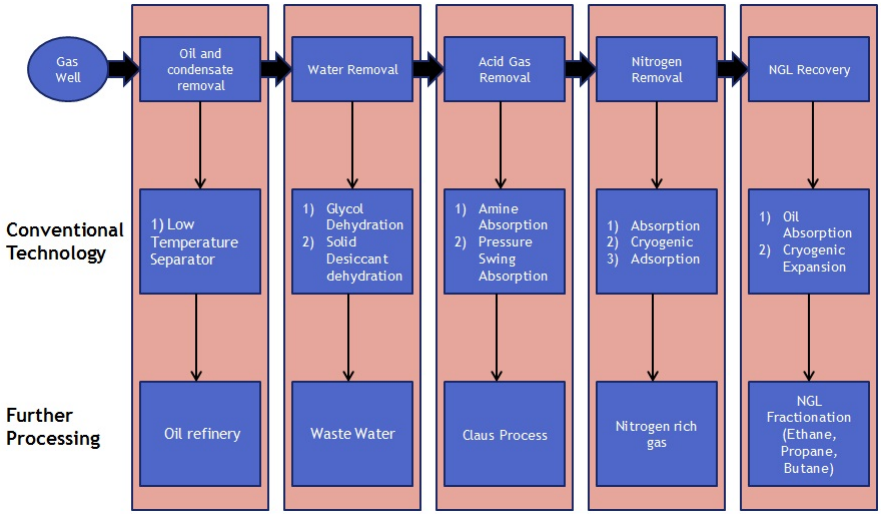

Fig. 1.3. Typical process stages involved in the separation of natural gas.

Membrane-based separation processes have proved very effective for NG processing [15, 26-29]. They offer potential advantages over conventional processes in terms of cost, simplicity, size, and energy efficiency [25, 26]. Furthermore, membrane processes are driven by high pressure [16, 30] which can be obtained directly from the NG wellhead (typically at 20-60 bar).

A schematic description of a membrane system for NG processing is shown in **Fig. 1.4.** The high-pressure feed stream is divided into two outlet streams: the low-pressure permeate and high-pressure retentate. In this example, CH_4 and C_{2+} hydrocarbons are present in the retentate, while CO_2 is enriched in the permeate. The gas separation mechanism is based on the principle that some gas species permeate more readily than others; more specifically, the difference in the condensability and gas molecular size determines how well the penetrants dissolve in the membrane and diffuse through it. For

example, in CO_2/CH_4 separation, CO_2 is smaller and more condensable than CH_4, and thus the membrane permeates CO_2 preferentially to CH_4.

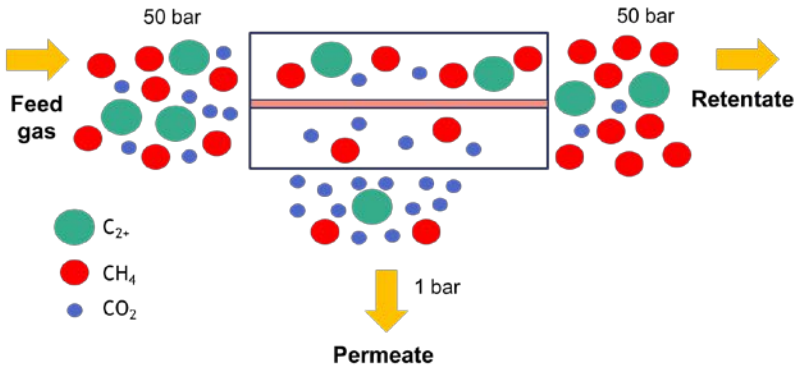

Fig. 1.4. Schematic representation of a membrane system for natural gas processing.

1.2.2. Membrane Plant Design

The most commonly used plant configuration for CO_2 removal in NG upgrading is shown in **Fig. 1.5** [14]. The practicality of the design depends on several factors, such as plant location, product purity, product recovery, and cost. In this schematic, the plant is designed to treat 10 million standard cubic feet per day (MMscfd) of gas containing 10% CO_2 using cellulose acetate (CA) membranes with a CO_2/CH_4 selectivity of 15. The goal is to reduce the CO_2 content of the product stream to less than 2%. One-stage designs are simple, consisting of one permeate stream and one retentate stream [14]. These designs achieve the targeted goal with CH_4 losses typically between 10-15%. Such losses are considered high and may make the process impractical. In a two-stage design, the permeate stream from the first stage is compressed and recycled to the feed of the second membrane unit. These designs achieve the targeted goal with minimal (< 2%) CH_4 loss;

however, the additional recompression stage makes them costly. Two-stage designs are employed for streams greater than 5 MMscfd, whereas one-stage designs are best for the 1-2 MMscfd streams typical of offshore platforms [14, 31].

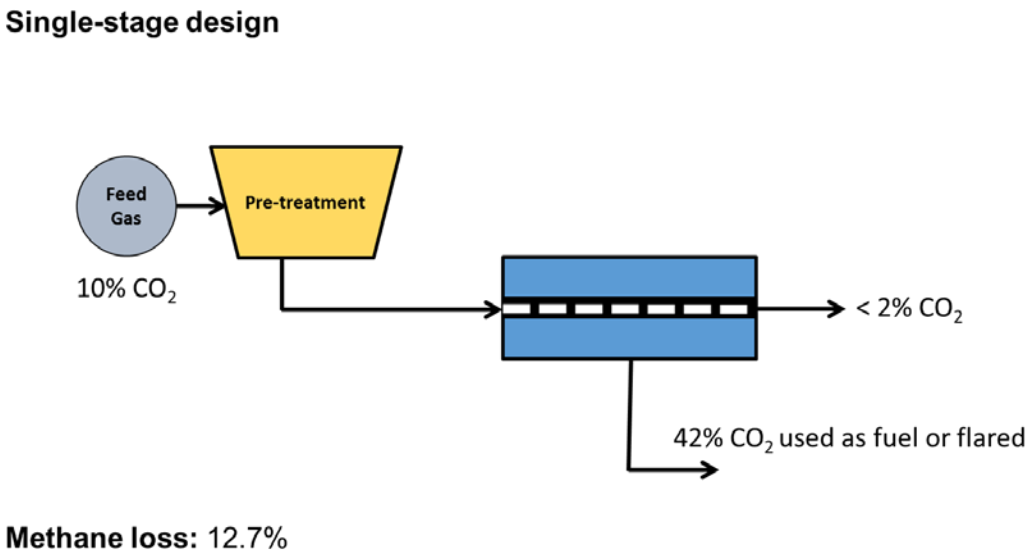

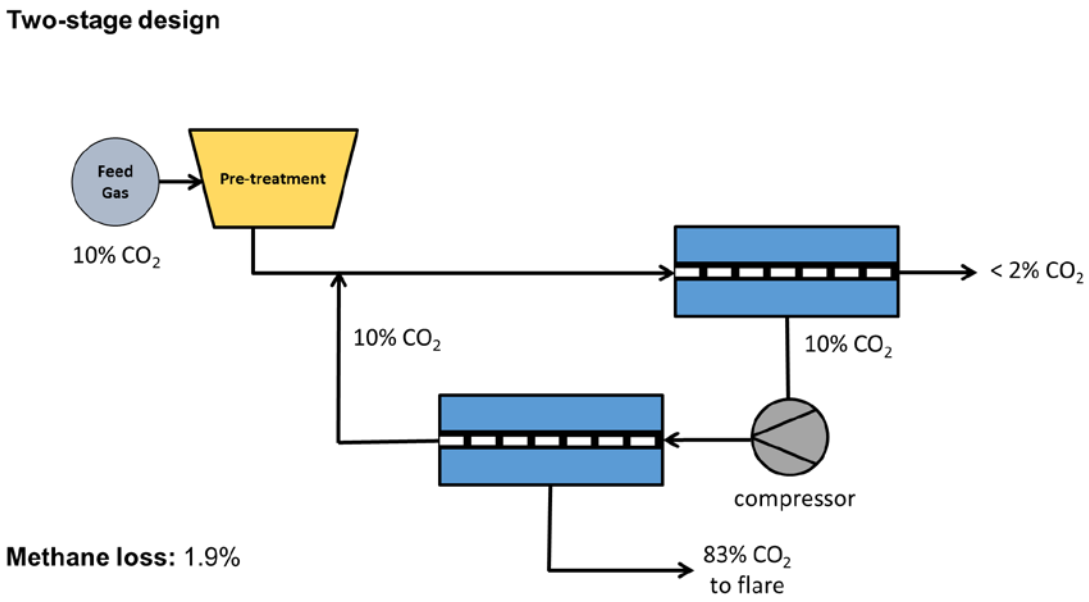

Fig. 1.5. Single- and two-stage membrane plant designs for the removal of carbon dioxide from natural gas.

Hybrid systems have been suggested as a low-cost alternative to conventional systems [28, 31]. These systems consist of a membrane system for bulk removal integrated with a conventional amine scrubbing system for pipeline-specific purity. For example, the gas plant in Mallet, Texas, U.S.A., which has been in place since 1994, employs a hybrid system (Cynara CA membranes + amine absorption unit) to remove CO_2 from associated gas (90% CO_2 + 4% CH_4 + 6% C_{2+} hydrocarbons) [18]. The first, membrane-based step of the separation process removes 70% of the CO_2, while the final step provides the pipeline-specified purity using an amine absorption system. Overall, the process successfully reduced the size and cost of downstream CO_2 removal equipment by 30%.

1.3. Polymeric Membranes for NG Applications

1.3.1. Membrane Classification

Polymeric membranes are classified into two main categories: glassy and rubbery polymers [32]. Glassy polymers have rigid structures and are commonly referred as 'size-selective' because separation is often dominated by differences in penetrant size [32, 33]. On the other hand, rubbery polymers have flexible chains and are commonly referred as 'solubility-selective' because separation is based on differences in penetrant condensability and polymer-penetrant interaction. The order of gas permeation in glassy and rubbery polymers relative to CH_4 is schematically illustrated in **Fig. 1.6** [14]. The figure provides a good starting reference for choosing the membrane type (glassy or rubbery) for a specific NG application. For example, glassy membranes may be suitable for CO_2/CH_4, He/CH_4, CO_2/C_{2+}, and H_2O/CH_4 separation because of the large size differences between the gas species, whereas rubbery membranes are more suitable for H_2O/CH_4, CH_4/N_2, and CH_4/C_{2+} separation because of their large solubility differences. Although both membrane types may qualify for a given separation process, the choice of membrane material depends on factors such as the membrane permeance and selectivity, process conditions (e.g., operating pressure, temperature), and impurities in the gas stream (SO_2, NOx, H_2S, etc.).

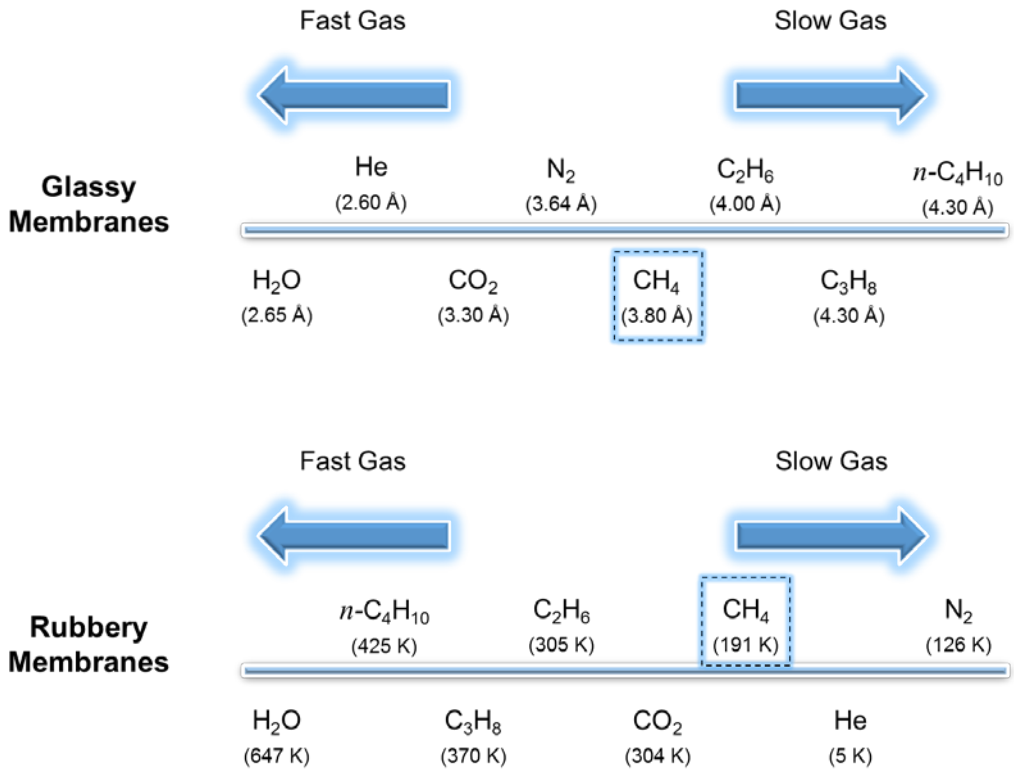

Fig. 1.6. Gas permeation order in glassy and rubbery polymeric membranes.

1.3.2. Selection Criteria and Challenges

Polymeric membranes have always been the prime focus for industrial commercialization because of their cost-effectiveness and high processability [25]. However, it is worth noting that, despite the development of several novel polymers, only a few have achieved commercial success. For example, in 2002, only nine polymeric membranes were used predominantly in 90% of gas separation applications [31]. This low implementation is due to the stringent industrial criteria for membrane fabrication and properties [12, 31]:

1) The polymer must be solution-processable.
2) Thin-film (~0.1-1 μm) asymmetric or composite membranes must be fabricated with a *defect-free* selective layer.
3) Both excellent gas permeance and excellent selectivity for the target separation.
4) Stable performance over prolonged periods (3-5 years).

In 1991, Robeson's pure gas permeability/selectivity 'upper-bound' curves identified a crucial tradeoff: membranes with high selectivity show low permeability and vice-versa [34]. This relationship limits the separation performance of membranes for a particular gas pair. Knowledge of this tradeoff is the critical first step in evaluating new materials for a particular application. Because pure-gas measurements do not account for non-idealities, such as plasticization and competitive sorption [35], the final assessment must include mixed-gas experiments [12]. Moreover, long-term membrane performance tests are crucial, especially for feeds containing highly sorbing gases [36]. The best-performing membranes used in industrial processes exhibit a 30% reduction in permeance over 3-5 years, with most of the decline occurring in the first six months [12]. Thus, membrane development efforts must not only improve membrane performance but also ensure chemical, thermal, and mechanical stability. The polymeric membrane materials that have been commercialized or identified as potential candidates for NG applications are discussed in the following section.

1.3.3. CO_2 Removal from NG

Membrane technology is predominantly used for removing CO_2 from NG. In 2008, this application represented nearly 5% of the total $5 billion market share, being by far

the largest application of membranes in NG processing [14]. To date, the most commonly used commercial membrane material for CO_2 removal is CA, with more than 100 NG treatment plants using CA membranes [31]. This membrane type exhibits low permeability and moderate mixed-gas CO_2/CH_4 selectivity of 10-15 under actual field conditions. Despite their high industrial popularity, the susceptibility of CA membranes to *plasticization* (leading to CH_4 loss) is still a major concern for their long-term reliability and economics [29, 31, 37]. In CO_2/CH_4 separation, CO_2 acts as a plasticizer. Plasticization occurs when large amounts of CO_2 sorb into the polymer matrix, which results in dilation of the polymer matrix and increases the polymer chain mobility [38-41]. Consequently, the separation performance of the membrane decreases. For example, CA membranes exhibited a 50% reduction in their mixed-gas selectivity, well below their low-pressure mixed-gas selectivity of ~30, as a result of CO_2-induced membrane plasticization [31, 42]. Moreover, they showed reduced CO_2 mixed-gas permeabilities due to the competitive sorption effect, commonly observed phenomenon in gas-mixture experiments in which penetrants compete for the available sorption sites, resulting in reduced solubility [43, 44]. To date, their industrial commercialization has been sustained by an excellent process design that incorporates the separation limit of CA membranes to achieve the target separation performances [12]. However, there is still great potential for the development of new materials with high permeability and selectivity that are inherently resistant to plasticization.

Polyimides are viewed as an alternative to CA membranes and thus have a share of the market [14, 22, 31]. They are robust and demonstrate higher separation performance

than CA membranes. Despite their attractive properties, polyimides also experience significant separation losses as a result of CO_2 plasticization. For example, the low-pressure mixed-gas selectivity of Matrimid® 5218, a commercial polyimide membrane, decreased from 45 to 25 (~45% reduction) as a result of plasticization [45, 46].

Some of the limitations of commercial gas separation membranes can potentially be mitigated by an emerging materials class based on perfluorinated, solution-processable glassy polymers, such as Teflon® AF (DuPont), Hyflon® AD (Solvay), and Cytop® (Asahi Glass) [47-52]. Their unique structure/gas transport property relationships have defined the 2008 Robeson upper-bound limit for the CO_2/CH_4 gas pair. For example, Teflon® AF 2400 exhibits a high CO_2 permeability of 3900 Barrer [53] owing to its large free volume. However, its CO_2/CH_4 selectivity is low (~6.5). In contrast, Hyflon® AD60 and Cytop® show superior performances, with CO_2 permeabilities of 216 and 150 and CO_2/CH_4 selectivities of 26 and 28, respectively [47]. In mixed-gas experiments, Hyflon® AD60 and Cytop® membranes exhibit CO_2/CH_4 selectivities of 17 and 22, respectively, with high CO_2 permeabilities [47]. Overall, there is a great potential for separation advances using perfluoro-based polymeric membranes, as apparent from the significant upper-bound transition of commercial perfluoropolymers in 1991 to the newly developed perfluoropolymers reported in 2008, as illustrated in **Fig. 1.7**. In fact, Membrane Technology and Research, Inc. (MTR) has successfully deployed perfluoropolymer-based membrane systems to treat gas wells with feeds containing > 40% CO_2 in Texas, U.S.A. (see **Fig. 1.8)** [54]. The system has successfully reduced the

CO_2 content down to a pipeline-specific value of < 2% with more than 95% hydrocarbon recovery.

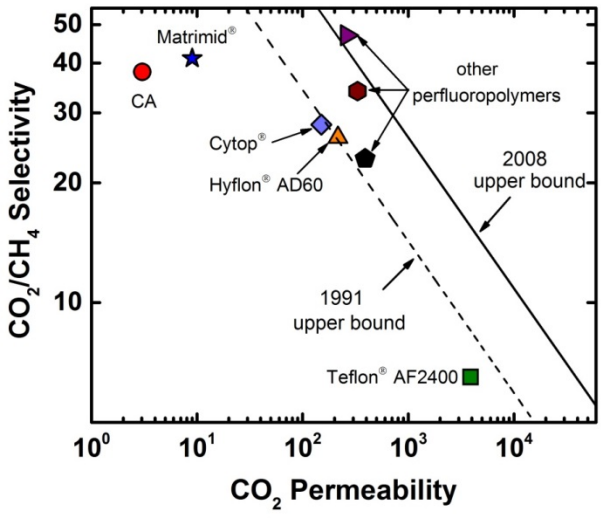

Fig. 1.7. Robeson upper-bound plot for CO_2/CH_4 separation.

Fig. 1.8. A membrane system using commercial perfluoropolymer for CO_2 removal and hydrocarbon recovery from NG in Texas, U.S.A.

1.3.4. C_{2+} Hydrocarbon Removal

The separation of higher hydrocarbons (C_2H_6, C_3H_8, *n*-C_4H_{10}, and C_{5+}) from NG is the second-largest application of membranes, after acid gas removal [22]. The total higher hydrocarbon content in associated NG is as high as ~20%, and its presence often causes membrane plasticization.

Rubbery polymeric membranes are suitable for this application because of their ability to preferentially permeate gases with high condensability. The most commonly used commercial material for hydrocarbon recovery is polydimethylsiloxane (PDMS) [12, 14] that exhibits high C_{2+} hydrocarbon permeabilities because of its highly flexible chain structure, which endows high solubility and low diffusional resistivity [55]. Consequently, hydrocarbons permeate more readily than CH_4. However, PDMS swells upon hydrocarbon sorption. For example, the mixed-gas *n*-butane/CH_4 selectivity of PDMS decreased to 5 from its pure-gas value of 18 (70% reduction) [56]. Other rubbery polymers have been reported with high *n*-butane/CH_4 mixed-gas selectivities up to 12 [56]; however, they are not yet employed in industrial processes. MTR developed rubbery membranes under their patented VaporSep® technology for hydrocarbon separation [57].

Conventional low free-volume glassy polymers such as CA and polysulfone are not suitable for this application because they preferentially permeate CH_4 over hydrocarbons due to their size-selective-based gas separation mechanism. Consequently, large membrane areas and compressor units are required to process NG, making the membrane systems impractical. Surprisingly, poly(1-trimethylsilyl-1-propyne) (PTMSP), a high-

free-volume glassy polymer, has demonstrated extraordinarily high mixed-gas C_{3+} hydrocarbon/CH_4 selectivity because of its large-hydrocarbon-preferential adsorption capacity [58]. PTMSP exhibited a *n*-butane/CH_4 mixed-gas selectivity of 30, which is almost 6-fold higher than its reported pure-gas values [58]. Despite this high performance, PTMSP membranes have not yet been considered for commercialization because of their poor chemical stability and physical aging issues [12].

Perfluoropolymers are known to possess an unusually low hydrocarbon vapor solubility [49]. For example, the propane solubility of Cytop® [49] was almost 5-fold lower than that of a partially fluorinated polyimide membrane [59]. This feature may enable an alternate strategy for NG treatment that is not possible using conventional hydrocarbon polymers because of their high hydrocarbon solubility-induced membrane plasticization. When tested under pure-gas conditions, Hyflon® AD60 and Cytop® composite membranes exhibited high CO_2/C_3H_8 selectivities of 360 and 88 [47], respectively. Furthermore, in the presence of CO_2 and hydrocarbons, CO_2/CH_4 selectivities of 10-15 (comparable to industry-standard CA membranes) with significantly higher CO_2 fluxes have been reported for these perfluoropolymers under actual NG operating conditions [49]. These results provide a good indication that perfluorinated membranes are suitable for NG upgrading, especially for feeds containing high concentrations of plasticizing components.

1.3.5. N_2 Removal from NG

The removal of N_2 from NG can allow access to 10 trillion standard cubic feet (tcf) of additional NG, worth $30 billion [31]. Membrane technology offers a potential economic

advantage, especially for smaller fields with flow rates of 1-20 MMscfd [22, 31]. For this separation, either glassy, N_2-selective polymers or rubbery, CH_4-selective polymers can be used. However, efficient separation of N_2 from CH_4 is difficult to achieve [20, 60]. Because N_2 is smaller than CH_4, diffusivity selectivity favors the permeation of N_2; whereas, because CH_4 is more condensable than N_2, solubility selectivity favors the permeation of CH_4. As a result of these contradictory effects, the overall N_2/CH_4 selectivities of polymeric membranes are generally low [20].

Ideally, N_2-selective membranes should be suitable for N_2 removal. In the case of CH_4-selective membranes, the bulk of NG (i.e., CH_4) requires an additional recompression stage to recycle the low-pressure permeate, making the process inefficient and costly [20]. However, Baker showed that, for a specific process design, a CH_4-selective membrane requires a CH_4/N_2 selectivity of 6, whereas a N_2-selective membrane requires a N_2/CH_4 selectivity of 17 [31]. At present, the best performing rubbery polymers are PDMS, Pebax® 2533, and Parel® 58, which provide CH_4/N_2 selectivities of 3-4, slightly below the required value [21]. However, the best-performing glassy polymers to date are Hyflon® AD80, Hyflon® AD60, Cytop®, and a few 6FDA-based polyimides, which provide N_2/CH_4 selectivities of 2-3. Thus, CH_4-selective membranes are currently used for this application [20, 60]. However, rubbery polymers are not without problems. To achieve CH_4/N_2 selectivities of 4 or greater, membrane processes must operate at low temperatures. This means that an additional refrigeration plant must be installed, which is impractical for small fields because of their high cost and complexity [60]. Moreover, NG contains CO_2, H_2S, and water vapor, which permeate

readily alongside CH_4 into the product stream. Therefore, an additional cost is associated with the pre- or post-treatment of the gas necessary to remove water and acid gas before delivery to the pipeline [61].

Perfluoropolymers that are N_2-selective provide a good alternative for this separation. Hyflon® AD60 and Cytop® showed high N_2 permeabilities with selectivities of 2-3. Even under mixture experiments containing 20% CO_2, their selectivities were well maintained [21, 61]. Moreover, these polymers exhibit low permeabilities for hydrocarbons, enabling the enrichment of hydrocarbons alongside CH_4 in the retentate. Perfluoropolymers with moderate selectivities may present a potentially viable alternative for separating nitrogen from CH_4 with economic benefits using the membrane configurations patented in reference [61].

1.4. Research Goals

Considerable efforts have been made to suppress the plasticization of polymers in NG applications. Several strategies have been employed to reduce plasticization, including the cross-linking of polymers, polymer blending, and thermal treatment [37, 45, 62-66]. These approaches tend to delay the onset of plasticization rather than removing its underlying cause, i.e., the high solubility of the plasticizing components. An alternative approach to counter the effect of plasticization may be to identify polymers that have a *low solubility* for plasticizing penetrants [49, 67]. Perfluoropolymers are known to have unusually low hydrocarbon gas solubilities, which provide unique separation properties well suited for NG applications [49]. This work aimed to assess the membrane

performance of Nafion®, a prototypical perfluorinated ionomer, for potential use in NG applications.

This dissertation comprises 8 chapters, including the introductory chapter, which has provided the background information necessary to understand the importance of NG, advantages of membrane technology for NG upgrading, and current commercial polymers used for specific NG applications.

Chapter 2 provides an overview of the physical and gas transport properties of perfluoropolymers. Moreover, a prototypical perfluorosulfonate ionomer, Nafion®, is presented as a potential membrane material for gas separation. The chapter explores earlier work on gas transport in Nafion® and its metal-complexed derivative forms. Additionally, the characterization techniques used in this work, such as wide-angle X-ray diffraction (WAXD), small-angle X-ray scattering (SAXS), differential scanning calorimetry (DSC), and dynamic mechanical analysis (DMA), are reviewed. Later in this work, these techniques are employed to obtain a fundamental understanding of Nafion®'s complex physical microstructure and its unique gas transport anomalies.

Chapter 3 introduces the fundamental and theoretical concepts necessary to understand gas transport through polymeric membranes.

Chapter 4 describes the materials, experimental procedures, equipment, and operation protocol used throughout this research.

In chapter 5, the transport properties of several gases including higher hydrocarbons and the mechanical properties of Nafion® are discussed to elucidate the physical state

(glass or rubber) of Nafion®. Correlations between the gas solubility and critical temperature, and between the gas permeability and penetrant critical volume, are highlighted to facilitate an understanding of gas transport through the complex microstructure of Nafion®. Temperature-dependent studies were conducted to measure the activation energies and quantify the structural chain tightness in Nafion® towards gas permeation.

Chapter 6 discusses the pressure dependence of the separation performances of Nafion® towards: (i) pure gas, (ii) binary CO_2/CH_4 mixed gas, and (iii) ternary $CO_2/CH_4/C_3H_8$ mixed gas. Interestingly, pressure-dependent pure-gas data revealed two divergent phenomena, namely, compression and plasticization, which altered the permeation properties in different ways. The interplay between the two phenomena was further investigated using (50:50) CO_2/CH_4 mixtures to determine their individual contributions towards the actual separation performance. A ternary (30:50:20) $CO_2/CH_4/C_3H_8$ mixture was used to evaluate the separation performance of Nafion® with two plasticizing components.

Chapter 7 examines the effect of crosslinking Nafion with trivalent Fe^{3+} cation to suppress CO_2-induced plasticization. The ionomer was characterized with WAXD, TGA and Raman techniques to develop a correlation between its physical properties and its gas permeation properties. Pressure-dependent pure- and mixed-gas properties were evaluated to compare the CO_2/CH_4 separation performances of Nafion H^+ and its Fe^{3+} exchanged form.

Finally, Chapter 8 presents the conclusions of this research project and outlines possibilities for future work in this area.

1.5. References

[1] M.J. Economides, D.A. Wood, The state of natural gas, J. Nat. Gas Sci. Eng. 1 (2009) 1-13.

[2] http://naturalgas.org/overview/background/.

[3] BP Statistical Review of World Energy, (2015).

[4] International Energy Outlook 2013, (access date 28 December 2015), http://www.eia.gov/forecasts/ieo/pdf/0484(2013).pdf.

[5] U.S. Energy Information Administration, (accessed on 29 December 2015) https://www.eia.gov.

[6] S. Mokhatab, W.A. Poe, J.G. Speight, Handbook of natural gas transmission and processing, second ed., Gulf Professional Publishing, MA, USA, 2006.

[7] A. Rojey, Natural Gas: Production, Processing, Transport, Editions Technip, 1997.

[8] G. Lockermann, The centenary of the bunsen burner, J. Chem. Educ. 33 (1956) 20.

[9] http://www.iangv.org/.

[10] International Energy Agency 2015, (accessed on 28 December 2015), https://www.iea.org/publications/freepublications/publication/WEO2015SpecialReportonEnergyandClimateChange.pdf.

[11] M. Safari, A. Ghanizadeh, M.M. Montazer-Rahmati, Optimization of membrane-based CO_2-removal from natural gas using simple models considering both pressure and temperature effects, International Journal of Greenhouse Gas Control 3 (2009) 3-10.

[12] R.W. Baker, B.T. Low, Gas separation membrane materials: a perspective, Macromolecules 47 (2014) 6999-7013.

[13] M.A. Al-Saleh, S.O. Duffuaa, M.A. Al-Marhoun, J.A. Al-Zayer, Impact of crude oil production on the petrochemical industry in Saudi Arabia, Energy 16 (1991) 1089-1099.

[14] R.W. Baker, K. Lokhandwala, Natural gas processing with membranes: an overview, Ind. Eng. Chem. Res. 47 (2008) 2109-2121.

[15] B.D. Bhide, S.A. Stern, Membrane processes for the removal of acid gases from natural gas. I. Process configurations and optimization of operating conditions, J. Membr. Sci. 81 (1993) 209-237.

[16] P. Bernardo, E. Drioli, G. Golemme, Membrane gas separation: a review/state of the art, Ind. Eng. Chem. Res. 48 (2009) 4638-4663.

[17] D. Dortmundt, K. Doshi, Recent development in CO_2 removal membranes, UOP, LLC, (1999).

[18] G. Blizzard, G. Parro, K. Hornback, Mallet gas processing facility uses membranes to efficiently separate CO_2, Oil Gas J. 103 (2005).

[19] J.A. Bullin, C. Fitz, T. Dustman, Practical hydrocarbon dew point specification for natural gas transmission lines, Bryan Research & Engineering Inc.

[20] R.W. Baker, K.A. Lokhandwala, I. Pinnau, S. Segelke, Methane/nitrogen separation process, US Patent 5669958, 1997.

[21] K.A. Lokhandwala, I. Pinnau, Z. He, K.D. Amo, A.R. DaCosta, J.G. Wijmans, R.W. Baker, Membrane separation of nitrogen from natural gas: a case study from membrane synthesis to commercial deployment, J. Membr. Sci. 346 (2010) 270-279.

[22] C.A. Scholes, G.W. Stevens, S.E. Kentish, Membrane gas separation applications in natural gas processing, Fuel 96 (2012) 15-28.

[23] Y. Yampolskii, Polymeric gas separation membranes, Macromolecules 45 (2012) 3298-3311.

[24] A. Legault, Mainstreaming efficient industrial separation systems (2008),

[25] Z.Y. Yeo, T.L. Chew, P.W. Zhu, A.R. Mohamed, S.-P. Chai, Conventional processes and membrane technology for carbon dioxide removal from natural gas: a review, J. Nat. Gas Chem. 21 (2012) 282-298.

[26] A.L. Lee, H.L. Feldkirchner, S.A. Stern, A.Y. Houde, J.P. Gamez, H.S. Meyer, Field tests of membrane modules for the separation of carbon dioxide from low-quality natural gas, Gas Sep. Purif. 9 (1995) 35-43.

[27] F.J.C. Fournie, J.P. Agostini, Permeation membranes can efficiently replace conventional gas treatment processes, J. Pet. Technol. 39 (1987) 707-712.

[28] R.L. Mckee, M.K. Changela, G.J. Reading, CO_2 removal: membranes plus amine, Hydrocarb Process 70 (1991) 63.

[29] B.D. Bhide, S.A. Stern, Membrane processes for the removal of acid gases from natural gas. II. effects of operating conditions, economic parameters, and membrane properties, J. Membr. Sci. 81 (1993) 239-252.

[30] R.W. Baker, Membrane Technology and Applications, 2nd ed., John Wiley & Sons, Ltd., Chichester, UK, 2004.

[31] R.W. Baker, Future directions of membrane gas separation technology, Ind. Eng. Chem. Res. 41 (2002) 1393-1411.

[32] S. Matteucci, Y. Yampolskii, B.D. Freeman, I. Pinnau, Transport of gases and vapors in glassy and rubbery polymers, in: Materials Science of Membranes for Gas and Vapor Separation, John Wiley & Sons, Ltd, 2006, pp. 1-47.

[33] K. Ghosal, B.D. Freeman, Gas separation using polymer membranes: an overview, Polym. Adv. Technol. 5 (1994) 673-697.

[34] L.M. Robeson, Correlation of separation factor versus permeability for polymeric membranes, J. Membr. Sci. 62 (1991) 165-185.

[35] L.M. Robeson, The upper bound revisited, J. Membr. Sci. 320 (2008) 390-400.

[36] X. He, M.B. Hägg, Membranes for environmentally friendly energy processes, Membranes 2 (2012) 706-726.

[37] J.D. Wind, D.R. Paul, W.J. Koros, Natural gas permeation in polyimide membranes, J. Membr. Sci. 228 (2004) 227-236.

[38] J.S. Chiou, D.R. Paul, Effects of CO_2 exposure on gas transport properties of glassy polymers, J. Membr. Sci. 32 (1987) 195-205.

[39] E.S. Sanders, Penetrant-induced plasticization and gas permeation in glassy polymers, J. Membr. Sci. 37 (1988) 63-80.

[40] M. Wessling, S. Schoeman, T. van der Boomgard, C.A. Smolders, Plasticization of gas separation membranes, Gas Sep. Purif. 5 (1991) 222-228.

[41] A. Bos, I.G.M. Pünt, M. Wessling, H. Strathmann, CO_2-induced plasticization phenomena in glassy polymers, J. Membr. Sci. 155 (1999) 67-78.

[42] A.Y. Houde, B. Krishnakumar, S.G. Charati, S.A. Stern, Permeability of dense (homogeneous) cellulose acetate membranes to methane, carbon dioxide, and their mixtures at elevated pressures, J. Appl. Polym. Sci. 62 (1996) 2181-2192.

[43] W.J. Koros, R.T. Chern, V. Stannett, H.B. Hopfenberg, A model for permeation of mixed gases and vapors in glassy polymers, J. Polym. Sci.: Polym. Phys. Ed. 19 (1981) 1513-1530.

[44] E.S. Sanders, W.J. Koros, H.B. Hopfenberg, V.T. Stannett, Mixed gas sorption in glassy polymers: Equipment design considerations and preliminary results, J. Membr. Sci. 13 (1983) 161-174.

[45] A. Bos, I.G.M. Pünt, M. Wessling, H. Strathmann, Plasticization-resistant glassy polyimide membranes for CO_2/CO_4 separations, Sep. Purif. Technol. 14 (1998) 27-39.

[46] L.S. White, T.A. Blinka, H.A. Kloczewski, I.F. Wang, Properties of a polyimide gas separation membrane in natural gas streams, J. Membr. Sci. 103 (1995) 73-82.

[47] I. Pinnau, Z. He, A.R. Da Costa, K.D. Amo, R. Daniels, Gas separation using C_{3+} hydrocarbon-resistant membranes, US Patent 6361582, 2002.

[48] V. Arcella, A. Ghielmi, G. Tommasi, High performance perfluoropolymer films and membranes, Ann. N.Y. Acad. Sci. 984 (2003) 226-244.

[49] T.C. Merkel, I. Pinnau, R. Prabhakar, B.D. Freeman, Gas and vapor transport properties of perfluoropolymers, in: Materials Science of Membranes for Gas and Vapor Separation, John Wiley & Sons, Ltd., Chichester, UK, 2006, pp. 251-270.

[50] Z. He, T.C. Merkel, Y. Okamoto, Y. Koike, Gas separation membranes based on perfluorinated polymers, US Patent 8828121, 2014.

[51] Y. Okamoto, H. Zhang, F. Mikes, Y. Koike, Z. He, T.C. Merkel, New perfluoro-dioxolane-based membranes for gas separations, J. Membr. Sci. 471 (2014) 412-419.

[52] Y. Okamoto, Q. Du, K. Koike, F. Mikeš, T.C. Merkel, Z. He, H. Zhang, Y. Koike, New amorphous perfluoro polymers: perfluorodioxolane polymers for use as plastic optical fibers and gas separation membranes, Polym. Adv. Technol. 27 (2016) 33-41.

[53] I. Pinnau, L.G. Toy, Gas and vapor transport properties of amorphous perfluorinated copolymer membranes based on 2,2-bistrifluoromethyl-4,5-difluoro-1,3-dioxole/tetrafluoroethylene, J. Membr. Sci. 109 (1996) 125-133.

[54] http://www.mtrinc.com/co2_removal.html, access date: 02/May/2016.

[55] T.C. Merkel, V.I. Bondar, K. Nagai, B.D. Freeman, I. Pinnau, Gas sorption, diffusion, and permeation in poly(dimethylsiloxane), J. Polym. Sci., Part B: Polym. Phys. 38 (2000) 415-434.

[56] J. Schultz, K.V. Peinemann, Membranes for separation of higher hydrocarbons from methane, J. Membr. Sci. 110 (1996) 37-45.

[57] K.A. Lokhandwala, M. Jacobs, New membrane applications in gas processing, MTR.

[58] I. Pinnau, L.G. Toy, Transport of organic vapors through poly(1-trimethylsilyl-1-propyne), J. Membr. Sci. 116 (1996) 199-209.

[59] C. Staudt-Bickel, W.J. Koros, Olefin/paraffin gas separations with 6FDA-based polyimide membranes, J. Membr. Sci. 170 (2000) 205-214.

[60] R.W. Baker, K.A. Lokhandwala, J.G. Wijmans, A.R. Da Costa, Nitrogen removal from natural gas using two types of membranes, US Patent 6630011, 2003.

[61] J.G. Wijmans, R.W. Baker, Z. He, I. Pinnau, Natural gas separation using nitrogen-selective membranes of modest selectivity, US Patent 6565626, 2003.

[62] S.S. Kulkarni, S.F. Yates, A.X. Swamikannu, Cross-linked gas selective membranes, US Patent 4932986, 1990.

[63] C. Staudt-Bickel, W. J. Koros, Improvement of CO_2/CH_4 separation characteristics of polyimides by chemical crosslinking, J. Membr. Sci. 155 (1999) 145-154.

[64] J.D. Wind, C. Staudt-Bickel, D.R. Paul, W.J. Koros, Solid-state covalent cross-linking of polyimide membranes for carbon dioxide plasticization reduction, Macromolecules 36 (2003) 1882-1888.

[65] C. Liu, S.T. Wilson, J.J. Chiou, D.A. Lesch, S. Kulprathipanja, Plasticization resistant membranes, US Patent 20100270234, 2010.

[66] J.D. Wind, S.M. Sirard, D.R. Paul, P.F. Green, K.P. Johnston, W.J. Koros, Carbon dioxide-induced plasticization of polyimide membranes: pseudo-equilibrium relationships of diffusion, sorption, and swelling, Macromolecules 36 (2003) 6433-6441.

[67] R.S. Prabhakar, B.D. Freeman, I. Roman, Gas and vapor sorption and permeation in poly(2,2,4-trifluoro-5-trifluoromethoxy-1,3-dioxole-co-tetrafluoroethylene), Macromolecules 37 (2004) 7688-7697.

Chapter 2. Literature Review of Perfluoropolymers

This chapter provides a brief overview of physical and gas transport properties of perfluoropolymers. More specifically, the potential use of Nafion®, a perfluorosulfonic acid ionomer, as a gas separation membrane material is discussed in light of its unique physical properties. Thus, the chapter thoroughly reviews the microstructure and molecular origins of Nafion® and its neutralized (cation and organic counterions) forms, as probed by techniques including wide-angle X-ray diffraction (WAXD), small-angle X-ray scattering (SAXS), differential scanning calorimetry (DSC), and dynamic mechanical analysis (DMA). Finally, previous research on the gas transport properties of Nafion® and its metal-ion-exchanged forms are summarized.

2.1. Overview of Perfluoropolymers

In general, there are two types of fluoropolymers: *perfluoropolymers* and *partially fluorinated polymers*. These fluoropolymers differ in that the chemical structure of perfluoropolymers contains mostly carbon and fluorine and no hydrogen, while that of partially fluorinated polymers contains carbon, fluorine, and hydrogen [1, 2].

The discovery of the first perfluoropolymer, polytetrafluoroethylene (PTFE), in 1938, sparked great interest in its industrial applications owing to its excellent chemical and thermal stability as well as useful electrical, optical, and surface properties [2-4]. These properties stem from its strong covalent carbon – carbon (360 kJ/mol) and carbon – fluorine bonds (485 kJ/mol) [2, 5]. Consequently, the polymer shows excellent resistance to chemicals, such as attack by acids, bases, organic solvents (aromatic amines, esters,

ketones, and ethers) and oils, making it useful for applications in harsh chemical environments [2, 6].

The first comprehensive gas transport measurements for PTFE were reported by Pasternak et al. [7]. Their study indicated that PTFE exhibits low permeability for all gases and vapors. However, the permeabilities for hydrocarbon vapors were unusually low relative to those of light gases. This was ascribed to the weak interactions between the hydrocarbon-fluorocarbon systems, which reduced hydrocarbon solubilities. In a later study, Yi-Yan et al. investigated the gas permeability of PTFE as a function of temperature and the effect of annealing on the structure and gas transport properties. The gas permeabilities correlated well with the Arrhenius-type relationship for the temperature range studied. Annealing the polymer significantly reduced the gas diffusivity and permeability due to an increase in crystallinity at elevated temperatures [8]. The use of PTFE as a gas separation membrane was limited by its low gas permeability [7], high crystallinity [9, 10], and insolubility in common solvents [2].

The more recent development of an amorphous class of perfluorinated solution-processable glassy polymers, such as Teflon AF® (DuPont), Hyflon® AD (Solvay), and Cytop® (Asahi Glass), rekindled the prospects of fluoropolymers for gas separation applications [2-4, 11-13]. These polymers exhibit a high free volume with excellent chemical and thermal properties [4, 11-13]. In fact, their unique structure/gas transport property relationships defined the 2008 Robeson upper bound curves for certain gas pairs, such as CO_2/CH_4, He/CH_4, He/H_2, N_2/CH_4, and H_2/CH_4 [14]. Because of their high selectivities and chemical inertness, these polymers were proposed for NG

treatment, in which condensable species degrade the performance of traditional polymers due to plasticization [2-4, 11, 12, 15].

2.2. Introduction to Nafion®

2.2.1. Structure of Nafion®

An important class of perfluorinated polymers based on sulfonated ionomers, Nafion®, developed by DuPont researchers in the 1960s, was capable of conducting ions [16]. Nafion® consists of a hydrophobic PTFE backbone with pendant side-chains of polyvinyl ether groups terminated by a highly hydrophilic sulfonic acid tail, as shown in **Fig. 2.1**. The ionic groups are phase-separated from the fluorocarbon matrix and aggregate to form clusters (according to a model first proposed by Gierke et al.) [17-27]. In the dry state, the 1.5-nm-diameter ionic clusters are dispersed in the perfluorocarbon matrix, as shown in **Fig. 2.2** [18, 21, 28]. In the presence of water, these clusters grow to approximately 4-5 nm in diameter and form interconnected channels [29] capable of transporting water and cations [21]. Nafion®'s high cation conductivity has led to its widespread use as a semipermeable barrier in electrolytic cells [28, 30].

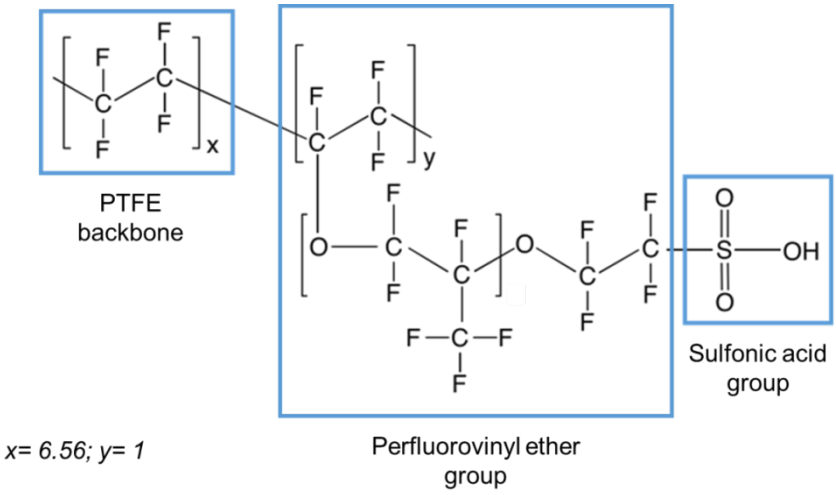

Fig. 2.1. Chemical structure of Nafion® (sulfonic acid form).

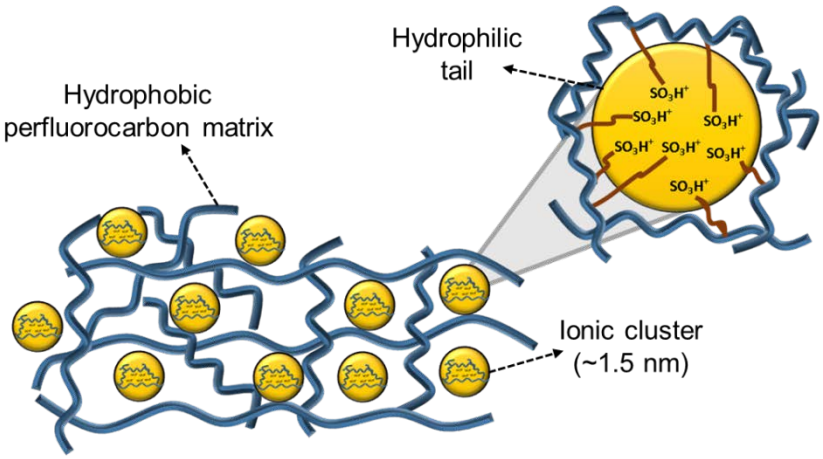

Fig. 2.2. Cluster-network model for dry Nafion®.

2.2.2. Applications of Nafion®

Nafion® was first used commercially in the chlor-alkali process (see **Fig. 2.3a**), in which chlorine gas and sodium hydroxide are produced by the electrolysis of sodium

chloride [16, 28]. In this application, a Nafion® membrane separates a sodium chloride solution at the anode of the electrolytic cell from a sodium hydroxide solution at its cathode, passing sodium ions while rejecting chloride and hydroxide. Nafion® has played a similar role as a proton-exchange membrane (PEM) in PEM fuel cells, facilitating the movement of hydrogen ions from the anode to the cathode and rejecting negatively charged electrons, which then pass through the external circuit as an electrical current (see **Fig. 2.3b)**. The first such cell, developed in the 1950s [31], used the ionomers available at the time. Nafion®'s higher proton conductivity and chemical stability made PEM fuel cells more practical, and since then, it has remained the benchmark material in this field [28, 30].

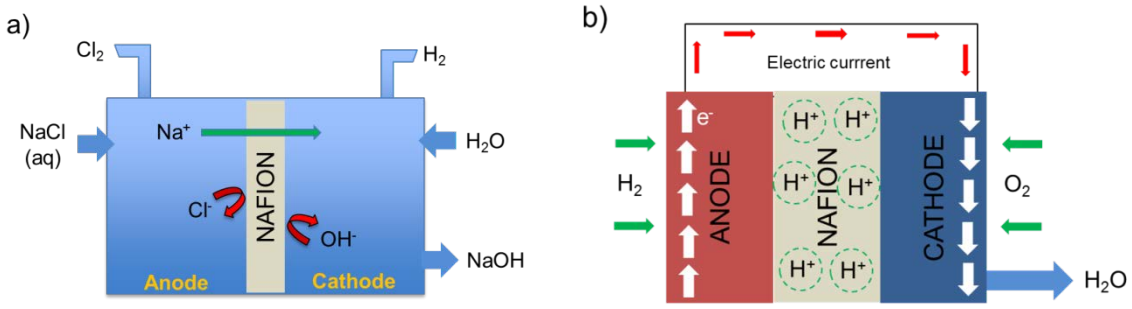

Fig. 2.3. (a) Chlor-alkali process; (b) polymer electrolyte membrane (PEM) fuel cell.

2.3. Structure-Property Characterization of Nafion®

A thorough knowledge of electrostatic interactions and thermomechanical properties is critical for developing a deeper understanding of the structure-property relationship of perfluorinated ionomers. Previous work investigating Nafion®'s chemical structure and morphology using WAXD and SAXS is discussed below. Additionally, the thermal

transitions and mechanical relaxations observed by DSC and DMA are explored to identify their molecular origins and thereby clarify Nafion®'s microstructure.

2.3.1. Scattering and Diffraction Techniques

It is difficult to accurately describe the morphology of Nafion® due to its unique chemical structure, as the crystalline and ionic domains organize in complicated forms [28]. Gierke's cluster-network model provided the first significant breakthrough in correlating several of the ion and water transport properties of Nafion® with its spatial morphology [21, 29]. The model was based on limited information gathered from SAXS and WAXD data. The SAXS curve identified two characteristic peaks representing two distinct regions [29]: one at $2\theta = \sim 0.5°$, corresponding to PTFE-like-crystallites, and one at $2\theta = \sim 2.6°$, attributed to 3nm diameter ionic clusters. As water sorbed into the polymer matrix, the ionomer peak increased in intensity and shifted to smaller angles ($2\theta = \sim 1.6°$), corresponding to a cluster size of 5 nm [29]. It was concluded that the ionic clusters in Nafion® undergo rearrangement upon hydration [29, 32-34], consistent with the hypothesis that the scattering behavior of Nafion® is best attributed to an interparticle origin [21, 28] rather than an intraparticle origin [35]. A water sorption study in Nafion® led Gierke to describe its water-swollen morphology as an inverted micellar structure with independent spherical clusters interconnected by 1-nm channels, as shown in **Fig. 2.4**.

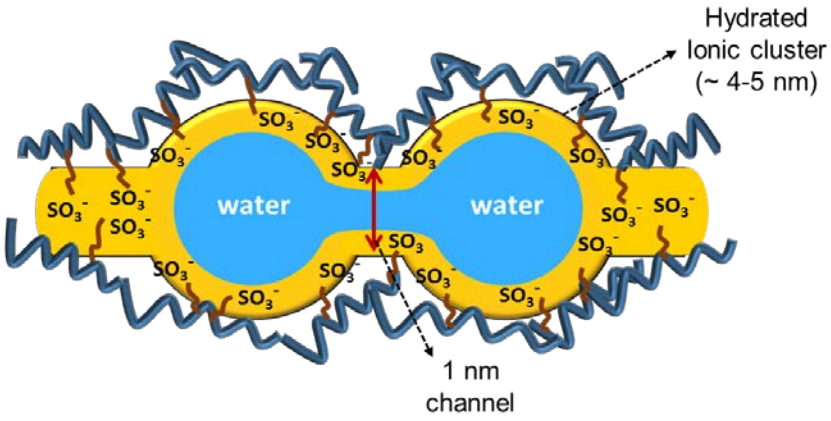

Fig. 2.4. Water-swollen morphology of Nafion® [28].

Subsequent data analysis of Nafion® using advanced scattering techniques led to the development of newer models that differed significantly in the geometry and spatial distribution of the ionic clusters [34-37]. However, common to all these models was the existence of interconnected ionic domains through which ions and solvent permeate [28]. The crystalline component has received less attention and was considered to provide structural integrity and resistance to solvent permeation [28]. The WAXD data for Nafion® showed a diffraction peak at $2\theta = 18°$, superimposed on a broad amorphous halo, indicating its semi-crystalline behavior. The degree of crystallinity in 1100 EW Nafion® was calculated as approximately 3-12% [28]. To date, Gierke's model has been used to successfully elucidate several of the structure-property anomalies of Nafion® in the context of fuel cell applications [38-40].

Gierke et al. extended their study by examining the cation-exchanged form of Nafion® membranes [21]. The SAXS results showed a decrease in the ionomer peak intensity with increasing cation size. This was attributed to the decreasing contrast

between the crystalline and ionic domains due to the high electron density of the heavier cations. However, no change in the Bragg spacing or scattering angle was observed. Transmission electron microscopy (TEM) images of Nafion® doped with silver and tin ions revealed ionic clusters with a *spherical-like* morphology and diameters of 3-10 nm [41], confirming Gierke's speculated spherical cluster network model [21]. Based on this geometrical verification and solvent absorption studies, Gierke estimated the average size of ionic clusters for several cations [21, 29]. The size of the ionic clusters decreased with an increase in the cation size.

Page et al. neutralized Nafion® with several alkylammonium ions and demonstrated a significant correlation between the magnitude of the electrostatic interactions and the size of the counterions, shedding light on *physical crosslinking* in ionomers [42]. Their study showed that the intensity of the ionomer peak strongly depended on the temperature and counterion size. They discovered that at a certain threshold temperature, the intensity abruptly decreased, and this temperature correlated well with the glass transition temperature of the ionomer domains as deduced from DMA (see next section). They attributed this decrease to the weakening of the electrostatic interactions between ion pairs responsible for physical crosslinking between the polymer chain molecules. The larger organic counterions exhibited a lower threshold value, representative of their higher plasticizing tendency.

2.3.2. Thermal Techniques

In an early DMA study by Yeo and Eisenberg, α-, β-, and γ-transitions were observed in Nafion® at ~111, 20, and -100 °C, respectively [18]. Based on their initial analysis, the

α- and β-relaxations were initially attributed to the glass transition temperature of the matrix and the ionic domains, respectively. The low-temperature transition (γ) was assigned to short-range motions in the PTFE unit but did not contribute substantially to the overall mechanical behavior of Nafion®. The two principal transitions (α and β) observed at two distinct temperatures confirmed the earlier interpretation that the Nafion® morphology consists of two distinct phase-separated regions [28]. Later, based on underwater stress relaxation measurements, Kyu and Eisenberg retained their assignment of the γ transition but reversed their assignment of α- and β-transitions. The high-temperature α-relaxation was reassigned to the glass transition of the ionic domains due to its strong dependence on the counterion type and water content. Meanwhile, the β-relaxation was reassigned to the perfluorocarbon matrix [43]. This revised assignment was subsequently complemented by several other researchers [44-46].

Later, Almeida et al. reported DSC studies of Nafion® membranes, in which two endothermic peaks were observed at 115 and 230 °C [45]. The peak at 115 °C disappeared during the first heating scan and then reappeared during the second heating scan. This low-temperature peak was primarily attributed due to thermally activated order-disorder transitions within the ionic clusters [45], analogous to other ionomers [47, 48]. In contrast, the high-temperature peak was ascribed to the melting of PTFE-like crystallites, consistent with the WAXD results, in which the crystalline peak at 275 °C disappeared [35].

Page et al. examined the molecular origins of alkali metal and alkylammonium counterion (sizes ranging between tetramethylammonium to tetradecylammonium) forms

of Nafion® membranes using DSC and DMA. The DSC behaviors of Na^+ and Cs^+ ions were consistent with those reported by Almeida et al. [45]; however, Page et al. contradicted their low-temperature peak assignment, attributing it to the melting of smaller crystallites [42]. The DMA data for Nafion® alkali and alkylammonium cation-exchanged membranes showed a profound effect on its thermomechanical properties. For Na^+ ions, the α- and β-relaxations shifted to higher temperatures relative to the acid form [42]. This transition to higher temperatures was previously reported for other metal ions using DMA, with higher temperature shifts for larger cations [49]. This trend was attributed to the increase in the polymer chain strength with increasing cation size, leading to higher stability and lower chain flexibility, as a result of the strong electrostatic interactions between the metal ions. Similarly, the α- and β-relaxation temperatures of alkylammonium counterions of different types and sizes shifted systematically. In contrast, the relaxation temperatures decreased with increasing counterion size. This was attributed to the bulky nature of the counterions, which plasticized the membrane and reduced the electrostatic interactions between ion pairs, thereby decreasing the relaxation temperatures. The weakening of the electrostatic interactions with increasing temperature was assigned as α-relaxation resulting from the onset of long-range backbone and side-chain motions caused by the complete destabilization of the physically crosslinked ionic network. The β-relaxation was attributed to the main chain motions of the fluorocarbon within the framework of a static physically crosslinked network.

In a later DMA study, Osborn et al. determined the true glass transition temperature in Nafion® by neutralizing it with various concentrations of alkylammonium ions and

analyzing the shifts in the α- and β-relaxation temperatures [50]. The DMA thermograms showed a systematic decrease in the β-relaxation temperature as the concentration decreased, while the α-relaxation temperature remained constant. It was concluded that the β-transition observed at -20 °C is the *true* glass transition temperature of Nafion®.

Mohamed et al. used positron annihilation lifetime spectroscopy (PALS) to analyze the effect of temperature on the free volume capacity in Nafion®-H^+ and determined its glass transition temperature. According to their study, the free volume increased with temperature, and at approximately 20 °C, an abrupt increase in free volume was observed. This increase was attributed to the β-relaxation temperature and assigned as its glass transition temperature [51, 52].

Because of the contradictory arguments and data inconsistencies regarding the glass transition temperature in the literature [42, 50-53], the true physical state of Nafion® is still under debate. To resolve this dispute, this study incorporated *direct* gas sorption measurements and stress-strain behavior correlations to reveal the physical state of Nafion®.

2.4. Gas Transport in Nafion®

2.4.1. Gas Permeation in Nafion®-H^+

Sakai and coworkers measured the gas permeability coefficients for H_2, O_2, and N_2 in the dried and hydrated forms of Nafion® membranes to determine whether gases diffuse through the ionic or fluorocarbon domains [54]. The gas permeability in the hydrated membrane was ten times greater than that in the dried membrane due to

significantly higher gas diffusion coefficients. The similar gas permeabilities in pure water led the researchers to conclude that the gas only diffuses through the ionic domains.

The first comprehensive study of the gas permeation properties of dry Nafion® was reported by Chiou and Paul [55]. Their study indicated a low permeability for all gases other than He and H_2. Surprisingly, Nafion® exhibited high He/H_2, N_2/CH_4, and He/CH_4 permselectivities. In fact, the permselectivity of He/H_2 was almost twice that of any other polymer with a similar helium permeability, as shown in **Fig. 2.5** [56, 57]. Robeson speculated that the unusually high He/H_2 permselectivity in Nafion® is primarily due to its perfluorinated nature, which is known to endow unique solubility properties not observed in conventional hydrocarbon polymers [14]. Chiou and Paul suggested a further detailed investigation of the gas sorption properties of Nafion® to refine the correlation between its structure and unusual gas transport properties.

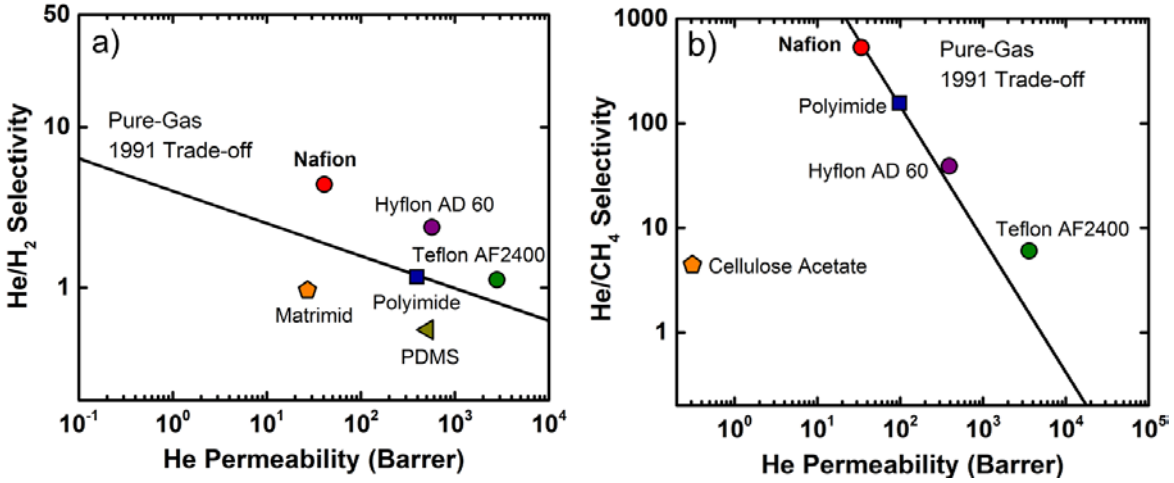

Fig. 2.5. Location of Nafion® on the 1991 Robeson upper-bound curve for (a) He/H_2 and (b) He/CH_4 gas pairs.

Fan et al. [58] reported gas permeability measurements conducted on dry Nafion® at different temperatures. Their values were lower than those reported by Chiou et al. [55] at 30 °C. Additionally, they compared the gas permeabilities of Nafion® and its backbone PTFE membrane, finding that the presence of sulfonate groups in Nafion® impedes gas transport, decreasing the gas permeability. Similar behavior was also reported for a Nafion®-H^+ carboxylate membrane [59]. It was proposed that the gas permeability occurs primarily through the perfluorocarbon chains [59], contrary to the earlier interpretation of gas transport through the ionic domains [54, 60].

Sarti's group evaluated the effects of temperature and relative humidity on Nafion® transport, finding 100-fold increases in the gas permeability relative to the values obtained under dry conditions [61, 62]. The increase in permeability was associated to the hydration of sulfonate groups in Nafion®, which allowed the permeability to approach those obtained in liquid water.

2.4.2. Gas Permeation in Nafion® Ion-Exchanged Membranes

The incorporation of metal ions into the Nafion® matrix has been known to physically crosslink the polymer chain molecules via electrostatic interactions [52, 54, 58, 60, 63-66]. As a result, the polymer exhibits higher mechanical stability and less chain flexibility [42, 52, 66, 67], leading to lower gas permeabilities but enhanced selectivity [52, 54, 60].

Sakai et al. measured the gas transport of H_2, O_2, and N_2 in dry Nafion® neutralized with K^+ ions [54, 60]. They reported that the gas diffusivity and permeability of Nafion®-K^+ was 14-56% lower than that of the acid form and suggested that the lower water-binding capacity and larger ionic radius of K^+ impede gas diffusion [54]. However, enhanced selectivities were observed for K^+ counterions.

Fan et al. studied Nafion® neutralized with monovalent (Li^+, Na^+, K^+) and divalent (Ca^{2+}) cations to investigate the effect of the magnitude of ionic interaction on the gas transport properties [58]. Their study showed a decrease in gas diffusivity for all metal-complexed Nafion® samples relative to the acid form, which was attributed to the commonly ascribed covalent crosslinking between ion pairs. Contrary to Sakai et al., Fan et al. observed an increase in gas permeability for all metal ions and suggested that the suppression of crystallinity and the increase in the ionic cluster size disrupted the polymer chains, increasing the solubility. The increase in ionic cluster size with cation radius is contradictory to Gierke's theoretical calculations [29]. Their study failed to provide any significant correlation between the cation type and gas transport properties. However, improvements in thermal stability and chain tightness were observed for divalent cations.

Mohammad et al. investigated the effect of neutralizing Nafion® with Na^+ and K^+ ions on its free volume and gas permeation properties [52]. The metal-exchanged membranes showed a ~26% increase in free volume measured using the PALS technique and decreases in the gas permeability by 45 and 72% for the Nafion® Na^+ and K^+ forms, respectively, relative to the acid form. This behavior was contradictory to the concept of

free volume, which states that a polymer with high free volume exhibits higher permeability [68, 69]. The increase in free volume was attributed to the increase of the chain spacing due to the incorporation of larger cations. The decrease in gas permeability was ascribed to chain tightening, as indicated by an increase in the Young's modulus and shifts of the α- and β-transitions to higher temperatures.

Lee et al. established a correlation between the ionic radius and gas permeability for several cation- and organic-counterion-exchanged perfluorocarboxylate Nafion® membranes [59]. It was shown that the permeability of O_2 and N_2 decreased with increasing ionic radius. The gas solubilities were nearly the same for all ionic forms; however, the diffusion coefficients were significantly reduced for larger cations, suggesting that the larger ions tended to crosslink more tightly. In contrast, the large alkylammonium counterions exhibited higher gas permeability than the small counterions. Again, the solubilities were independent of ionic size, but the diffusivity increased with the counterion size. This result was consistent with the DMA study reported by Page et al., which demonstrated the weakening of physical crosslinking with increasing size of the alkylammonium ions [42].

Cussler et al. studied the permeability of ammonia in Nafion®-H^+ and other metal-exchanged forms as a function of temperature and pressure. Their study revealed the highest NH_3 permeability and strikingly high selectivity for NH_3/N_2 (> 3000) in the Nafion®-H^+ form. The high permeability of NH_3 was ascribed to its special interaction with the polar sulfonic acid groups [70].

Kobayashi et al. studied the permeability of ethylene and propylene through Nafion® and Nafion® doped with Ag^+ ions [71]. Their study revealed that the permeability was doubled upon Ag^+ doping as a result of Ag-olefin complex formation in the ionic domains of the membrane [13]. This work was continued by Eriksen et al. under humidified conditions, finding that the ethylene permeability of the humidified membrane was nearly two orders of magnitude greater than that in the dry state [72].

Several research groups have investigated the incorporation of metal ions into polymers, including polysulfone [64], polystyrene [63], poly(phenylene oxide) [73], polyimides [74], and others [66]. The selectivities were higher for divalent cations, which provided better separation performance than monovalent cations.

To date, most gas permeation studies of Nafion® have aimed at optimizing its fuel cell performance or olefin/paraffin separation via metal complexation. In contrast, there have been no reported studies assessing the performance of Nafion® and its metal counterpart as a potential membrane material for NG application. This assessment is the core objective of this thesis.

2.5. References

[1] H. Teng, Overview of the development of the fluoropolymer industry, Appl. Sci. 2 (2012) 496-512.

[2] T.C. Merkel, I. Pinnau, R. Prabhakar, B.D. Freeman, Gas and vapor transport properties of perfluoropolymers, in: Materials Science of Membranes for Gas and Vapor Separation, John Wiley & Sons, Ltd., Chichester, UK, 2006, pp. 251-270.

[3] V. Arcella, A. Ghielmi, G. Tommasi, High performance perfluoropolymer films and membranes, Ann. N.Y. Acad. Sci. 984 (2003) 226-244.

[4] Y. Okamoto, H. Zhang, F. Mikes, Y. Koike, Z. He, T.C. Merkel, New perfluoro-dioxolane-based membranes for gas separations, J. Membr. Sci. 471 (2014) 412-419.

[5] T. Davidson, R. N. Gounder, D. K. Weber, S.M. Wecker, A perspective on solid state microstructure in polytetrafluoroethylene, in: Fluorpolymers 2, Springer, Berlin, 2002, pp. 3-22.

[6] V. Arcella, P. Colaianna, P. Maccone, A. Sanguineti, A. Gordano, G. Clarizia, E. Drioli, A study on a perfluoropolymer purification and its application to membrane formation, J. Membr. Sci. 163 (1999) 203-209.

[7] R.A. Pasternak, M.V. Christensen, J. Heller, Diffusion and permeation of oxygen, nitrogen, carbon dioxide, and nitrogen dioxide through polytetrafluoroethylene, Macromolecules 3 (1970) 366-371.

[8] N.Y. Yan, R.M. Felder, W.J. Koros, Selective permeation of hydrocarbon gases in poly(tetrafluoroethylene) and poly(fluoroethylene–propylene) copolymer, J. Appl. Polym. Sci. 25 (1980) 1755-1774.

[9] P.J. Rae, D.M. Dattelbaum, The properties of poly(tetrafluoroethylene) (PTFE) in compression, Polymer 45 (2004) 7615-7625.

[10] Teflon PTFE properties handbook Access date: 02/May/2015.

[11] I. Pinnau, Z. He, A.R. Da Costa, K.D. Amo, R. Daniels, Gas separation using C_{3+} hydrocarbon-resistant membranes, US Patent 6361582, 2002.

[12] Z. He, T.C. Merkel, Y. Okamoto, Y. Koike, Gas separation membranes based on perfluorinated polymers, US Patent 8828121, 2014.

[13] Y. Okamoto, Q. Du, K. Koike, F. Mikes, T.C. Merkel, Z. He, H. Zhang, Y. Koike, New amorphous perfluoro polymers: perfluorodioxolane polymers for use as plastic optical fibers and gas separation membranes, Polym. Adv. Technol. 27 (2016) 33-41.

[14] L.M. Robeson, The upper bound revisited, J. Membr. Sci. 320 (2008) 390-400.

[15] T.C. Merkel, L.G. Toy, Comparison of hydrogen sulfide transport properties in fluorinated and nonfluorinated polymers, Macromolecules 39 (2006) 7591-7600.

[16] W. Grot, History, in: Fluorinated Ionomers (Second Edition), William Andrew Publishing, 2011, pp. 5-10.

[17] A. Eisenberg, Clustering of ions in organic polymers. a theoretical approach, Macromolecules 3 (1970) 147-154.

[18] S.C. Yeo, A. Eisenberg, Physical properties and supermolecular structure of perfluorinated ion-containing (Nafion) polymers, J. Appl. Polym. Sci. 21 (1977) 875-898.

[19] H.L. Yeager, B. Kipling, Ionic diffusion and ion clustering in a perfluorosulfonate ion-exchange membrane, J. Phys. Chem. 83 (1979) 1836-1839.

[20] H.L. Yeager, A. Steck, Cation and water diffusion in Nafion ion exchange membranes: influence of polymer structure, J. Electrochem. Soc. 128 (1981) 1880-1884.

[21] T.D. Gierke, W.Y. Hsu, The cluster-network model of ion clustering in perfluorosulfonated membranes, in: Perfluorinated Ionomer Membranes, 180, American Chemical Society, Washington DC, 1982, pp. 283-307.

[22] W.Y. Hsu, T.D. Gierke, Ion transport and clustering in Nafion perfluorinated membranes, J. Membr. Sci. 13 (1983) 307-326.

[23] R.S. Yeo, Ion clustering and proton transport in Nafion membranes and its applications as solid polymer electrolyte, J. Electrochem. Soc. 130 (1983) 533-538.

[24] N.G. Boyle, V.J. McBrierty, A. Eisenberg, NMR investigation of molecular motion in Nafion membranes, Macromolecules 16 (1983) 80-84.

[25] N.G. Boyle, V.J. McBrierty, D.C. Douglass, The behavior of water in Nafion membranes, Macromolecules 16 (1983) 75-80.

[26] V.K. Datye, P.L. Taylor, A.J. Hopfinger, Simple model for clustering and ionic transport in ionomer membranes, Macromolecules 17 (1984) 1704-1708.

[27] A. Eisenberg, B. Hird, R.B. Moore, A new multiplet-cluster model for the morphology of random ionomers, Macromolecules 23 (1990) 4098-4107.

[28] K.A. Mauritz, R.B. Moore, State of understanding of Nafion, Chem. Rev. 104 (2004) 4535-4586.

[29] T.D. Gierke, G.E. Munn, F.C. Wilson, The morphology in Nafion perfluorinated membrane products, as determined by wide- and small-angle x-ray studies, J. Polym. Sci.: Polym. Phys. Ed. 19 (1981) 1687-1704.

[30] B.C.H. Steele, A. Heinzel, Materials for fuel-cell technologies, Nature 414 (2001) 345-352.

[31] J.W.T. Grubb, Fuel cell, US Patent 2913511, 1959.

[32] F.P. Orfino, S. Holdcroft, The morphology of Nafion: are ion clusters bridged by channels or single ionic sites?, J. New Mater. Electrochem. Syst. 3 (2000) 287-292.

[33] J.A. Elliott, S. Hanna, A.M.S. Elliott, G.E. Cooley, Interpretation of the small-angle X-ray scattering from swollen and oriented perfluorinated ionomer membranes, Macromolecules 33 (2000) 4161-4171.

[34] G. Gebel, Structural evolution of water swollen perfluorosulfonated ionomers from dry membrane to solution, Polymer 41 (2000) 5829-5838.

[35] M. Fujimura, T. Hashimoto, H. Kawai, Small-angle x-ray scattering study of perfluorinated ionomer membranes. 1. Origin of two scattering maxima, Macromolecules 14 (1981) 1309-1315.

[36] H.G. Haubold, T. Vad, H. Jungbluth, P. Hiller, Nano structure of Nafion: a SAXS study, Electrochim. Acta 46 (2001) 1559-1563.

[37] L. Rubatat, A.L. Rollet, G. Gebel, O. Diat, Evidence of elongated polymeric aggregates in Nafion, Macromolecules 35 (2002) 4050-4055.

[38] R.A. Komoroski, K.A. Mauritz, A sodium-23 nuclear magnetic resonance study of ionic mobility and contact ion pairing in a perfluorosulfonate ionomer, J. Am. Chem. Soc. 100 (1978) 7487-7489.

[39] W.Y. Hsu, J.R. Barkley, P. Meakin, Ion percolation and insulator-to-conductor transition in Nafion perfluorosulfonic acid membranes, Macromolecules 13 (1980) 198-200.

[40] P.C. Lee, D. Meisel, Luminescence quenching in the cluster network of perfluorosulfonate membrane, J. Am. Chem. Soc. 102 (1980) 5477-5481.

[41] T. D. Gierke, 152nd meeting of electrochemical society, Atlanta, GA, Oct. 1977. Abstract No. 438, Journal of Electrochemical Society 124, 319C (1977).

[42] K.A. Page, K.M. Cable, R.B. Moore, Molecular origins of the thermal transitions and dynamic mechanical relaxations in perfluorosulfonate ionomers, Macromolecules 38 (2005) 6472-6484.

[43] T. Kyu, A. Eisenberg, Mechanical relaxations in perfluorosulfonate ionomer membranes, in: Perfluorinated Ionomer Membranes, 180, American Chemical Society, 1982, pp. 79-110.

[44] R.B. Moore, C.R. Martin, Chemical and morphological properties of solution-cast perfluorosulfonate ionomers, Macromolecules 21 (1988) 1334-1339.

[45] S.H. de Almeida, Y. Kawano, Thermal behavior of Nafion membranes, J. Therm. Anal. Calorim. 58 (1999) 569-577.

[46] Y. Miura, H. Yoshlda, Effects of water and alcohols on molecular motion of perfluorinated ionomer membranes, Thermochim. Acta 163 (1990) 161-168.

[47] E. Hirasawa, Y. Yamamoto, K. Tadano, S. Yano, Formation of ionic crystallites and its effect on the modulus of ethylene ionomers, Macromolecules 22 (1989) 2776-2780.

[48] K. Tadano, E. Hirasawa, H. Yamamoto, S. Yano, Order-disorder transition of ionic clusters in ionomers, Macromolecules 22 (1989) 226-233.

[49] T. Kyu, M. Hashiyama, A. Eisenberg, Dynamic mechanical studies of partially ionized and neutralized Nafion polymers, Can. J. Chem. 61 (1983) 680-687.

[50] S.J. Osborn, M.K. Hassan, G.M. Divoux, D.W. Rhoades, K.A. Mauritz, R.B. Moore, Glass transition temperature of perfluorosulfonic acid ionomers, Macromolecules 40 (2007) 3886-3890.

[51] F.M.M. Hamdy, Y. Kobayashi, C.S. Kuroda, A. Ohira, Free volume and gas permeation in ion-exchanged forms of the Nafion® membrane, J. Phys. Conf. Ser. 225 (2010) 012038.

[52] H.F.M. Mohamed, Y. Kobayashi, C.S. Kuroda, A. Ohira, Effects of ion exchange on the free volume and oxygen permeation in Nafion for fuel cells, J. Phys. Chem. B 113 (2009) 2247-2252.

[53] H.Y. Jung, J.W. Kim, Role of the glass transition temperature of Nafion 117 membrane in the preparation of the membrane electrode assembly in a direct methanol fuel cell (DMFC), Int. J. Hydrogen Energy 37 (2012) 12580-12585.

[54] T. Sakai, H. Takenaka, E. Torikai, Gas diffusion in the dried and hydrated Nafions, J. Electrochem. Soc. 133 (1986) 88-92.

[55] J.S. Chiou, D.R. Paul, Gas permeation in a dry Nafion membrane, Ind. Eng. Chem. Res. 27 (1988) 2161-2164.

[56] L.M. Robeson, Correlation of separation factor versus permeability for polymeric membranes, J. Membr. Sci. 62 (1991) 165-185.

[57] Z.P. Smith, R.R. Tiwari, M.E. Dose, K.L. Gleason, T.M. Murphy, D.F. Sanders, G. Gunawan, L.M. Robeson, D.R. Paul, B.D. Freeman, Influence of diffusivity and sorption on helium and hydrogen separations in hydrocarbon, silicon, and fluorocarbon-based polymers, Macromolecules 47 (2014) 3170-3184.

[58] Y. Fan, D. Tongren, C.J. Cornelius, The role of a metal ion within Nafion upon its physical and gas transport properties, Eur. Polym. J. 50 (2014) 271-278.

[59] Y.T. Lee, K. Iwamoto, M. Seno, Gas permeabilities of perfluorocarboxylate membranes in various ionic forms, J. Membr. Sci. 49 (1990) 85-93.

[60] T. Sakai, H. Takenaka, N. Wakabayashi, Y. Kawami, E. Torikai, Gas permeation properties of solid polymer electrolyte (SPE) membranes, J. Electrochem. Soc. 132 (1985) 1328-1332.

[61] J. Catalano, T. Myezwa, M.G. De Angelis, M.G. Baschetti, G.C. Sarti, The effect of relative humidity on the gas permeability and swelling in PFSI membranes, Int. J. Hydrogen Energy 37 (2012) 6308-6316.

[62] M. Giacinti Baschetti, M. Minelli, J. Catalano, G.C. Sarti, Gas permeation in perflurosulfonated membranes: influence of temperature and relative humidity, Int. J. Hydrogen Energy 38 (2013) 11973-11982.

[63] W.J. Chen, C.R. Martin, Gas-transport properties of sulfonated polystyrenes, J. Membr. Sci. 95 (1994) 51-61.

[64] H.B. Park, S.Y. Nam, J.W. Rhim, J.M. Lee, S.E. Kim, J.R. Kim, Y.M. Lee, Gas transport properties through cation-exchanged sulfonated polysulfone membranes, J. Appl. Polym. Sci. 86 (2002) 2611-2617.

[65] S. Bai, S. Sridhar, A.A. Khan, Metal-ion mediated separation of propylene from propane using PPO membranes, J. Membr. Sci. 147 (1998) 131-139.

[66] Y. Fan, C.J. Cornelius, Raman spectroscopic and gas transport study of a pentablock ionomer complexed with metal ions and its relationship to physical properties, J. Mater. Sci. 48 (2013) 1153-1161.

[67] D.L. Feldheim, D.R. Lawson, C.R. Martin, Influence of the sulfonate countercation on the thermal stability of Nafion perfluorosulfonate membranes, J. Polym. Sci., Part B: Polym. Phys. 31 (1993) 953-957.

[68] S. Matteucci, Y. Yampolskii, B.D. Freeman, I. Pinnau, Transport of gases and vapors in glassy and rubbery polymers, in: Materials Science of Membranes for Gas and Vapor Separation, John Wiley & Sons, Ltd, 2006, pp. 1-47.

[69] K. Ghosal, B.D. Freeman, Gas separation using polymer membranes: an overview, Polym. Adv. Technol. 5 (1994) 673-697.

[70] Y. He, E.L. Cussler, Ammonia permeabilities of perfluorosulfonic membranes in various ionic forms, J. Membr. Sci. 68 (1992) 43-52.

[71] T. Kanno, S. Fujita, M. Kobayashi, Enhancement of the permeabilities of ethylene and propylene gases in the Nafion-Ag composite, J. Chem. Soc., Chem. Commun. (1989) 1854-1855.

[72] O.I. Eriksen, E. Aksnes, I.M. Dahl, Facilitated transport of ethene through Nafion membranes. Part I. water swollen membranes, J. Membr. Sci. 85 (1993) 89-97.

[73] J.W. Rhim, G. Chowdhury, T. Matsuura, Development of thin-film composite membranes for carbon dioxide and methane separation using sulfonated poly(phenylene oxide), J. Appl. Polym. Sci. 76 (2000) 735-742.

[74] A. Taubert, J.D. Wind, D.R. Paul, W.J. Koros, K.I. Winey, Novel polyimide ionomers: CO_2 plasticization, morphology, and ion distribution, Polymer 44 (2003) 1881-1892.

Chapter 3. Fundamental and Theoretical Background of Gas Transport

3.1. Gas Permeability

The permeation of gases and vapors through a non-porous membrane is generally described by the solution-diffusion model [1-3]. According to this model, gas transport occurs in three successive steps: (i) the penetrant molecules dissolve on the side of the membrane with the higher chemical potential (upstream), (ii) diffuse through the membrane, and (iii) finally desorb on the side with the lower chemical potential (downstream). The steady-state gas permeability through a membrane of thickness *l* is defined by

$$P = \frac{Nl}{p_{up} - p_{down}} \tag{3.1}$$

where *P* is the gas permeability coefficient (cm^3 (STP) cm/cm^2 s cmHg), *N* is the steady-state gas flux (cm^3 (STP)/cm^2 s) through the membrane, and p_{up} and p_{down} are the upstream and downstream pressures at the membrane interface, respectively.

The flux through the membrane is given by the expression [4, 5]:

$$N = -D\frac{dC}{dx} \tag{3.2}$$

where *D* (cm^2/s) is the effective diffusion coefficient in the polymer and *C* (cm^3 (STP)/cm^3 (polymer)) is the penetrant concentration in the membrane. Penetrant diffusion is believed to occur by the jumping of the molecules through the transient free-

volume openings, triggered by thermal fluctuations within polymer chains. Combining equations 1 and 2 and integrating across the membrane thickness gives:

$$P = D_{eff}\frac{C_{up} - C_{down}}{p_{up} - p_{down}} \tag{3.3}$$

where D_{eff} is the concentration-averaged effective diffusion coefficient and C_{up} and C_{down} are the penetrant concentrations at the upstream and downstream side of the membrane, respectively. When the downstream pressure is much lower than the upstream pressure, equation 3 can be simplified to:

$$P = D_{eff}\frac{C_{up}}{p_{up}} = D_{eff}S \tag{3.4}$$

where S (cm^3 (STP)/cm^3 (polymer) cmHg) is the solubility coefficient at the upstream side of the membrane.

3.2. Selectivity

The performance of a membrane material is characterized by its ideal selectivity, $\alpha_{A/B}$, defined as the ratio of the most permeating gas A to the least permeating gas B [3, 4, 6, 7]:

$$\alpha_{A/B} = \frac{P_A}{P_B} = \frac{D_A}{D_B}\ x\ \frac{S_A}{S_B} \tag{3.5}$$

where P_A and P_B are the pure-gas permeability coefficients of gases A and B, respectively; D_A/D_B is the diffusivity selectivity, defined as the ratio of the diffusion coefficients of gases A and B; and S_A/S_B is the solubility selectivity, defined as the ratio

of the solubility coefficients of gases A and B. The diffusivity selectivity describes the size-sieving capability of the membrane and increases as the size difference between the penetrants increases. In contrast, the solubility selectivity describes the relative condensability of the penetrants and their interaction with the polymer and increases as the condensability difference between the penetrants increases. It is worth noting that larger penetrants have lower diffusion coefficients and higher condensabilities (see **Fig. 1.6**). Thus, a trade-off exists between the two selectivity terms, which often oppose each other to reduce the overall selectivity. Generally, diffusivity selectivity dominates gas separation in glassy polymers because of their rigid structure. Meanwhile, solubility selectivity dominates gas separation in rubbery polymers because of their flexible chain microstructure.

3.3. Gas Solubility

3.3.1. Solubility in Rubbery Polymers

The solubility of sparingly soluble gases in rubbery polymers is characterized by a linear isotherm in which the gas concentration in the polymer obeys Henry's law: $C = K_D \cdot p$, where K_D is Henry's constant and p is the gas pressure [3, 7-10]. However, for strongly sorbing gases (at high penetrant activities), the sorbed concentration deviates from ideal Henry's law behavior [10-13]. In this case, the isotherm is convex to the pressure axis, and the curvature depends upon the level of gas interaction with the polymer matrix. The magnitude of the polymer-penetrant interaction can then be expressed using the Flory-Huggins equation:

$$ln\, a = ln\, \Phi + (1 - \Phi) + \chi(1 - \Phi)^2 \quad (3.6)$$

where a is the penetrant activity, Φ is the volume fraction occupied by the sorbed penetrant molecule, and χ is the Flory-Huggins interaction parameter. The penetrant activity is expressed as p/p_{sat}, where p_{sat} is penetrant saturation vapor pressure at the temperature of the sorption experiment.

3.3.2. Solubility in Glassy Polymers

Gas sorption in glassy polymers differs markedly from that in rubbery polymers [10]. The sorbed gas concentration shows a characteristic concave behavior at low pressure and is linear at high pressure. Such isotherms are most commonly described by the dual-mode sorption model (**Fig. 3.1a**), where the initial gas sorption occurs in the non-equilibrium excess free-volume portion of the polymer matrix, generally referred to as 'Langmuir sites' or 'holes' [9, 14-18]. At a given temperature, a fixed number of holes is available, which are randomly distributed within the polymer matrix. Upon hole saturation, the solubility coefficient approaches the asymptotic value of k_D (**Fig. 3.1b**), at which point the gas molecules dissolve in the equilibrium dense portion of the polymer matrix – referred to as the 'Henry's mode' or 'dissolved mode' of sorption. The cumulative sorption C occurring in the Langmuir holes and Henry's mode is mathematically represented as:

$$C = C_D + C_H$$

$$C = K_D p + \left(\frac{C'_H bp}{1+bp}\right) \quad (3.7)$$

where C_D represents the ordinary gas dissolution described by Henry's law; C'_H is the Langmuir saturation capacity parameter, which describes the non-equilibrium excess free-volume feature of the glassy state; and b characterizes the affinity between the penetrant and the Langmuir sites. Another characteristic feature of glassy polymers is the sorption/desorption hysteresis curve, which represents the slow chain relaxation process upon desorption [19]. The gas solubility is higher in glassy polymers than in rubber polymers because of the non-equilibrium excess free volume [10, 17, 18].

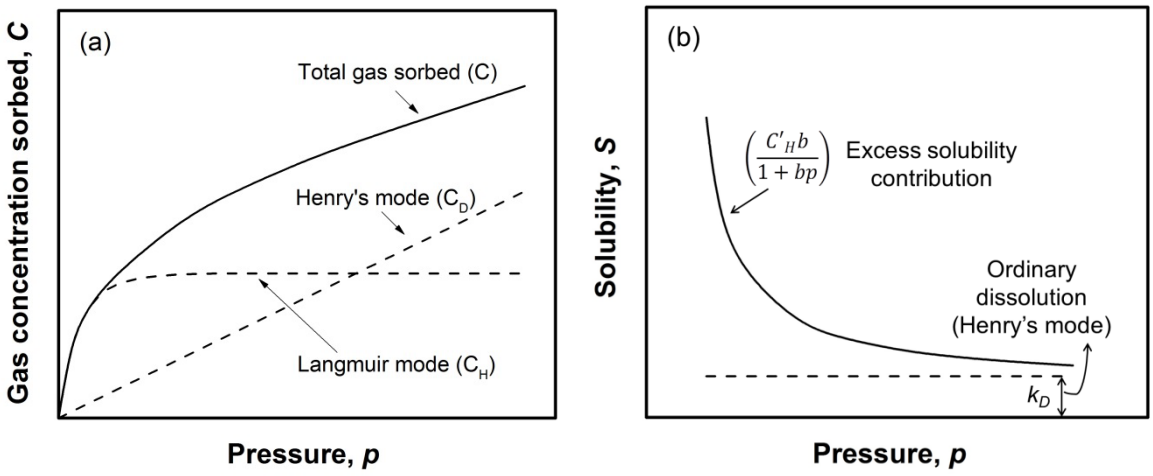

Fig. 3.1. Dual-mode sorption in glassy polymers. (a) Contribution of the Langmuir mode and Henry's mode to the total gas uptake. (b) The solubility coefficient, $S = c/p$, decreases upon hole saturation and reaches the asymptotic solubility limit, k_D, as the pressure increases.

The gas solubility in glassy polymers can be correlated with the fractional free volume (FFV), defined as the volume fraction of the polymer unoccupied by the polymer chain molecules [3]:

$$FFV = \frac{v - v_o}{v} \tag{3.8}$$

where v is the polymer specific volume (cm^3/g) and v_0 is the volume occupied by the polymer chain molecules. At high temperatures, the polymer chains are flexible and rubber-like, and the material is at thermodynamic equilibrium. Upon cooling, the polymer transitions from rubber to glass at the *glass transition temperature* (T_g). As the temperature decreases further, the free volume also decreases, and the polymer enters the non-equilibrium state, with significantly long chain relaxation times. Segmental motions cease, and an *excess free volume* is frozen into the polymer matrix, as illustrated in **Fig. 3.2** [3, 20].

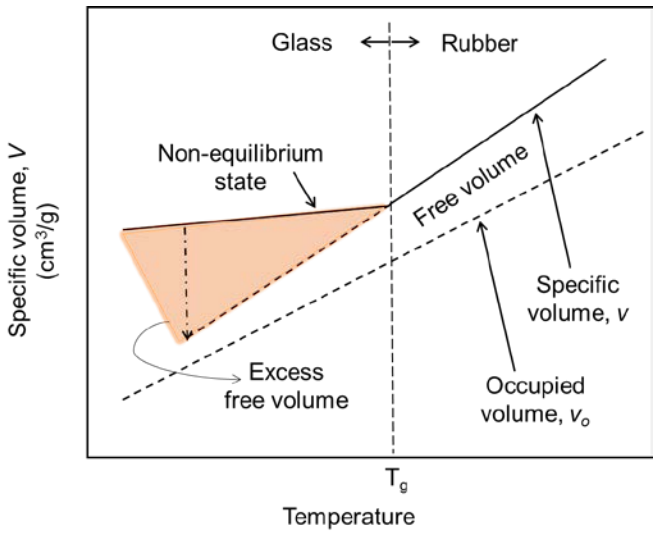

Fig. 3.2. Effective polymer volume (cm^3) occupied by gas molecules (g) above and below the glass transition temperature.

3.3.3. Gas Solubility Correlations

The solubility of gases depends on the relative affinity between the gas and polymer as well as the penetrant condensability, which is generally correlated with the Lennard-Jones force constant (ε/k), gas critical temperature (T_c), or normal boiling point (T_b) [3, 21]. The relationship between the solubility and penetrant condensability is generally expressed as:

$$\ln S = a + bT_c \tag{3.9}$$

The constant a is a measure of the overall sorption capacity, while the slope b represents the increase in solubility with penetrant condensability. The solubility of common gases in hydrocarbon polymers (rubbery and glassy) generally obeys the trend described in equation 3.9, with b values in the range of 0.017 – 0.019 K^{-1} [3]. However, deviations from the trend are seen for hydrocarbon gas solubility in perfluorocarbon polymers as a result of unfavorable thermodynamic interactions [22]. The gas solubility in perfluorocarbon polymers is lower than that in hydrocarbon-based polymers, and the slope values range from 0.009 – 0.011 K^{-1} [22].

3.3.4. Flory-Huggins Interactions

Flory-Huggins theory relates the gas solubility of a rubbery polymer with the thermodynamic interaction between the penetrant and the polymer. The interaction parameter χ, which measures the magnitude of polymer-penetrant interaction, depends on the partial molar volume (V_o) (cm^3/mol) of the gas dissolved in the polymer. V_o is defined as the volume increment in the polymer upon gas sorption [23] and is measured

by calculating the change in the volume of a polymer sheet upon dilation (assuming the dilation to be isotropic). The V_o values for penetrants differ by polymer. V_o depends on the gas concentration (C) in the polymer according to the following equation:

$$\Phi = \frac{CV_0}{(V_S + CV_0)} \tag{3.10}$$

where V_s is the volume of a mole of ideal gas at standard temperature and pressure (STP) (22410 cm^3/mol).

Wong et al. demonstrated that V_o for all gases in rubbery polymers correlates *linearly* with the critical molar volume (V_C) of the gases [24]. Later, Kamiya et al. confirmed this result by measuring V_o for several fluorinated and non-fluorinated gases in PDMS and linear-density polyethylene (LDPE) using a dilatometer [13]. Their study also showed that the fluorinated gases exhibited lower solubility and higher V_o than the hydrocarbon polymers. For example, in PDMS, C_2H_6 exhibited a k_D value of 2.34 (cm^3 (STP)/cm^3 atm), which is nearly 7-fold higher than its fluorinated analog C_2F_6, which has a k_D of 0.382 (cm^3 (STP)/cm^3 atm). However, the V_o value of C_2H_6 (70 cm^3/mol) was nearly half that of C_2F_6 (119 cm^3/mol). The low solubilities of perfluorocarbon gases in hydrocarbon polymers were ascribed to the weak polymer-penetrant interactions [22, 25]. It was then concluded that V_o of the non-fluorinated and fluorinated gases should be described by different equations [13]:

$$V_o = 26.3 + 0.28\,V_C \quad (non - fluorinated) \tag{3.11}$$

$$V_o = 26.3 + 0.4\,V_C \quad (fluorinated) \tag{3.12}$$

Using the values of V_o from equations 3.11 and 3.12 and substituting it into equation 3.10, the value of Φ can be obtained. The polymer-penetrant interaction parameter χ can then be deduced from equation 3.6.

3.4. Temperature Dependence of Gas Permeability

The temperature dependence of the gas permeability, diffusivity, and solubility coefficient is often described by the Arrhenius-van't Hoff equations [26-29]:

$$P = P_o exp\left(\frac{-E_P}{RT}\right) \tag{3.13}$$

$$D = D_o exp\left(\frac{-E_D}{RT}\right) \tag{3.14}$$

$$S = S_o exp\left(\frac{-H_S}{RT}\right) \tag{3.15}$$

In these equations, E_P, E_D, and H_S *(kJ/mol)* are the activation energies of permeation, diffusion, and the enthalpy of sorption, respectively; P_o, D_o, and S_o are pre-exponential factors; *R (J/mol·K)* is the universal gas constant; and *T (K)* is the absolute temperature. The activation energies provide meaningful insights into the structure/gas transport property relationships of a polymer [7]. The temperature dependence of E_P is based on the individual contributions of: (i) E_D, a kinetic parameter whose value depends on the penetrant size, polymer chain mobility, and polymer inter-chain spacing [28, 30] and (ii) H_S, whose value depends on thermodynamic parameters, such as the gas condensability and polymer-penetrant interaction [7, 30]. The activation energy parameters are related by the equation [3, 7, 28-30]:

$$E_P = E_D + H_S \tag{3.16}$$

The activation energy of diffusion is *always* positive (i.e., $E_d > 0$) and increases with the penetrant size [7, 30, 31]. The heat associated with condensation is typically exothermic (i.e., $H_S < 0$), and its magnitude increases with the penetrant condensability [29, 31]. Generally, for conventional low-free-volume glassy polymers, $E_D >> |H_S|$ [7, 30]. As a result, E_P is positive, and the permeability coefficients increase with temperature [3, 30]. For rubbery polymers, the polymer chains are more flexible and offer less diffusional restrictions, weakening the effect of temperature on the diffusion coefficients ($E_D > |H_S|$) [7]. Therefore, E_p in rubbery polymers for low-sorbing gases is lower than that in conventional glassy polymers but still positive.

3.5. Stress-Strain Mechanical Properties

Stress (σ)-strain (ε) relationships are an extremely important measure of a material's mechanical properties. The *σ/ε* curve is generated by stretching a sample at a constant rate by applying tensile force. In the early portion of the curve, the stress is proportional to the strain and is mathematically represented by Hooke's law [32]:

$$\sigma = E \cdot \varepsilon \tag{3.17}$$

where the slope *E* represents Young's modulus, which defines the viscoelasticity of the polymer or, more simply, its stiffness. As the strain increases, the curve deviates from linear behavior because the polymer undergoes internal rearrangements, in which the atoms are moved to new equilibrium positions [32]. For glassy polymers, the chains are

rigid; consequently, the materials break in the early stages, and their stress-strain curves are nearly linear [32, 33]. High values of this modulus, which are characteristic of such materials, reflect the large force required to overcome the chain interaction energy. Meanwhile, the internal molecular reorganization in a rubbery polymer upon applied stress is different. The mechanical response of rubbers produces a low modulus and large deformations characterized by high degrees of elongation at break.

3.6. Mixed-Gas Non-Idealities

Membrane transport properties using gas-mixture feeds are typically estimated from pure-gas transport parameters, namely, the diffusion and solubility coefficients. However, for gas mixtures containing condensable components, the transport properties of one component are altered by co-permeation of another component. In such cases, pure-gas calculations can lead to erroneous estimates of actual separation performance [34].

Plasticization occurs when large quantities of condensable gases sorb into the polymer matrix, increasing polymer chain mobility [34-37]. Macroscopic effects of plasticization include concentration-dependent volume dilation [36, 38-41], reduced mechanical stability [34, 42-44], and depression of the glass transition temperature [34, 36, 43, 45-47]. The observed physical modification due to the plasticization of polymers can affect the gas transport properties as follows [34, 48]: (i) increase the CO_2 permeability with pressure [35, 37, 47, 49, 50], (ii) further increase the mixed-gas CH_4 permeability [49, 51], (iii) decrease the mixed-gas selectivity [36, 51], (iv) increase the CO_2 permeability in a time-dependent manner (conditioning) [17, 34-36, 49-52], (v) decrease the activation energy of diffusion with increasing CO_2 concentration [36], (vi)

decrease the diffusional time-lag with increasing CO_2 concentration [47], (vi) unsteady-state sorption kinetics [34], and (vii) transition the sorption isotherm from concave to linear for low T_g glassy polymers [10, 47]. These observations originate from the increased segmental chain mobility of the polymers upon significant CO_2 sorption [34-37]. Bos et al. demonstrated that, for several glassy polymers, a CO_2 concentration of approximately 38 ± 7 cm^3 (STP)/cm^3 inside the polymer matrix is high enough to induce plasticization [37, 53]. However, Wind et al. argued that a critical CO_2 partial molar volume of 29 ± 2 cm^3/mol is required to plasticize the membrane [19]. Later, Visser et al. combined the individual contributions from the penetrant concentration (C) and partial molar volume (V_o) into the volume dilation $\left(\frac{\Delta V}{V_i} = CV_o\right)$ and demonstrated that, for any gas tested, the same critical amount of volume dilation was necessary to induce membrane plasticization [54].

Polymers containing polar functional groups (acetate, ester, nitro, carbonyl, hydroxyl, sulfonyl and carboxylic) usually have high CO_2 solubility and thus high permeability due to specific polar-quadrupolar interactions [4, 21, 47, 52, 55-58]. For example, the incorporation of polar carboxylic acid into poly(2,6-dimethylphenylene oxide) (PPO) increased the CO_2 permeability significantly relative to the unmodified PPO polymer [59]. Puleo et al. showed that the CO_2 solubility and permeability of CA membranes increased when the degree of the polar acetate group increased [50]. Koros demonstrated that the solubility selectivity (S_{CO_2}/S_{CH_4}) of several conventional low-free-volume glassy polymeric membranes can be tailored by increasing the concentration of the polar carbonyl and sulfonyl groups in the polymer [4]. This theory was later applied for

polysulfone (PS) substituted with polar nitro groups, wherein S_{CO_2}/S_{CH_4} increased by ~13% relative to the unmodified PS [57]. Such polymer-penetrant interactions, though effective in increasing the solubility selectivity, may lead to high CO_2 solubility-induced membrane plasticization [4, 34, 47, 52, 56]. The polymer-penetrant interaction can be so strong that it disrupts the polymer inter-chain interactions such that the membrane loses its size-sieving capabilities [37, 47, 58]. Consequently, the diffusivity selectivity of the membrane decreases significantly more than the solubility selectivity (modestly) increases.

3.6.1. Competitive Sorption

In multicomponent gas mixture experiments, each feed component competes for available sorption sites in the membrane. As a result, their relative concentration is lower than their pure-gas concentration at an equivalent penetrant partial pressure [4, 60]. An early example of this effect was observed in the binary mixed-gas CO_2/C_2H_4 experiment for PMMA membranes, wherein the CO_2 and C_2H_4 solubilities were reduced by 25 and 15% respectively, relative to their pure-gas values [52, 61]. The more condensable gas outcompetes the less condensable gas, and the overall mixed-gas solubility selectivity favors the more condensable gas. In the absence of plasticization, the permeability of each penetrant is affected similarly. However, the preferential solubility of the condensable gas often increases the polymer chain mobility, resulting in a relatively large increase in the diffusivity of the larger penetrant molecule [37, 52]. For example, in mixed-gas CO_2/CH_4 separation using CA membranes, the CO_2 permeability decreased by up to half relative to the pure-gas value, whereas the permeability of CH_4 tripled due

to CO_2-induced plasticization [62]. Consequently, the mixed-gas selectivity was reduced significantly due to two effects of competitive sorption: reduced CO_2 permeability and plasticization.

3.7. References

[1] T. Graham, On the absorption and dialytic separation of gases by colloid septa, J. Chem. Soc. 20 (1867) 235-288.

[2] J.G. Wijmans, R.W. Baker, The solution-diffusion model: a review, J. Membr. Sci. 107 (1995) 1-21.

[3] S. Matteucci, Y. Yampolskii, B.D. Freeman, I. Pinnau, Transport of gases and vapors in glassy and rubbery polymers, in: Materials Science of Membranes for Gas and Vapor Separation, John Wiley & Sons, Ltd, 2006, pp. 1-47.

[4] W.J. Koros, Simplified analysis of gas/polymer selective solubility behavior, J. Polym. Sci.: Polym. Phys. Ed. 23 (1985) 1611-1628.

[5] R. B. Bird, W.E. Stewart, E.N. Lightfoot, Diffusivity and the mechanism of mass transport, in: Transport Phenomena, John Wiley & Sons, Inc., New York, 1990, pp. 514.

[6] J.M.S. Henis, M.K. Tripodi, Composite hollow fiber membranes for gas separation: the resistance model approach, J. Membr. Sci. 8 (1981) 233-246.

[7] K. Ghosal, B.D. Freeman, Gas separation using polymer membranes: an overview, Polym. Adv. Technol. 5 (1994) 673-697.

[8] A.S. Michaels, R.B. Parker, Sorption and flow of gases in polyethylene, J. Polym. Sci. 41 (1959) 53-71.

[9] T.A. Barbari, R.M. Conforti, Recent theories of gas sorption in polymers, Polym. Adv. Technol. 5 (1994) 698-707.

[10] J.S. Chiou, Y. Maeda, D.R. Paul, Gas and vapor sorption in polymers just below Tg, J. Appl. Polym. Sci. 30 (1985) 4019-4029.

[11] P.J. Flory, Thermodynamics of high polymer solutions, J. Chem. Phys. 10 (1942) 51-61.

[12] M.L. Huggins, Theory of solutions of high polymers, J. Am. Chem. Soc. 64 (1942) 1712-1719.

[13] Y. Kamiya, Y. Naito, K. Terada, K. Mizoguchi, A. Tsuboi, Volumetric properties and interaction parameters of dissolved gases in poly(dimethylsiloxane) and polyethylene, Macromolecules 33 (2000) 3111-3119.

[14] R.M. Barrer, J.A. Barrie, J. Slater, Sorption and diffusion in ethyl cellulose. part III. Comparison between ethyl cellulose and rubber, J. Polym. Sci. 27 (1958) 177-197.

[15] A.S. Michaels, W.R. Vieth, J.A. Barrie, Solution of gases in polyethylene terephthalate, J. Appl. Phys. 34 (1963) 1-12.

[16] W.R. Vieth, J.M. Howell, J.H. Hsieh, Dual sorption theory, J. Membr. Sci. 1 (1976) 177-220.

[17] D.R. Paul, Gas sorption and transport in glassy polymers, Ber. Bunsen Ges. Phys. Chem. 83 (1979) 294-302.

[18] S.A. Stern, V. Saxena, Concentration-dependent transport of gases and vapors in glassy polymers, J. Membr. Sci. 7 (1980) 47-59.

[19] J.D. Wind, S.M. Sirard, D.R. Paul, P.F. Green, K.P. Johnston, W.J. Koros, Carbon dioxide-induced plasticization of polyimide membranes: pseudo-equilibrium relationships of diffusion, sorption, and swelling, Macromolecules 36 (2003) 6433-6441.

[20] R.W. Baker, Membrane Technology and Applications, 2nd ed., John Wiley & Sons, Ltd., Chichester, UK, 2004.

[21] G.J. Van Amerongen, Influence of structure of elastomers on their permeability to gases, J. Polym. Sci. 5 (1950) 307-332.

[22] T.C. Merkel, I. Pinnau, R. Prabhakar, B.D. Freeman, Gas and vapor transport properties of perfluoropolymers, in: Materials Science of Membranes for Gas and Vapor Separation, John Wiley & Sons, Ltd., Chichester, UK, 2006, pp. 251-270.

[23] N.F.A. van der Vegt, V.A. Kusuma, B.D. Freeman, Basis of solubility versus TC correlations in polymeric gas separation membranes, Macromolecules 43 (2010) 1473-1479.

[24] B. Wong, Z. Zhang, Y.P. Handa, High-precision gravimetric technique for determining the solubility and diffusivity of gases in polymers, J. Polym. Sci., Part B: Polym. Phys. 36 (1998) 2025-2032.

[25] T.C. Merkel, V. Bondar, K. Nagai, B.D. Freeman, Hydrocarbon and perfluorocarbon gas sorption in poly(dimethylsiloxane), poly(1-trimethylsilyl-1-propyne), and copolymers of tetrafluoroethylene and 2,2-bis(trifluoromethyl)-4,5- difluoro-1,3-dioxole, Macromolecules 32 (1999) 370-374.

[26] G.J. Van Amerongen, Diffusion in elastomers, Rubber Chem. Technol. 37 (1964) 1065-1152.

[27] V.T. Stannett, Simple gases in: Diffusion in polymers, Wiley, New York, 1971.

[28] L.M. Costello, W.J. Koros, Temperature dependence of gas sorption and transport properties in polymers: measurement and applications, Ind. Eng. Chem. Res. 31 (1992) 2708-2714.

[29] L.M. Costello, W.J. Koros, Effect of structure on the temperature dependence of gas transport and sorption in a series of polycarbonates, J. Polym. Sci., Part B: Polym. Phys. 32 (1994) 701-713.

[30] I. Pinnau, L.G. Toy, Gas and vapor transport properties of amorphous perfluorinated copolymer membranes based on 2,2-bistrifluoromethyl-4,5-difluoro-1,3-dioxole/tetrafluoroethylene, J. Membr. Sci. 109 (1996) 125-133.

[31] H. Lin, B.D. Freeman, Gas solubility, diffusivity and permeability in poly(ethylene oxide), J. Membr. Sci. 239 (2004) 105-117.

[32] D. Roylance, Stress-strain curves, MIT, (2001), <http://ocw.mit.edu/courses/materials-science-and-engineering/3-11-mechanics-of-materials-fall-1999/modules/ss.pdf>, (27/Jan/2016).

[33] A.K. Bhowmick, Mechanical properties of polymers, in: Material Science and Engineering, 1, Encyclopedia of Life Support Systems (EOLSS), Eolss Publishers, Paris, France.

[34] E.S. Sanders, Penetrant-induced plasticization and gas permeation in glassy polymers, J. Membr. Sci. 37 (1988) 63-80.

[35] J.S. Chiou, D.R. Paul, Effects of CO_2 exposure on gas transport properties of glassy polymers, J. Membr. Sci. 32 (1987) 195-205.

[36] M. Wessling, S. Schoeman, T. van der Boomgard, C.A. Smolders, Plasticization of gas separation membranes, Gas Sep. Purif. 5 (1991) 222-228.

[37] A. Bos, I.G.M. Pünt, M. Wessling, H. Strathmann, CO_2-induced plasticization phenomena in glassy polymers, J. Membr. Sci. 155 (1999) 67-78.

[38] J.D. Wind, C. Staudt-Bickel, D.R. Paul, W.J. Koros, Solid-state covalent cross-linking of polyimide membranes for carbon dioxide plasticization reduction, Macromolecules 36 (2003) 1882-1888.

[39] G.K. Fleming, W.J. Koros, Dilation of polymers by sorption of carbon dioxide at elevated pressures. 1. Silicone rubber and unconditioned polycarbonate, Macromolecules 19 (1986) 2285-2291.

[40] G.K. Fleming, W.J. Koros, Dilation of substituted polycarbonates caused by high-pressure carbon dioxide sorption, J. Polym. Sci., Part B: Polym. Phys. 28 (1990) 1137-1152.

[41] M. Wessling, I. Huisman, T. van der Boomgard, C.A. Smolders, Dilation kinetics of glassy, aromatic polyimides induced by carbon dioxide sorption, J. Polym. Sci., Part B: Polym. Phys. 33 (1995) 1371-1384.

[42] J.R. Fried, H.C. Liu, C. Zhang, Effect of sorbed carbon dioxide on the dynamic mechanical properties of glassy polymers, J. Polym. Sci., Polym. Lett. 27 (1989) 385-392.

[43] W.C.V. Wang, E.J. Kramer, W.H. Sachse, Effects of high-pressure CO_2 on the glass transition temperature and mechanical properties of polystyrene, J. Polym. Sci.: Polym. Phys. Ed. 20 (1982) 1371-1384.

[44] H. Hojo, W.N. Findley, Effect of gas diffusion on creep behavior of polycarbonate, Polym. Eng. Sci. 13 (1973) 255-265.

[45] J.S. Chiou, J.W. Barlow, D.R. Paul, Plasticization of glassy polymers by CO_2, J. Appl. Polym. Sci. 30 (1985) 2633-2642.

[46] H. Hachisuka, T. Sato, T. Imai, Y. Tsujita, A. Takizawa, T. Kinoshita, Glass transition temperature of glassy polymers plasticized by CO_2 gas, Polym. J. 22 (1990) 77-79.

[47] J.S. Chiou, D.R. Paul, Gas sorption and permeation in poly(ethyl methacrylate), J. Membr. Sci. 45 (1989) 167-189.

[48] A. Bos, High pressure CO_2/CH_4 separation with glassy polymer membranes: aspects of CO_2-induced plasticization, Ph.D. Thesis, University of Twente, Netherlands, 1996.

[49] A.Y. Houde, B. Krishnakumar, S.G. Charati, S.A. Stern, Permeability of dense (homogeneous) cellulose acetate membranes to methane, carbon dioxide, and their mixtures at elevated pressures, J. Appl. Polym. Sci. 62 (1996) 2181-2192.

[50] A.C. Puleo, D.R. Paul, S.S. Kelley, The effect of degree of acetylation on gas sorption and transport behavior in cellulose acetate, J. Membr. Sci. 47 (1989) 301-332.

[51] A. Bos, I.G.M. Pünt, M. Wessling, H. Strathmann, Plasticization-resistant glassy polyimide membranes for CO_2/CO_4 separations, Sep. Purif. Technol. 14 (1998) 27-39.

[52] E.S. Sanders, S.M. Jordan, R. Subramanian, Penetrant-plasticized permeation in polymethylmethacrylate, J. Membr. Sci. 74 (1992) 29-36.

[53] R.W. Baker, K. Lokhandwala, Natural gas processing with membranes: an overview, Ind. Eng. Chem. Res. 47 (2008) 2109-2121.

[54] T. Visser, M. Wessling, When do sorption-induced relaxations in glassy polymers set in?, Macromolecules 40 (2007) 4992-5000.

[55] S.G. Kazarian, M.F. Vincent, F.V. Bright, C.L. Liotta, C.A. Eckert, Specific intermolecular interaction of carbon dioxide with polymers, J. Am. Chem. Soc. 118 (1996) 1729-1736.

[56] P.C. Raymond, D.R. Paul, Sorption and transport of pure gases in random styrene/methyl methacrylate copolymers, J. Polym. Sci., Part B: Polym. Phys. 28 (1990) 2079-2102.

[57] K. Ghosal, R.T. Chern, B.D. Freeman, R. Savariar, The effect of aryl nitration on gas sorption and permeation in polysulfone, J. Polym. Sci., Part B: Polym. Phys. 33 (1995) 657-666.

[58] A.F. Ismail, W. Lorna, Penetrant-induced plasticization phenomenon in glassy polymers for gas separation membrane, Sep. Purif. Technol. 27 (2002) 173-194.

[59] W.J. Koros, B.J. Story, S.M. Jordon, K. O'Brien, G.R. Husk, Material selection considerations for gas separation processes, presented at the Spring National Meeting of the AIChE, New Orleans, LA, April 1986.

[60] W.J. Koros, R.T. Chern, V. Stannett, H.B. Hopfenberg, A model for permeation of mixed gases and vapors in glassy polymers, J. Polym. Sci.: Polym. Phys. Ed. 19 (1981) 1513-1530.

[61] E.S. Sanders, W.J. Koros, H.B. Hopfenberg, V.T. Stannett, Mixed gas sorption in glassy polymers: Equipment design considerations and preliminary results, J. Membr. Sci. 13 (1983) 161-174.

[62] M.D. Donohue, B.S. Minhas, S.Y. Lee, Permeation behavior of carbon dioxide-methane mixtures in cellulose acetate membranes, J. Membr. Sci. 42 (1989) 197-214.

Chapter 4. Experimental Techniques

This chapter describes the investigated materials and the preparation of the Fe^{3+}-ion-exchanged membranes. The experimental methods used to measure the gas sorption and pure- and mixed-gas permeation are also presented in this chapter, as are the physical characterization techniques.

4.1. Materials

4.1.1. As-received Nafion®-H^+ Films

Isotropic Nafion® NRE 211 dispersion-cast films were obtained from Ion Power, Inc., in the H^+ form. These ion-exchange membranes had a nominal thickness of 25 μm and equivalent weight of 1100 g $equiv^{-1}$. Because Nafion® tends to sorb water readily from the atmosphere, the films were dried at 80 °C under vacuum for 2 days prior to all measurements. The film density was determined as 2.01 g/cc ± 0.014 using mass-volumetric and non-solvent buoyancy techniques; this value is consistent with previously reported density values for dry Nafion® [1].

4.1.2. Preparation of Nafion® Cation-Exchanged Membranes

The as-received Nafion® H^+ films (as mentioned above) were used for the preparation of Fe^{3+} cation-exchanged membrane. The Nafion® H^+ membrane exhibited an ion-exchange capacity (IEC) of 0.91 meq/g (IEC = 1/equiv. wt). The films were first washed with distilled water to remove any surface impurities. Next, the films were immersed in the Fe^{3+} nitrate solution of 0.05 molar concentrations. The exchange process was monitored using a pH meter until the pH value stabilized. To ensure complete

complexation, the films were stored in the solution for at least 10 days. The wet films were gently wiped with soft tissue paper to remove any excess salt or water from the surface. The films were then air dried for 12 h by sandwiching between two filter papers and dried under vacuum at 80 °C for 2 days prior to testing. The film density was determined as 2.14 g/cc ± 0.014 using mass-volumetric and non-solvent buoyancy techniques.

4.2. Gas Sorption

4.2.1. Barometric Gas Sorption

Nafion® was subjected to high-pressure gas sorption using a custom-built dual-volume pressure decay apparatus based on an original design described elsewhere [2]. Gas sorption isotherms were determined in the following order: He, H_2, N_2, O_2, CH_4, CO_2, C_2H_6, C_3H_8, and *n*-C_4H_{10}. All measurements were performed at 35 °C up to pressures of 20 atm (except for C_3H_8, ~ 7 atm, and *n*-C_4H_{10}, ~ 2 atm). After drying the polymer film sample (~ 1.5 g) in a vacuum oven at 80 °C for 2 days, the sample was placed in a sample holder and allowed to outgas under high vacuum for 12 h at 35 °C. After introducing the gas into the system at the desired pressure, the pressure decay over time due to gas sorption was continuously recorded with a data acquisition system using LabVIEW software (National Instruments) until the sample chamber pressure stabilized. The amount of gas sorbed into the polymer was determined by mass balance. Additional gas was then introduced into the system to increase the pressure for the next measurement. This process was repeated until a complete isotherm was recorded for the given gas as a function of pressure. The sample was then degassed under high vacuum for

up to 5 days. To ensure that the sample reverted to its initial physical state after each gas was tested, the N_2 measurement was repeated. Finally, the system was degassed again, and the next gas was introduced into the system.

4.2.2. Gravimetric Gas Sorption

The gas solubility of Nafion® H^+ was also measured using a Hiden Intelligent Gravimetric Analyzer (IGA-003, Hiden Isochema, UK), which measures gas isotherms up to 20 atm. After drying a polymer film sample (~ 100 mg) in a vacuum oven at 80 °C for 2 days, it was mounted in the sorption apparatus and degassed under high vacuum (< 10^{-7} mbar) at 35 °C until the sample weight readings stabilized. Then, to collect the isotherm points, the appropriate gas was introduced into the sample chamber by a stepwise pressure ramp of 100 mbar/min until the desired pressure was reached. After the equilibrium weight uptake was recorded, the next pressure point was set, and this process was continued until the complete isotherm was determined. After the measurement, the sample was degassed as described for the barometric method, and all other gas sorption isotherms were determined in consecutive order.

4.3. Gas Permeation

4.3.1. Permeation Apparatus Schematic

Fig 4.1 shows a schematic design of the custom-made permeation system. The permeation cell (3) used was a circular stainless steel holder purchased from Millipore Corporation with an effective area of 13.8 cm^2. The temperature inside the system was

regulated by a temperature controller (Omega®) connected to the heater (2) and two fans (1), which heated and circulated the air inside the permeation box.

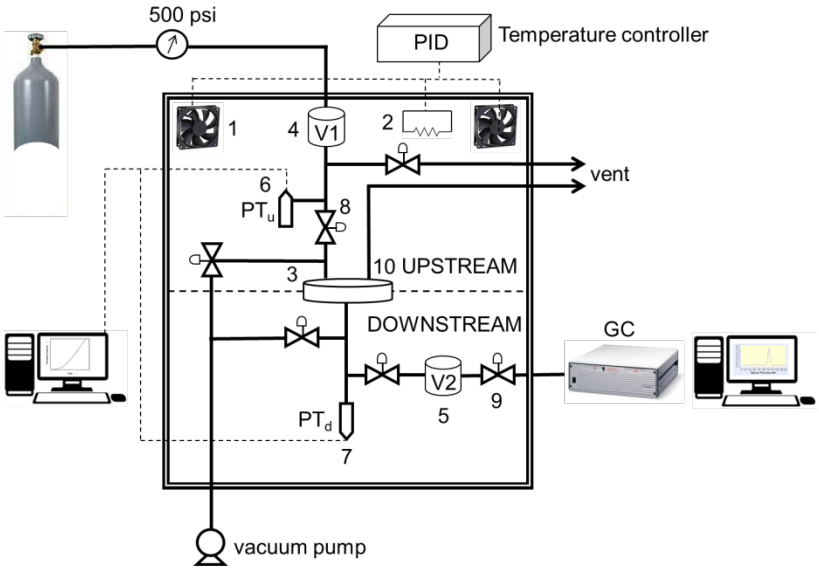

Fig. 4.1. Schematic design of a constant-volume/variable-pressure permeation system for pure- and mixed-gas experiments. System components: (1) fans for air circulation, (2) heaters, (3) permeation cell, (4) upstream volume, (5) downstream volume, (6) upstream pressure transducer, (7) downstream pressure transducer, (8) long bellow sealed feed gas valve, (9) short bellow sealed valve for GC sampling, (10) exit port.

The system was integrated to allow mixed-gas permeation testing. The permeation cell was modified to include an exit port (10) so that the feed gas could flow along the surface and exit. The stage cut (permeate flow/feed flow) was maintained below 1% by purging the upstream of the permeation cell at an appropriate flow rate. This step ensured that the residue gas concentration was essentially equal to the feed gas concentration

throughout the permeation process and prevented concentration polarization at the upstream end of the permeation cell. A gas chromatograph (GC) (Agilent 3000A) with thermal conductivity detector (TCD) fitted with two different columns was calibrated with several gases from Abdullah Hashim Group (AHG). Binary 50:50 and 90:10 CO_2/CH_4 mixtures was used to calculate the calibration constant for CO_2/CH_4. Additionally, 50:50 CO_2/C_3H_8 and 30:50:20 $CO_2/CH_4/C_3H_8$ mixtures were used to calculate the calibration constant for CO_2/C_3H_8. Ultra-high purity helium was used as the carrier gas. The column temperature was set between 80 and 120 °C for all measurements.

4.3.2. Membrane Masking and Loading

The polymer film samples were partially masked with an impermeable aluminum tape to expose a membrane area of approximately 5.0 cm^2. The masked sample was positioned in the permeation cell, and another layer of aluminum tape was added to mount the masked sample firmly in the cell. The interface between the aluminum tape and the membrane was carefully masked with epoxy glue to prevent leakage through the openings. The epoxy was allowed to fully cure for approximately 24 h. The complete cell with the mounted sample was then placed in a vacuum oven at 80 °C for 2 days. Because of the sample's sensitivity to humidity, the cell was immediately re-installed in the permeation system and exposed to vacuum from both the upstream and downstream sides for at least 24 h at 35 °C to degas the film.

4.3.3. Pure-Gas Permeation

The gas permeability through a dense polymeric membrane was determined using the constant-volume/variable-pressure method [3, 4]. After degassing the sample, the upstream and downstream valves were isolated from the vacuum. Thereafter, the change in permeate pressure with time, *dp/dt*, was measured to ensure that the leak rate of the system was below 10^{-7} torr/s. The upstream gas reservoir was then purged and pressurized with the desired feed gas, after which the feed gas valve was opened and the permeate pressure was continuously monitored until a steady-state *dp/dt* was achieved. The gas permeability of the membrane was then obtained from *dp/dt* as follows:

$$P = D \cdot S = 10^{10} \frac{V_d \; l}{p_{up} \; ART} \frac{dp}{dt} \tag{4.1}$$

where P is the permeability in Barrers (1 Barrer = 10^{-10} cm^3(STP) cm/cm^2 s cmHg), p_{up} is the upstream pressure (cmHg), *dp/dt* is the steady-state permeate-side pressure increase (cmHg/s), V_d is the calibrated permeate volume (cm^3), l is the membrane thickness (cm), A is the effective membrane area (cm^2), T is the operating temperature (K), and R is the gas constant (0.278 cm^3 cmHg /cm^3(STP) K). The ideal selectivity for a gas pair is given by the following relationship:

$$\alpha_{A/B} = \frac{P_A}{P_B} x \frac{S_A}{S_B} \tag{4.2}$$

The apparent diffusion coefficient D (cm^2/s) was calculated from individual measurements of P and S (cm^3(STP)/cm^3·cmHg) by the relationship $D=P/S$, where the S values were determined from the barometric sorption technique.

The diffusion coefficient was also determined using the *time-lag* technique described by Frisch [5] based on the following expression:

$$D = \frac{l^2}{6\theta} \tag{4.3}$$

where l is the membrane thickness and θ is the time lag of the permeation. The response from the downstream pressure transducer was employed for the time lag calculation. The time lag is attributed to the time required for the gas to leave the transient state and establish equilibrium, as shown in **Fig. 4.2**. The time lag was obtained by extrapolating the pressure increase-time curve to the time axis after the equilibrium state was reached. To ensure that the diffusion coefficient calculations were reliable, steady-state readings over a period of at least ten time lags were used.

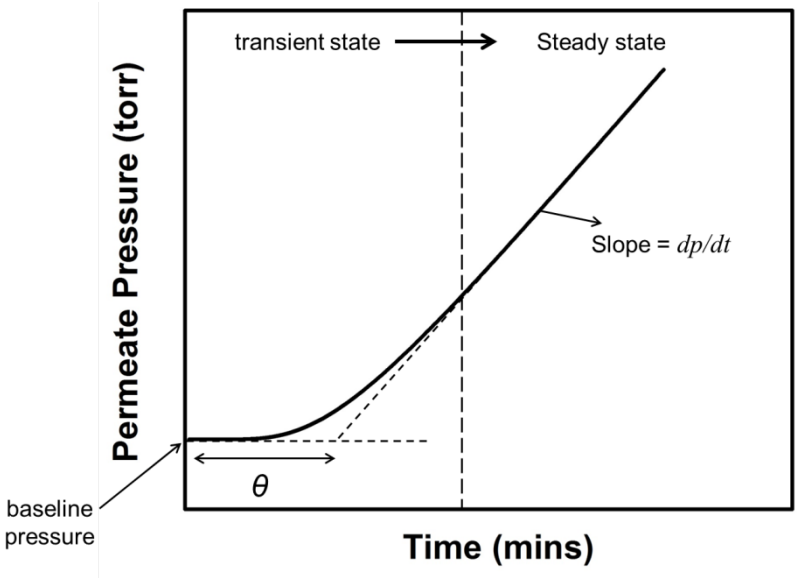

Fig. 4.2. Graphical representation of a time-lag behavior in the constant-volume/variable-pressure technique.

4.3.4. Mixed-Gas Permeation

The binary and ternary mixed-gas permeation properties were measured using feed gas mixtures of 50:50 CO_2:CH_4 and 30:50:20 CO_2:CH_4:C_3H_8, respectively, at 35 °C by the method described above [4]. Samples were tested at total pressures of 4, 10, 14, 20, 24 and 30 atm for the binary experiments and 16 atm for the ternary experiments. The mixed-gas permeabilities were calculated by:

$$P_{CO_2} = 10^{10} \frac{y_{CO_2} V_d \; l}{x_{CO_2} p_{up} \; ART} \frac{dp}{dt} \tag{4.4}$$

$$P_{CH_4} = 10^{10} \frac{y_{CH_4} V_d \; l}{x_{CH_4} p_{up} \; ART} \frac{dp}{dt} \tag{4.5}$$

$$P_{C_3H_8} = 10^{10} \frac{y_{C_3H_8} V_d \ l}{x_{C_3H_8} p_{up} \ ART} \frac{dp}{dt} \quad (4.6)$$

where *x* and *y* are the mole fractions in the feed and permeate, respectively. A GC was used to measure the permeate mole fraction (*y*), and a minimum of six GC runs were conducted to ensure the accuracy of the analysis at each pressure. Because the downstream pressure was negligible, the mixed-gas CO_2/CH_4 and CO_2/C_3H_8 selectivities were obtained from:

$$\alpha_{CO_2/CH_4} = \frac{y_{CO_2}/y_{CH_4}}{x_{CO_2}/x_{CH_4}} \quad (4.7)$$

$$\alpha_{CO_2/C_3H_8} = \frac{y_{CO_2}/y_{C_3H_8}}{x_{CO_2}/x_{C_3H_8}} \quad (4.8)$$

4.4. Thermal and Physical Characterization

4.4.1. Dynamic Mechanical Analysis (DMA)

Stress-strain curves were obtained using a TA Instruments Q800 dynamic mechanical analyzer (DMA) at various temperatures under controlled forced oscillation mode. The samples were cut into rectangles with a length, width, and thickness of ~6 mm, 5.3 mm, and 0.025 mm, respectively. The samples were dehydrated under vacuum at 80 °C for 2 days and then carefully installed in the DMA clamp for thin film samples. The mechanical response was obtained for temperatures ranging from -120 to 100 °C by applying a tensile force at a uniform rate of 1 N/min up to a maximum of 18 N at a frequency of 1 Hz. For each curve, the Young's modulus was calculated from the initial

slope of the linear elastic region at strain levels below 2.5 % using Hooke's law: $E = \sigma/\varepsilon$. The experiments were conducted under a N_2 purge (10 mL/min) to minimize the influence of moisture. The preload force was 0.01 N, the isothermal temperature was 80 °C, and the duration was 30 min.

4.4.2. Thermogravimetric Analysis (TGA)

The thermal stability of Nafion®-H^+ and Fe^{3+} samples were investigated on a TA instrument 2950 thermogravimetric analyzer (TGA) in a nitrogen atmosphere to prevent the sample from adsorbing any moisture. Approximately 3-5 mg of the sample was placed in an HT-aluminum pan, and it was flamed and tarred prior to each analysis. The temperature was ramped from room temperature to 800 °C at a rate of 3 K/min.

4.4.3. Wide-Angle X-Ray Diffraction (WAXD)

Wide-angle x-ray diffraction (WAXD) measurements were conducted on a Bruker D8 Advance diffractometer using a Cu Kα X-ray source of characteristic wavelength λ = 1.54 Å from 11 to 50° with a step size of 0.05° and a rate of 5 s/step. The membrane samples were pre-dried under vacuum at 80 °C for 2 days. The diffraction patterns were corrected for background scattering, and the crystalline/amorphous peaks were fit to the Pearson VII distribution function, with correlation coefficients greater than 99%. The relative crystallinity was calculated by integrating the area under the crystalline peak and dividing by the sum of the fitted integrated peaks using the following equation:

$$x_c = \frac{\int_0^\infty I_{cr}\,(2\theta)d(2\theta)}{\int_0^\infty I_{cr}\,(2\theta)d(2\theta) + \int_0^\infty I_{am}\,(2\theta)d(2\theta)} \tag{4.9}$$

where x_c is the amount of crystallinity in the polymer; I_{cr} and I_{am} are the sum of the intensities of the fitted crystalline and amorphous peaks, respectively; and 2θ is the diffraction angle.

4.4.4. Raman Spectroscopy

Raman spectra of Nafion® H^+ and Fe^{3+} were collected on a LABRAM ARAMIS (Horiba Jobin Yvon, Inc.) instrument. The excitation source was a 473-nm laser focused with a 100x objective with a laser spot of 1 μm and 0.5 mW power. The scattered signal was dispersed by a 1800-mm^{-1} grating. Spectra within the region of 400 to 1400 cm^{-1} were collected in backscattering geometry.

4.5. References

[1] T. Takamatsu, A. Eisenberg, Densities and expansion coefficients of Nafion polymers, J. Appl. Polym. Sci. 24 (1979) 2221-2235.

[2] W.J. Koros, D.R. Paul, Design considerations for measurement of gas sorption in polymers by pressure decay, J. Polym. Sci.: Polym. Phys. Ed. 14 (1976) 1903-1907.

[3] D.G. Pye, H.H. Hoehn, M. Panar, Measurement of gas permeability of polymers. I. permeabilities in constant volume/variable pressure apparatus, J. Appl. Polym. Sci. 20 (1976) 1921-1931.

[4] K.C. O'Brien, W.J. Koros, T.A. Barbari, E.S. Sanders, A new technique for the measurement of multicomponent gas transport through polymeric films, J. Membr. Sci. 29 (1986) 229-238.

[5] H.L. Frisch, The time lag in diffusion, J. Phys. Chem. 61 (1957) 93-95.

Chapter 5. Gas Sorption, Diffusion and Permeation in Nafion®

5.1. Abstract

The gas permeability of dry Nafion® films was determined at 2 atm and 35 °C for He, H_2, N_2, O_2, CO_2, CH_4, C_2H_6 and C_3H_8. In addition, gas sorption isotherms were determined by gravimetric and barometric techniques as a function of pressure up to 20 atm. Nafion® exhibited linear sorption uptake for low-solubility gases, following Henry's law, and convex behavior for highly sorbing condensable gases, indicating rubber-like behavior at 35 °C. To complement this result, a detailed analysis on the mechanical properties of Nafion® was provided over a temperature range from -120 to 100 °C. The stress-strain profile clearly revealed the onset of rubbery behavior in Nafion® at -60 ^{o}C, indicated by a significant ~180% increase in elongation at break. XRD results demonstrated that Nafion® contains bimodal amorphous chain domains with average d-spacing values of 2.3 and 5.3 Å. Only helium and hydrogen showed relatively high gas permeability of 37 and 7 Barrer, respectively; all other gases exhibited low permeability that decreased significantly as penetrant size increased. Dry Nafion® was characterized by extraordinarily high selectivities: He/H_2 = 5.2, He/CH_4 = 445, He/C_2H_6 = 1275, He/C_3H_8 = 7400, CO_2/CH_4 = 28, CO_2/C_2H_6 = 79, CO_2/C_3H_8 = 460, H_2/CH_4 = 84, H_2/C_2H_6 = 241, and H_2/C_3H_8 = 1400. These high selectivities could make Nafion® a potential candidate membrane material for dry feeds for helium recovery and carbon dioxide separation from natural gas, and removal of higher hydrocarbons from hydrogen-containing refinery gases. Gas permeation temperature dependence studies revealed very

high activation energy of permeation for Nafion® that resulted primarily from its tightly packed ionic chain structure in the dry state.

5.2. Introduction

Separation processes account for ~45% of all process energy used in chemical and petroleum refining industries [1]. As the drive for energy savings and sustainability intensifies, more efficient separation technology becomes increasingly important. Membrane-based technology offers potential advantages over traditional processes such as cryogenic distillation and amine absorption in terms of cost, simplicity, size, and energy efficiency [2, 3]. Commercial applications using membranes include onsite nitrogen production from air, hydrogen recovery from various refinery and petrochemical process streams, dehydration of air and carbon dioxide removal from natural gas [4-8]. Glassy polymers currently used for gas separations (polysulfone, cellulose acetate, polyimide) are limited in their commercial application spectrum due to their moderate permeability and selectivity and limited resistance to penetrant-induced plasticization. For feeds containing condensable components (such as CO_2, water vapor, C_{3+} hydrocarbons, aromatics etc.) membrane plasticization often leads to highly undesirable loss in mixed-gas selectivity [4, 7-13].

An emerging materials class that can potentially mitigate some limitations of commercial gas separation membranes is based on perfluorinated solution-processable glassy polymers, including Teflon AF® (Du Pont), Hyflon® AD (Solvay), Cytop® (Asahi Glass) and others [14-19]. These polymers are known for their excellent chemical and thermal properties as a result of their strong C-F bond energy (485 kJ/mole) in

comparison to C-C (360 kJ/mole) bonds in hydrocarbon polymers [19]. Their unique structure/gas transport property relationships have set the limits of permeability-selectivity combinations on the 2008 Robeson upper bound for certain gas pairs such as He/CH_4, He/H_2, N_2/CH_4, and H_2/CH_4 [20]. Because of their high selectivities and chemical inertness, these polymers were proposed for gas separation applications, specifically natural gas treatment, where condensable species were detrimental to the performance of traditional polymers as a result of plasticization [14-16].

Another important class of perfluorinated polymers is based on sulfonated ionomers. Nafion® (Du Pont), the prototypical perfluorinated ionomer, has been the benchmark material in the fuel cell industry for several decades owing to its high proton conductivity and good chemical and thermal stability [21, 22]. The structure of dry Nafion® consists of a hydrophobic perfluorocarbon backbone and a highly hydrophilic sulfonic acid tail (**Fig. 5.1 (a**)), which forms a dispersed phase of ionic clusters with diameters of 1.5 nm in the perfluorocarbon matrix (**Fig. 5.1 (b**)) [22-25]. Surprisingly, only very limited pure-gas transport data have been reported for Nafion® [26-32]. The first comprehensive study on the gas permeation properties of dry Nafion® was reported by Chiou and Paul using the constant-volume/variable-pressure technique [29]. The gas diffusion coefficients were then deduced from the time-lag method. Their study indicated low permeability in dry Nafion® for all gases other than He and H_2. Recently, Fan et al. reported gas permeability measurements in dry Nafion® at different temperatures using the same technique [30]. Sarti's group evaluated the effects of temperature and relative humidity on Nafion®

transport and found up to 100-fold increases in gas permeability relative to the values obtained under dry test conditions [31, 32].

The physical state of dry Nafion® (glass or rubber) has been under debate because of the significantly varying glass transition temperature values reported by several researchers [22, 25, 33]. As Nafion® consists of a phase-separated structure, it is expected to have two glass transition temperatures; one that represents the rubbery PTFE phase and another one induced by the ionic sulfonic acid clusters. Osborn et al. performed a comprehensive study on the glass transition of Nafion® using dynamic mechanical analysis (DMA) and concluded that the β transition observed at -20 °C in Nafion® H^+ is the glass transition temperature of the rubbery phase in Nafion® [33]. This transition results from fluorocarbon main-chain motions within the framework of a *static* physically cross-linked network [33].

Chiou and Paul showed that the CO_2 permeability increased with pressure, a typical behavior observed in rubbers, and suggested that this could possibly indicate that the rubbery phase dominates gas transport [29]. It was concluded that *direct* gas sorption measurements are necessary to gain more definitive insight into the role of the rubbery phase and the ionic cluster domains with respect to gas permeation in Nafion®. To date, to the best of our knowledge, only one study has reported directly measured gas sorption isotherms in Nafion®, and was limited to He and H_2 [34].

In this work, comprehensive data on the pure-gas permeability of He, H_2, N_2, O_2, CO_2, CH_4, C_2H_6, and C_3H_8 in Nafion® are reported. Additionally, extensive high-pressure gas sorption studies were performed using barometric and gravimetric sorption

techniques at 35 °C. Diffusion coefficients were deduced using the solution-diffusion model and the directly measured permeability and solubility coefficients.

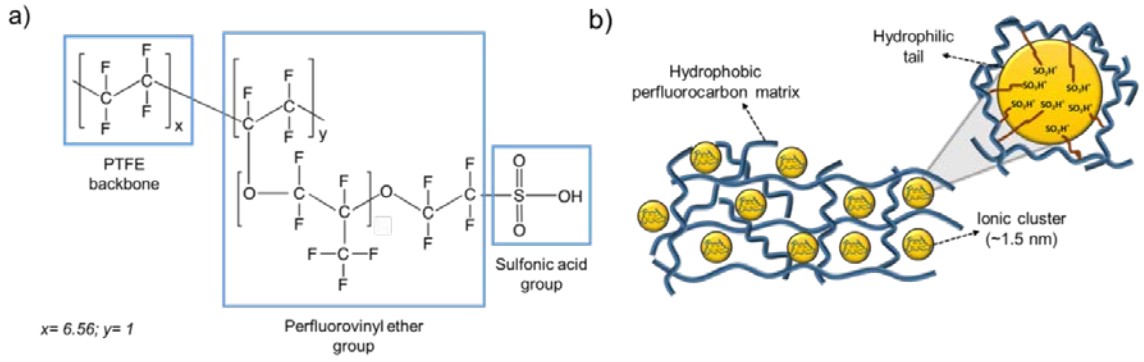

Fig. 5.1. (a) Chemical structure of Nafion® (sulfonic acid form); x=6.56, y=1; (b) Cluster-network model for dry Nafion®.

5.3. Results and Discussion

5.3.1. Microstructure of Nafion®

The chain packing in Nafion® can be qualitatively assessed with the WAXD spectrum presented in **Fig. 5.2**. The spectrum indicates semi-crystalline behavior of Nafion® represented by the crystalline peak at 2θ =17.7° and two amorphous halo peaks at 2θ = 16.8 and 39.3° consistent with previously reported data [35-38]. The relative crystallinity calculated by fitting the crystalline and amorphous peaks from **Fig. 5.2** is 9%. These results agree with previously reported WAXD data for Nafion® with crystallinity values ranging between 12-22% [22, 37]. Nafion® shows a bimodal amorphous distribution comprising regions with average chain d-spacings of 2.3 Å and 5.3 Å calculated from

Bragg's equation, ($d= \lambda/2\sin\theta$). The region of very tight chain packing in Nafion® (average d-spacing ~2.3 Å over a wide diffraction angle range of 30-50°) is a consequence of several diffraction peaks from intermolecular correlations [36]. This observation has significant implications for the ability of Nafion® to selectively permeate helium (d_k = 2.6 Å) over all other gases, including hydrogen (d_k = 2.89 Å).

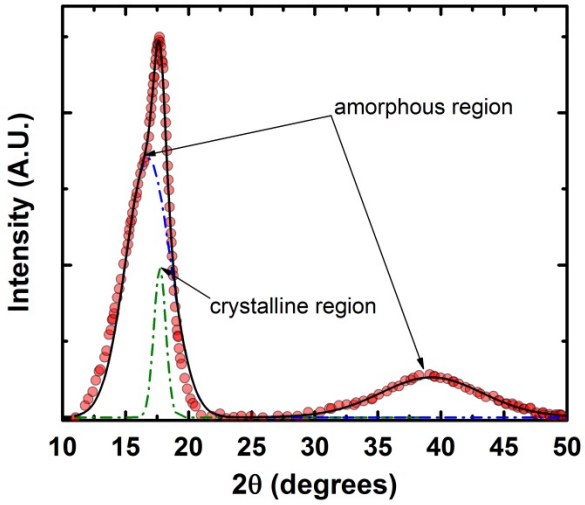

Fig. 5.2. WAXD profile of Nafion® dried under vacuum at 80 °C for 2 days. The diffraction spectrum was corrected for background scattering and the crystalline and amorphous peaks were obtained by applying the Pearson VII distribution function on the original convoluted peak (red symbols). The black smooth line is the sum of crystalline and amorphous regions in the polymer.

5.3.2. Stress-Strain Profile of Nafion®

The influence of temperature on the mechanical properties of Nafion® was qualitatively assessed by analyzing the stress-strain curves presented in **Fig. 5.3**. The

curve provides valuable information about the polymer's Young modulus and elongation at break offering meaningful insight about the variation in the physical state of Nafion® with changes in temperature. Nafion® undergoes a decrease in Young modulus and increase in elongation at break with increasing temperature. An increase in temperature weakens the ionic interaction between the sulfonate groups, which enhances the polymer chain mobility. A similar qualitative trend has been reported previously by Kawano et al. for Nafion® studied at temperatures above room temperature [39].

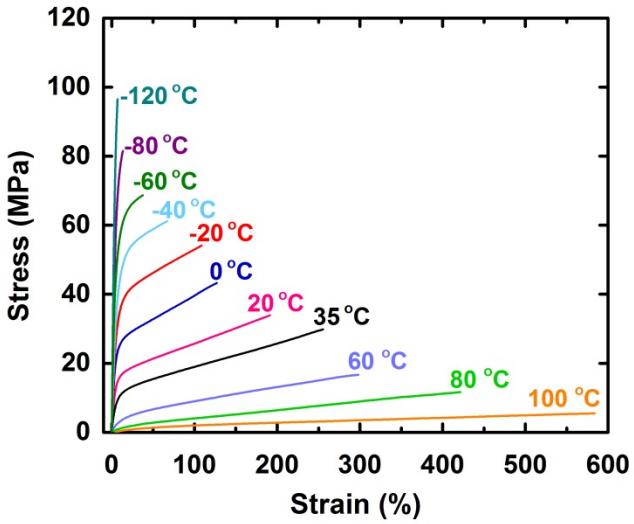

Fig. 5.3. Stress-strain curves for Nafion® at temperatures ranging from -120 to 100 °C

Table 5.1 summarizes the Young's modulus and elongation at break in Nafion® at each temperature. The elongations at break reported in our study were significantly higher than the values reported by Kawano et al.; however, our strain value at 20 °C is consistent with values reported by DuPont [40].

Table 5.1. Young's modulus and elongation at break values of Nafion® calculated from the stress-strain curves at each temperature.

Temperature (°C)	Elongation at break (%)	Young's Modulus (GPa)
-120	7	2.4
-80	13	1.5
-60	38	1.2
-40	67	0.85
-20	95	0.63
0	127	0.46
20	191	0.34
35	255	0.22
60	342	0.03
80	421	0.008
100	>580	0.006

The stress-strain curves for Nafion® at low temperatures between -120 and -80 °C were almost linear, with large modulus values and low degrees of elongation indicative of a stiff glassy polymer profile [41]. Upon transitioning from -80 to -60 °C, the polymer starts to shift from the glassy to the rubbery state, as indicated by an abrupt increase in elongation at break value (see **Fig. 5.4 (a)**). At higher temperatures, the stress-strain profile of Nafion® was similar to that of a rubbery polymer. Above room temperature, a

noticeable decrease in modulus was observed as shown in **Fig. 5.4 (b)**, which progressively decreased further with increase in temperature. This can be correlated to the *onset* of destabilization of the physically crosslinked hydrogen-bonded network or cluster disordering effect entailing large chain mobility. Upon further increase in temperature, the polymer underwent its maximum drop in modulus at 60 °C (**Fig. 5.4(b)**) of about one order of magnitude while only a subtle increase in elongation was observed. At higher temperature, the stress-strain curve of Nafion® was similar to that of a soft and weak plastic material. Finally, at temperatures above 100 °C, the film did not break upon reaching the instrument maximum strain limit emphasizing a destabilized hydrogen-bonded network.

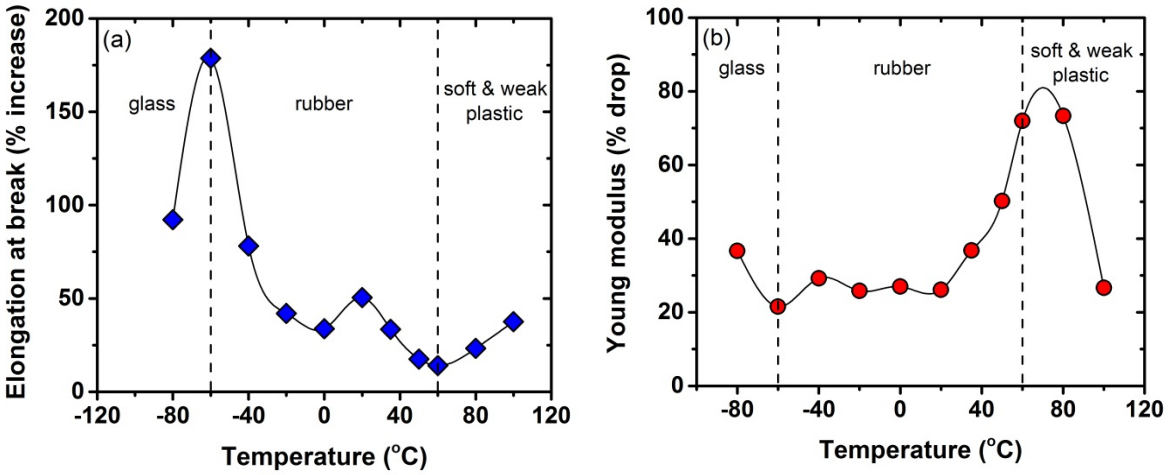

Fig. 5.4. (a) elongation at break (b) Young modulus represented by the percentage change as we go up in temperature from -120 to 100 ^{o}C.

5.3.3. Pure-Gas Permeability

The pure-gas permeation properties of He, H_2, N_2, O_2, CO_2, CH_4, C_2H_6 and C_3H_8 in Nafion® are presented in **Table 5.2**. The gas permeabilities follow the order of kinetic diameters (d_k): He > H_2 > CO_2 > O_2 > N_2 > CH_4 > C_2H_6 > C_3H_8 indicative of the strongly size-dependent permeation mechanism in Nafion®. The gas permeabilities at 35 °C reported in this study are in reasonably good agreement with those reported by Chiou and Paul [29]. However, the values reported by Fan et al. at 30 °C are approximately 20-40% lower than those reported here [30]. Possible reasons for this difference include: (i) Different film drying protocol; (ii) different permeation test conditions. In our study, the same film drying and permeation test protocol was applied for each film, which minimized possible errors due to sample variations.

Table 5.2. Gas permeability in dry Nafion® at 2 atm and 35 °C.

Gas	**Permeability (Barrer)**		
	This study	**[29]**[a]	**[30]**[b]
He	37	41	29
H_2	7	9.3	5.2
O_2	1.01	1.08	0.72
N_2	0.24	0.26	0.18
CO_2	2.3	2.4	1.4

CH_4	0.083	0.102	0.08
C_2H_6	0.029	-	-
C_3H_8	0.005	-	-

[a] 1 atm and 35 °C [29].

[b] 4 atm and 30 °C [30].

The permeability properties of Nafion® and rubbery polydimethylsiloxane (PDMS) [42], as a function of critical volume for several gases, are compared in **Fig. 5.5**. In Nafion®, the permeability decreases significantly as the sizes of the gas molecules increase as is typically observed for low free volume glassy polymers. C_2H_6 and C_3H_8 exhibited *very* low permeability owing to their large size (low diffusivity) and commonly ascribed unfavorable hydrocarbon-fluorocarbon interaction (low gas solubility) [16]. On the other hand, highly flexible rubbery PDMS shows markedly different permeation behavior: more condensable gases with large molecular size such as C_2H_6 and C_3H_8 exhibit higher permeability than smaller gases such as He and H_2 [42]. In fact, PDMS shows about 6 orders of magnitude higher C_3H_8 permeability than Nafion®. This behaviour results directly from the highly flexible chain architecture of PDMS (high diffusivity) and the tight polymer chain packing of Nafion® in its rubbery fluorocarbon and ionic sulfonic acid domains (low diffusivity). In addition, but to a lesser extent, Nafion® also has lower gas solubility than conventional rubbery or glassy polymers, as discussed below.

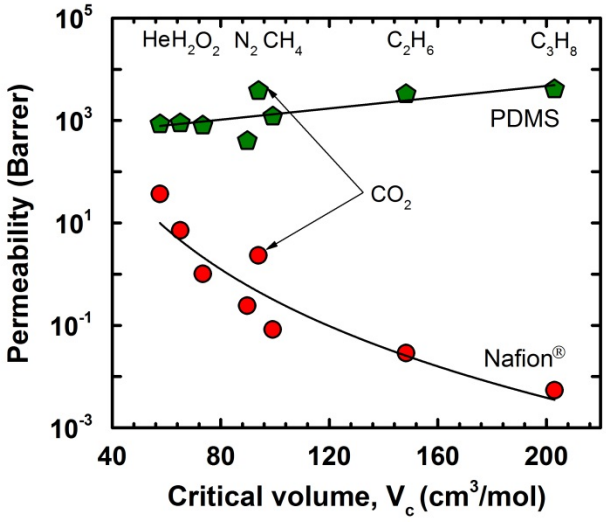

Fig. 5.5. Gas permeability in dry Nafion® and rubbery PDMS [42] as a function of penetrant critical volume, V_c at 35 °C.

5.3.4. Gas Solubility and Diffusion Coefficients

The pure-gas solubility coefficients for He, H_2, N_2, O_2, CO_2, CH_4, C_2H_6, C_3H_8 and *n*-C_4H_{10} are presented in **Table 5.3**. In this study, the gas solubilities were *directly* measured using barometric and gravimetric methods and are generally in good agreement. Previously reported solubility values by Chiou et al. [29] and Fan et al. [30] were calculated from the diffusion time-lag method, which is prone to errors especially for polymers with low gas solubility [43]. The solubility data for He and H_2, measured using the barometric method in this study agree reasonably well with the gravimetrically measured values reported by Smith et al [34].

Table 5.3. Gas solubility coefficients in dry Nafion® at 2 atm and 35 °C

	This work		Reference		
Gas	(Gravimetric)	(Barometric)	(Time lag)[a]	(Time lag)[b]	(Gravimetric)[c]
	Gas Solubility, S (10^{-3} cm^3(STP)/cm^3 cmHg)				
He	-	0.52	-	0.28	0.49
H_2	-	0.69	0.97	0.75	0.84
N_2	1.3	1.3	1.5	0.97	-
O_2	2.4	1.7	2.4	2.3	-
CH_4	2.4	1.9	3.6	1.2	-
CO_2	9.5	8.7	14.5	9.0	-
C_2H_6	4.8	4.9	-	-	-
C_3H_8	7.9	7.2	-	-	-
n-C_4H_{10}	16.2[d]	17.3[d]	-	-	-

[a] Solubility coefficients calculated by $S=P/D$ from permeability and diffusion time-lag method (1 atm; 35 °C) [29].

[b] Solubility coefficients calculated by $S=P/D$ from permeability and diffusion time-lag method (4 atm; 30 °C) [30].

[c] Solubility coefficients measured directly by gravimetric method (10 atm; 35 °C) [34].

[d] Solubility coefficients measured at 1 atm and 35 °C.

Sorption isotherms for He, H_2, N_2, O_2, CO_2, CH_4, and C_2H_6 in Nafion® measured at 35 °C using the barometric technique, shown in **Fig. 5.6 (a)** and **(b)**, were linear up to 20 atm, following Henry's law. The isotherms of propane and *n*-butane in **Fig. 5.6 (c)** were convex to the pressure axis, which is well described by the Flory-Huggins theory for gas

sorption in polymers. Such effects have been reported earlier wherein the solubility of vapors were sufficient enough to allow convex behavior in rubbers owing to its high condensability values [42, 44-47].

The linear and convex solubility isotherm for condensable gases (CO_2, propane and *n*-butane) are strong evidences to indicate Nafion®'s rubber like behavior at 35 ^oC. However, it has been observed for some glassy polymers that the sorption of such gases caused lowering of glass transition temperature that allowed them to exhibit rubbery sorption isotherms [48]. This has been attributed to high solubility induced chain plasticization effect. Based on the mechanical stress-strain results shown above, such effect is highly unlikely for Nafion® because the polymer shows rubbery characteristics at 35 ^oC highlighted by its significantly high elongation at break value of 255%.

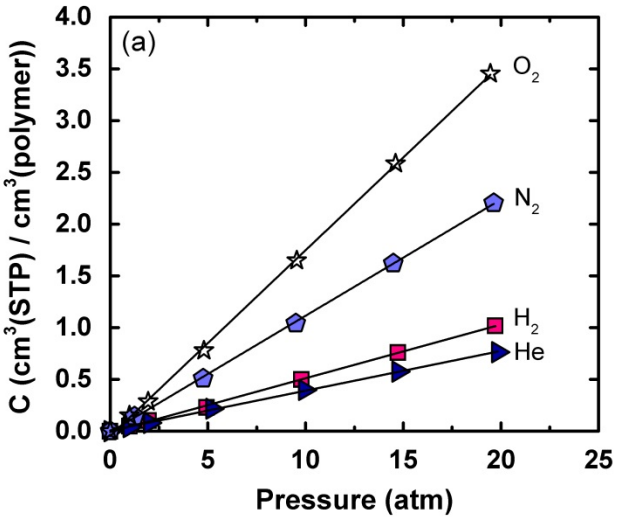

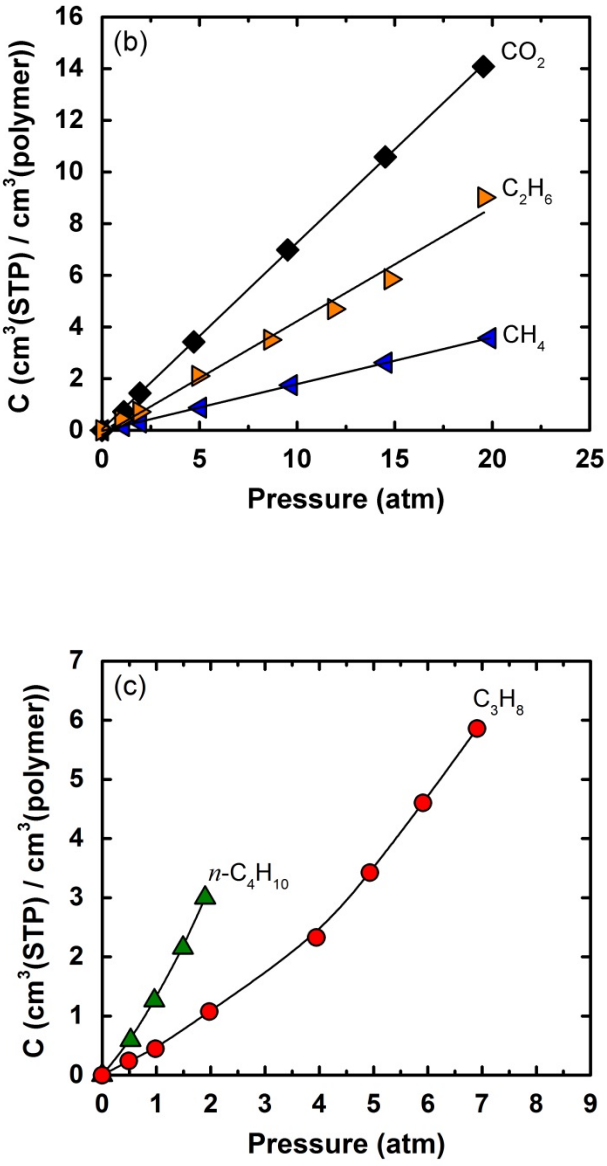

Fig. 5.6. Sorption isotherms in dry Nafion® measured barometrically at 35 °C: (a) He, H_2, N_2, O_2; (b) CO_2, CH_4, C_2H_6; and (c) C_3H_8, *n*-C_4H_{10}.

The solubility of each penetrant in Nafion® as a function of pressure (**Fig. 5.7 (a)**) is compared with solubility values in rubbery PDMS (**Fig. 5.7 (b)**) [42]. Both polymers show similar qualitative solubility trends. For low sorbing gases, such as H_2 and N_2, the

absolute solubility values are similar in both polymers. However, for more highly sorbing hydrocarbon gases, such as C_3H_8, Nafion® exhibits up to 10-fold lower gas sorption than PDMS, most likely due to unfavorable fluorocarbon polymer-hydrocarbon gas interactions [16].

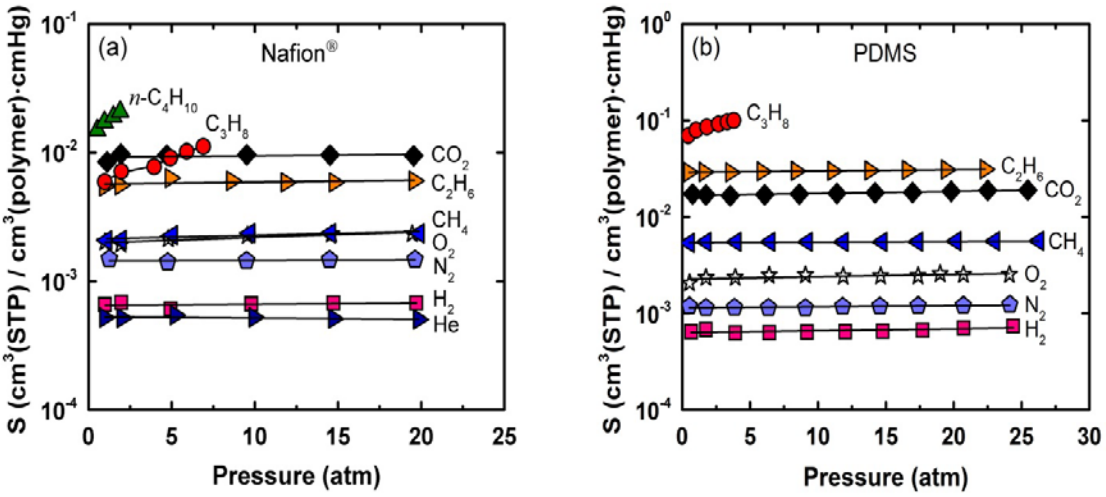

Fig. 5.7. (a) Pressure dependent gas solubility in dry Nafion® measured barometrically at 35 °C for He, H_2, N_2, O_2, CH_4, CO_2, C_2H_6, C_3H_8, and *n*-C_4H_{10} and (b) Pressure dependent solubility data for PDMS from reference [42] at 35 °C for H_2, N_2, O_2, CH_4, CO_2, C_2H_6, and C_3H_8.

Fig. 5.8 presents gas solubility in Nafion® and a perfluorinated glassy polymer (Cytop®) [16] at 35 °C as a function of critical temperature. The solubility coefficients generally scale with gas condensability: He < H_2 < N_2 < O_2 ≈ CH_4 < C_2H_6 < C_3H_8. However, Nafion® and Cytop® have unusually high CO_2 solubility which deviates from the general trendline in **Fig. 5.8**. Previous studies highlighted the unusual CO_2/perfluorocarbon interactions responsible for enhanced CO_2 solubility in

perfluorinated liquids, which may also explain the observed higher solubility of CO_2 in Nafion® and Cytop® [49, 50]. Additionally, it is well known that polymers containing polar moieties exhibit larger interaction with polar gases such as CO_2 [51]. Thus, the interaction of quadrupolar CO_2 with the highly polar sulfonic acid group in Nafion® may have significant influence on its overall solubility.

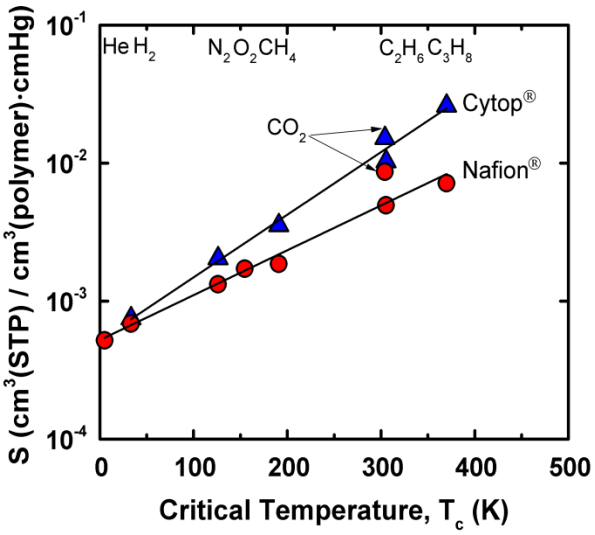

Fig. 5.8. Solubility of gases in perfluorinated polymers at 35 °C: Nafion® and glassy Cytop® [16], as a function of critical temperature, T_c. The best-fit trendline through the experimental data for Nafion® is: $\ln S = -7.56 + 0.0078\ T_c$ [K].

Interestingly, the trend line through the solubility data of Nafion® differs from that of other perfluorinated polymers, such as Cytop®. This is primarily due to the extremely low hydrocarbon solubility observed in Nafion® with a slope value of 0.0078 K^{-1} which is significantly lower than the general slope value for gas solubility in hydrocarbon- (0.017–0.019 K^{-1}) [52] and other perfluorocarbon-based (0.009–0.011 K^{-1}) [16] polymers. The

deviation in slope for Nafion® compared to other perfluorinated polymers may be due to the hydrophilic sulfonic acid group that creates an additional unfavorable environment for sorption of the hydrocarbon penetrants in the polymer matrix. This lower solubility has significant implications for the separation properties of gas pairs with large size differences: diffusivity selectivity to dominate overall permselectivity.

Pure-gas diffusion (D) coefficients in Nafion® calculated from the ratio of permeabilities and directly measured barometric sorption data at 2 atm and 35 °C are shown in **Table 5.4**. As expected, diffusivity decreases with increasing kinetic diameter (except for CO_2): He > H_2 > O_2 > CO_2 > N_2 > CH_4 > C_2H_6 > C_3H_8. The extent of these differences is extraordinary: the diffusivity of He is ~ 4 and 5 orders of magnitude higher than that of C_2H_6 and C_3H_8, respectively. This result highlights the exceptional molecular sieving properties of Nafion® for He/C_{2+} hydrocarbons as well as H_2/C_{2+} hydrocarbons and CO_2/C_{2+} hydrocarbons, as shown in **Table 5.5**. Even similarly sized He (d_k= 2.60 Å) and H_2 (d_k= 2.89 Å) can efficiently be separated due to the strikingly high He/H_2 diffusivity selectivity of 6.8 and permselectivity of 5.2, which are the highest values for the He/H_2 pair of any known polymer reported to date. It is important to note that the high permselectivities of Nafion® do not solely result from its high diffusivity selectivities. The extremely low hydrocarbon gas solubilities lead to relatively small "inverse" solubility selectivity values for small, low sorbing gases over large, more condensable hydrocarbon gases (S (He) and S (H_2) over $S_{hydrocarbons}$ < 1).

Table 5.4. Summary of gas diffusivity coefficients in dry Nafion® at 2 atm and 35 °C.

Gas	This study[a]	Reference [29][b]	Reference [30][c]
	Diffusivity (10^{-8} cm^2/s)		
He	714	-	1076
H_2	104	95.8	69
O_2	5.9	4.57	3.19
CO_2	2.7	1.68	1.56
N_2	1.8	1.73	1.82
CH_4	0.45	0.28	0.66
C_2H_6	0.058	-	-
C_3H_8	0.007	-	-

[a] Diffusion data were calculated from gas permeability and barometrically measured gas solubility values via solution-diffusion model (D=P/S).

[b] Determined by diffusion time-lag method at 35 °C.

[c] Determined by diffusion time-lag method at 30 °C.

Table 5.5. Selectivity of common gas pairs in dry Nafion® at 2 atm and 35 °C.

Gas Pair	P_a/P_b	D_a/D_b	S_a/S_b
He/H_2	5.2	6.9	0.75
He/CH_4	445	1590	0.28
He/C_2H_6	1275	12750	0.10

He/C_3H_8	7400	102800	0.072
H_2/CH_4	84	232	0.36
H_2/C_2H_6	241	1790	0.135
H_2/C_3H_8	1400	14580	0.096
CO_2/CH_4	28	6	4.67
CO_2/C_2H_6	79	47	1.68
CO_2/C_3H_8	460	300	1.53

Note: Solubility data were calculated using barometric technique and diffusion data were obtained from *D=P/S*.

It is important to point out that this study was only focused on detailed evaluation of the intrinsic pure-gas transport properties of dry Nafion®. A water-swollen Nafion® membrane would certainly exhibit poorer gas separation performance due to loss of its size-sieving capabilities induced by enhanced chain mobility.

5.3.5. Flory-Huggins Interaction

Flory-Huggins provides a measure of thermodynamic interaction (χ) between the polymer and penetrant rationalizing the complex gas solubility behavior in Nafion®. In the evaluation of χ, the saturation vapor pressure (p_{sat}) and partial molar volume (V_o) at the studied temperature are essential. The p_{sat} values for gases with critical temperature (T_c) above 35 °C were estimated from the Wagner equation [53]. For gases with T_c below 35 °C, the p_{sat} values were estimated from the linear relation ln p_{sat} versus 1/T

because experimentally the liquefied phase pressure cannot be achieved at 35 °C [53]. The p_{sat} and V_o values are presented in **Table 5.6**.

The dependence of χ upon penetrant activity for CO_2, C_2H_6, C_3H_8 and *n*-C_4H_{10} is illustrated in **Fig. 5.9 (a).** The magnitude of χ parameter follows the order: $CO_2 < C_2H_6 < C_3H_8 <$ *n*-C_4H_{10}. The smaller value of χ indicates higher interaction and thus is consistent with the gas solubility isotherm shown in **Fig. 5.9 (b)**. The χ value for CO_2 and C_2H_6 shows constant value up to penetrant activity of 0.4 corresponding to linear sorption isotherm. However, for C_3H_8 and *n*-C_4H_{10}, the χ value decreases with increase in penetrant activity indicative of increasing interaction. This is highlighted by the convex curvature shown in **Fig. 5.9 (b).**

Table 5.6. Penetrant critical volumes (V_c), Saturation vapor pressures (p_{sat}) and partial molar volumes (V_o) at 35 °C.

Gas	**V_c (cc/mol)**	**p_{sat} (atm)**	**V_o (cc/mol)**
He	57.6	42	49
H_2	65.1	341	52
O_2	73.4	864	56
N_2	89.8	902	62
CO_2	93.9	81.9	64
CH_4	99.2	359	66
C_2H_6	148.3	53.2	85
C_3H_8	203	12.4	106
n-C_4H_{10}	255	3.2	128

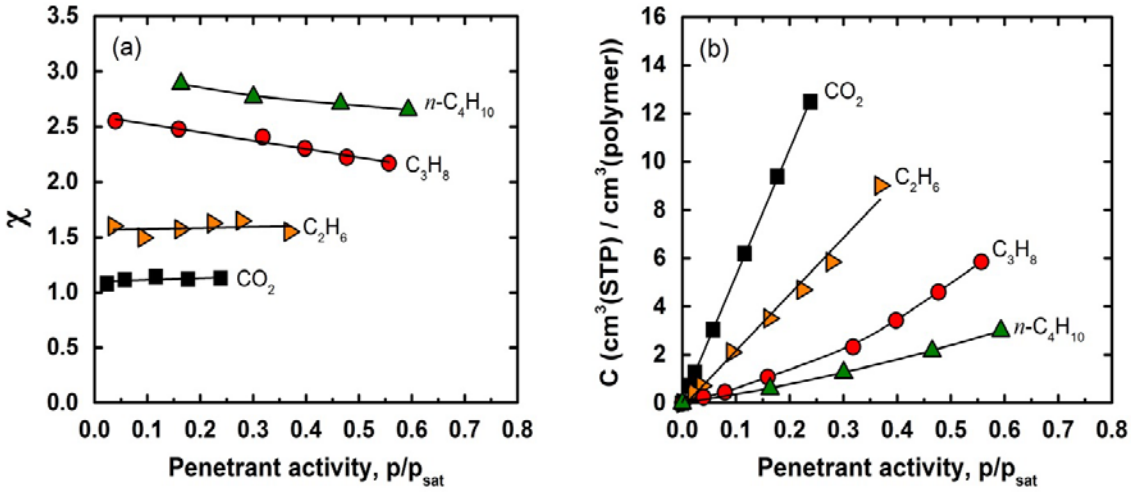

Fig. 5.9. (a) Flory-Huggins interaction parameter values, and (b) gas solubility for CO_2, C_2H_6, C_3H_8 and *n*-C_4H_{10} in Nafion® as a function of penetrant activity at 35 ºC.

5.3.6. Temperature Dependence of Gas Permeation

The permeability of He, H_2, O_2, N_2, CO_2, CH_4, C_2H_6 and C_3H_8 in Nafion® was determined at a feed pressure of 2 atm in the temperature range from 23-50 °C. The permeability of gases obeyed typical Arrhenius behavior, as shown in **Fig. 5.10**. The permeability of all gases increased with temperature, which indicates that the increase in diffusion coefficient overcame the simultaneous decrease in solubility coefficients.

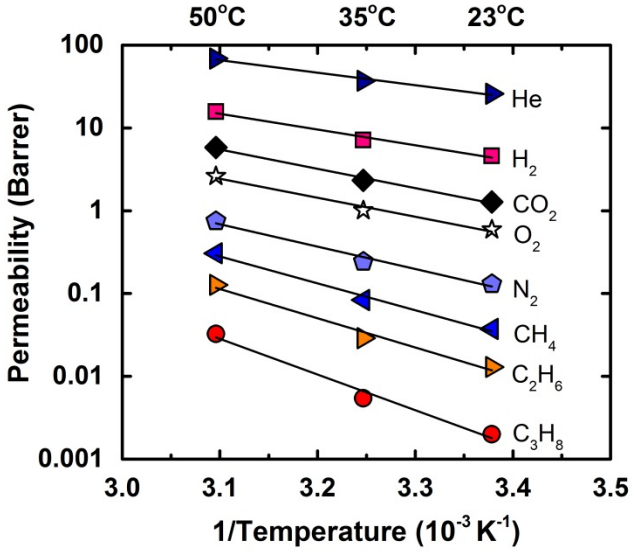

Fig. 5.10. Permeability of He, H_2, N_2, O_2, CH_4, CO_2, C_2H_6, and C_3H_8 in Nafion® as a function of temperature ranging from 23-50 °C measured at 2 atm.

The activation energy of permeation (E_P) was calculated from the data in **Fig. 5.9** using equation 3.12. It followed the order: He < H_2< O_2< CO_2< N_2 < CH_4 < C_2H_6< C_3H_8 representative of diffusion dominated permeation behavior in Nafion®. The values reported in this study are in reasonably good agreement with previously reported E_P data for Nafion® [30, 32]. The largest effect of temperature on permeability was observed for hydrocarbon gases (CH_4, C_2H_6 and C_3H_8) with large kinetic diameters. This translates into significant variations in gas separation performance where an increase in temperature results in decrease in gas selectivity. For example, important gas pairs with large size differences such as He/CH_4 and H_2/C_3H_8 observed significant drops in selectivity from 700 at 23 °C to 225 at 50 °C (68% decrease) and 2300 at 23 °C to 483 at 50 °C (79% decrease), respectively, as a result of a decrease in diffusivity selectivity. From an industrial perspective, however, selectivities of 225 and 483 for He/CH_4 and H_2/C_3H_8 at

high temperatures may still show potential for economic implementation of membranes in helium production from natural gas and hydrogen recovery from various refinery and petrochemical process streams.

The activation energies of permeation, E_P are reported in **Table 5.7** and compared to glassy polycarbonate [54]. The E_P values in Nafion® are almost two times higher than PC for He, O_2 and N_2, whereas for CH_4 and CO_2 it is almost three times higher. This is indicative of extremely tight chain packing in Nafion® entailing large diffusional restrictions for gas molecules with large sizes. It is therefore reasonable to compare Nafion® to an ultra-low free volume glassy polymer with strong molecular sieving capabilities at the temperature range investigated.

Table 5.7. Summary of activation energy of permeation, E_p (kJ/mole) for He, H_2, N_2, O_2, CH_4, CO_2, C_2H_6, and C_3H_8 in Nafion® measured at 2 atm. E_p reference data of glassy polycarbonate (PC) [54] is included for comparison.

Gas	Nafion[a]	Nafion[b]	Nafion[c]	PC[d]
He	28.9	22.1	22.0	17.6
H_2	36.4	-	32.5	-
N_2	51.7	49.7	48.8	25.1
O_2	43.9	34.6	36.4	20.9
CO_2	44.7	36.7	36.1	12.6

CH_4	62.2	-	54.7	25.9
C_2H_6	67.5			
C_3H_8	82.4			

Test conditions:

a. 2 atm, 25-50 °C [this work].

b. 1-2 bar, 25-65 °C [32].

c. 4 atm, 30-90 °C [30].

d. 5 atm for O_2, 35-175 °C; 5 atm for CO_2, 35-175 °C; 10 atm for He, N_2 and CH_4, 35-175 °C [54].

5.4. Conclusions

Nafion® exhibits rubber-like gas solubility behavior at 35 °C as evidenced by linear sorption isotherms for low sorbing gases (e.g. N_2, O_2, CH_4 etc.) and convex sorption isotherms of more highly sorbing propane and *n*-butane. Hydrocarbon gas sorption in Nafion® is significantly lower compared to that observed in other perfluorinated glassy polymers; the best-fit trendline through the experimental gas sorption data as function of critical gas temperature for Nafion® is: $\ln S = -7.56 + 0.0078\ T_c$. The stress-strain profile of Nafion® indicated that its transition from a glassy to a rubbery polymer began at temperatures as low as -60 °C represented by the significant increase in elongation at break and loss of a linear profile corresponding to the hard and brittle glassy state. WAXD data showed that Nafion® contains tightly packed amorphous chain domains with sharp size-sieving regions separating gases based on their molecular sizes, which is more commonly observed in stiff-chain, low free volume glassy polymers. The temperature dependence study in Nafion® confirmed the diffusion based permeation mechanism in Nafion commonly observed for ultra-low free volume glassy polymers. The strong size-

sieving effect of dry Nafion® resulted in *extraordinarily* high permselectivity and was especially pronounced between small gases (He, H_2, CO_2) and large hydrocarbon gases (C_{1+}). This attribute can potentially be harnessed for dry feed steams for helium recovery and CO_2 removal in natural gas applications, and hydrogen recovery from refinery gas streams. However, it is important to point out that this study was only focused on detailed evaluation of the intrinsic pure-gas transport properties of *dry* Nafion®. A water-swollen Nafion® membrane would certainly exhibit much poorer gas separation performance due to loss of its size-sieving capabilities induced by enhanced chain mobility, resulting in a significant loss in selectivity [31].

5.5. References

[1] A. Legault, Mainstreaming efficient industrial separation systems in IEA OPEN Energy Technology Bulletin, (2008).

[2] R.W. Baker, Future directions of membrane gas separation technology, Ind. Eng. Chem. Res. 41 (2002) 1393-1411.

[3] P. Bernardo, E. Drioli, G. Golemme, Membrane gas separation: a review/state of the art, Ind. Eng. Chem. Res. 48 (2009) 4638-4663.

[4] R.W. Baker, K. Lokhandwala, Natural gas processing with membranes: an overview, Ind. Eng. Chem. Res. 47 (2008) 2109-2121.

[5] P. Bernardo, E. Drioli, Membrane gas separation progresses for process intensification strategy in the petrochemical industry, Petroleum Chemistry 50 (2010) 271-282.

[6] Y. Yampolskii, Polymeric gas separation membranes, Macromolecules 45 (2012) 3298-3311.

[7] R.W. Baker, B.T. Low, Gas separation membrane materials: a perspective, Macromolecules 47 (2014) 6999-7013.

[8] D.F. Sanders, Z.P. Smith, R. Guo, L.M. Robeson, J.E. McGrath, D.R. Paul, B.D. Freeman, Energy-efficient polymeric gas separation membranes for a sustainable future: A review, Polymer 54 (2013) 4729-4761.

[9] L.S. White, T.A. Blinka, H.A. Kloczewski, I.F. Wang, Properties of a polyimide gas separation membrane in natural gas streams, J. Membr. Sci. 103 (1995) 73-82.

[10] A.Y. Houde, B. Krishnakumar, S.G. Charati, S.A. Stern, Permeability of dense (homogeneous) cellulose acetate membranes to methane, carbon dioxide, and their mixtures at elevated pressures, J. Appl. Polym. Sci. 62 (1996) 2181-2192.

[11] A. Bos, I.G.M. Pünt, M. Wessling, H. Strathmann, CO_2-induced plasticization phenomena in glassy polymers, J. Membr. Sci. 155 (1999) 67-78.

[12] J.D. Wind, C. Staudt-Bickel, D.R. Paul, W.J. Koros, Solid-state covalent cross-linking of polyimide membranes for carbon dioxide plasticization reduction, Macromolecules 36 (2003) 1882-1888.

[13] J.D. Wind, D.R. Paul, W.J. Koros, Natural gas permeation in polyimide membranes, J. Membr. Sci. 228 (2004) 227-236.

[14] I. Pinnau, Z. He, A.R. Da Costa, K.D. Amo, R. Daniels, Gas separation using C_{3+} hydrocarbon-resistant membranes, US Patent 6361582, 2002.

[15] R.S. Prabhakar, B.D. Freeman, I. Roman, Gas and vapor sorption and permeation in poly(2,2,4-trifluoro-5-trifluoromethoxy-1,3-dioxole-co-tetrafluoroethylene), Macromolecules 37 (2004) 7688-7697.

[16] T.C. Merkel, I. Pinnau, R. Prabhakar, B.D. Freeman, Gas and vapor transport properties of perfluoropolymers, in: Materials Science of Membranes for Gas and Vapor Separation, John Wiley & Sons, Ltd., Chichester, UK, 2006, pp. 251-270.

[17] Z. He, T.C. Merkel, Y. Okamoto, Y. Koike, Gas separation membranes based on perfluorinated polymers, US Patent 8828121, 2014.

[18] Y. Okamoto, H. Zhang, F. Mikes, Y. Koike, Z. He, T.C. Merkel, New perfluoro-dioxolane-based membranes for gas separations, J. Membr. Sci. 471 (2014) 412-419.

[19] V. Arcella, P. Colaianna, P. Maccone, A. Sanguineti, A. Gordano, G. Clarizia, E. Drioli, A study on a perfluoropolymer purification and its application to membrane formation, J. Membr. Sci. 163 (1999) 203-209.

[20] L.M. Robeson, The upper bound revisited, J. Membr. Sci. 320 (2008) 390-400.

[21] B.C.H. Steele, A. Heinzel, Materials for fuel-cell technologies, Nature 414 (2001) 345-352.

[22] K.A. Mauritz, R.B. Moore, State of understanding of Nafion, Chem. Rev. 104 (2004) 4535-4586.

[23] S.C. Yeo, A. Eisenberg, Physical properties and supermolecular structure of perfluorinated ion-containing (Nafion) polymers, J. Appl. Polym. Sci. 21 (1977) 875-898.

[24] T.D. Gierke, W.Y. Hsu, The cluster-network model of ion clustering in perfluorosulfonated membranes, in: Perfluorinated Ionomer Membranes, 180, American Chemical Society, Washington DC, 1982, pp. 283-307.

[25] H.R. Corti, F. Nores-Pondal, M.P. Buera, Low temperature thermal properties of Nafion 117 membranes in water and methanol-water mixtures, J. Power Sources 161 (2006) 799-805.

[26] T. Sakai, H. Takenaka, N. Wakabayashi, Y. Kawami, E. Torikai, Gas permeation properties of solid polymer electrolyte (SPE) membranes, J. Electrochem. Soc. 132 (1985) 1328-1332.

[27] M.L. Wu, Gas separations using membranes comprising perfluorinated polymers with pendant ionomeric moieties, EP Patent 0239888, 1987.

[28] Y. He, E.L. Cussler, Ammonia permeabilities of perfluorosulfonic membranes in various ionic forms, J. Membr. Sci. 68 (1992) 43-52.

[29] J.S. Chiou, D.R. Paul, Gas permeation in a dry Nafion membrane, Ind. Eng. Chem. Res. 27 (1988) 2161-2164.

[30] Y. Fan, D. Tongren, C.J. Cornelius, The role of a metal ion within Nafion upon its physical and gas transport properties, Eur. Polym. J. 50 (2014) 271-278.

[31] J. Catalano, T. Myezwa, M.G. De Angelis, M.G. Baschetti, G.C. Sarti, The effect of relative humidity on the gas permeability and swelling in PFSI membranes, Int. J. Hydrogen Energy 37 (2012) 6308-6316.

[32] M. Giacinti Baschetti, M. Minelli, J. Catalano, G.C. Sarti, Gas permeation in perflurosulfonated membranes: influence of temperature and relative humidity, Int. J. Hydrogen Energy 38 (2013) 11973-11982.

[33] S.J. Osborn, M.K. Hassan, G.M. Divoux, D.W. Rhoades, K.A. Mauritz, R.B. Moore, Glass transition temperature of perfluorosulfonic acid ionomers, Macromolecules 40 (2007) 3886-3890.

[34] Z.P. Smith, R.R. Tiwari, M.E. Dose, K.L. Gleason, T.M. Murphy, D.F. Sanders, G. Gunawan, L.M. Robeson, D.R. Paul, B.D. Freeman, Influence of diffusivity and sorption on helium and hydrogen separations in hydrocarbon, silicon, and fluorocarbon-based polymers, Macromolecules 47 (2014) 3170-3184.

[35] M. Laporta, M. Pegoraro, L. Zanderighi, Recast Nafion-117 thin film from water solution, Macromolecular Materials and Engineering 282 (2000) 22-29.

[36] P.C. van der Heijden, L. Rubatat, O. Diat, Orientation of drawn Nafion at molecular and mesoscopic scales, Macromolecules 37 (2004) 5327-5336.

[37] J.E. Hensley, J.D. Way, S.F. Dec, K.D. Abney, The effects of thermal annealing on commercial Nafion® membranes, J. Membr. Sci. 298 (2007) 190-201.

[38] H.F.M. Mohamed, Y. Kobayashi, C.S. Kuroda, A. Ohira, Impact of heating on the structure of perfluorinated polymer electrolyte membranes: a positron annihilation study, Macromol. Chem. Phys. 212 (2011) 708-714.

[39] Y. Kawano, Y. Wang, R.A. Palmer, S.R. Aubuchon, Stress-Strain Curves of Nafion Membranes in Acid and Salt Forms, Polímeros 12 (2002) 96-101.

[40] http://www.fuelcellmarkets.com/content/images/articles/nae201.pdf.

[41] A.K. Bhowmick, Mechanical properties of polymers, in: Material Science and Engineering, 1, Encyclopedia of Life Support Systems (EOLSS), Eolss Publishers, Paris, France.

[42] T.C. Merkel, V.I. Bondar, K. Nagai, B.D. Freeman, I. Pinnau, Gas sorption, diffusion, and permeation in poly(dimethylsiloxane), J. Polym. Sci., Part B: Polym. Phys. 38 (2000) 415-434.

[43] Z.P. Smith, R.R. Tiwari, T.M. Murphy, D.F. Sanders, K.L. Gleason, D.R. Paul, B.D. Freeman, Hydrogen sorption in polymers for membrane applications, Polymer 54 (2013) 3026-3037.

[44] H. Lin, B.D. Freeman, Gas solubility, diffusivity and permeability in poly(ethylene oxide), J. Membr. Sci. 239 (2004) 105-117.

[45] V.I. Bondar, B.D. Freeman, I. Pinnau, Gas transport properties of poly(ether-b-amide) segmented block copolymers, J. Polym. Sci., Part B: Polym. Phys. 38 (2000) 2051-2062.

[46] H. Lin, B.D. Freeman, Gas and vapor solubility in cross-linked poly(ethylene glycol diacrylate), Macromolecules 38 (2005) 8394-8407.

[47] J.S. Chiou, Y. Maeda, D.R. Paul, Gas and vapor sorption in polymers just below Tg, J. Appl. Polym. Sci. 30 (1985) 4019-4029.

[48] J.S. Chiou, D.R. Paul, Gas sorption and permeation in poly(ethyl methacrylate), J. Membr. Sci. 45 (1989) 167-189.

[49] F.D. Evans, R. Battino, The solubility of gases in liquids 3. The solubilities of gases in hexafluorobenzene and in benzene, J. Chem. Thermodyn. 3 (1971) 753-760.

[50] M.F. Costa Gomes, A.A.H. Pádua, Interactions of carbon dioxide with liquid fluorocarbons, The Journal of Physical Chemistry B 107 (2003) 14020-14024.

[51] S.G. Kazarian, M.F. Vincent, F.V. Bright, C.L. Liotta, C.A. Eckert, Specific intermolecular interaction of carbon dioxide with polymers, J. Am. Chem. Soc. 118 (1996) 1729-1736.

[52] S. Matteucci, Y. Yampolskii, B.D. Freeman, I. Pinnau, Transport of gases and vapors in glassy and rubbery polymers, in: Materials Science of Membranes for Gas and Vapor Separation, John Wiley & Sons, Ltd, 2006, pp. 1-47.

[53] R.C. Reid, J.M. Prausnitz, B.E. Poling, The Properties of Gases and Liquids, McGraw Hill, New York, 1987.

[54] L.M. Costello, W.J. Koros, Temperature dependence of gas sorption and transport properties in polymers: measurement and applications, Ind. Eng. Chem. Res. 31 (1992) 2708-2714.

Chapter 6. Pressure-Dependent Pure- and Mixed-Gas Permeation Properties of Nafion®

6.1. Abstract

The permeation properties of Nafion® at 35 °C are presented for pure gases H_2, N_2, O_2, CH_4, CO_2, C_2H_6 and C_3H_8, as a function of pressure between 2 and 20 atm. The effect of pressure on permeability and selectivity is analyzed to understand two observed phenomena: compression and plasticization. In pure-gas experiments, at increasing feed pressure, compression of the polymer matrix reduced the permeability of low-sorbing penetrants H_2, N_2, O_2, and CH_4. In contrast, permeabilities of more soluble penetrants CO_2 and C_2H_6 increased by 18 and 46% respectively, as plasticization effects overcame compression effects. Permeability of C_3H_8 decreased slightly with increasing pressure up to 4.6 atm as a result of compression, then increased by 3-fold at 9 atm as a result of plasticization associated with high C_3H_8 solubility. Binary CO_2/CH_4 (50:50) mixed-gas experiments at total feed pressures up to 36 atm quantified the effect of CO_2 plasticization on separation performance. At 10 atm CO_2 partial pressure, CH_4 permeability increased by 23% relative to its pure-gas value of 0.078 Barrer, while CO_2 permeability decreased by 28%. Consequently, CO_2/CH_4 selectivity decreased to 19, i.e., 42% below its pure-gas value of 32.

6.2. Introduction

The importance of natural gas (NG) as a fuel source and chemical feedstock has grown in tandem with advances in technologies for its bulk removal and purification [1, 2]. Separation of contaminants such as CO_2 and H_2S from raw NG streams, traditionally

accomplished using large amine absorption towers, is now often done using membrane systems – particularly on offshore platforms where space is at a premium [2-4]. The most common commercial membrane material in this application is cellulose acetate (CA), which can provide CO_2/CH_4 selectivity of 10-15 under high-pressure mixed-gas conditions [5]. Polyimide-based membranes are viewed as an alternative to CA membranes and also have a share of the market [2, 4-6].

Plasticization limits real-world membrane performance primarily by reducing selectivity, resulting in methane loss [5-7]. Plasticization occurs when large quantities of condensable gases such as CO_2, ethane, propane, butane and C_{5+} hydrocarbons sorb into the polymer matrix, increasing polymer chain mobility [8-11]. Macroscopic effects of plasticization include volume dilation, reduced mechanical stability, and depression of glass transition temperature [9, 10, 12-14]. The effects of CO_2 plasticization on gas transport include: (i) higher CO_2 permeability, (ii) even higher relative increase in mixed-gas CH_4 permeability, (iii) lower mixed-gas selectivity and (iv) time-dependent increases in CO_2 permeability (conditioning) [8-11, 15, 16]. These observations stem from the fact that polymers undergo reorganization of local segmental chains upon significant CO_2 sorption [8]. It has been shown for several glassy polymers that a CO_2 concentration of about 38 $cm^3(STP)/cm^3$ inside the polymer matrix is high enough to induce plasticization [2, 11].

Several strategies have been employed to reduce plasticization, including cross-linking of polymers, polymer blending, and thermal treatment [17-19]. These approaches have been more successful in delaying the onset of plasticization than in treating its

underlying cause, i.e., the high solubility of plasticizing components. An alternative approach to counter the effect of plasticization may be to identify polymers that have *lower solubility* for plasticizing penetrants [20, 21].

Nafion's® polytetrafluoroethylene (PTFE) backbone places this ionomer in the class of perfluoropolymers. Materials in this class have already found important commercial applications in chemical, electronic and medical industries [22-26], owing in large part to their exceptional chemical and mechanical stability. Semi-crystalline PTFE shows low gas permeability [27] and cannot be solvent cast into thin films [21], but newer amorphous glassy perfluoropolymers such as Teflon® AF (Du Pont), Hyflon® AD (Solvay), Cytop® (Asahi Glass) and others have shown promise in several gas separation applications [20, 21, 28-35]. These polymers are soluble in perfluorinated solvents and thus can be fabricated into thin-film composite membranes. Their unique ability to combine restricted, efficient chain packing with low gas solubilities has allowed permeability-selectivity combinations to surpass 2008 Robeson upper bound curves for several gas pairs: He/CH_4, He/H_2, N_2/CH_4, and H_2/CH_4 [21, 30-32, 36, 37]. Nafion® is unusual in that its phase-separated microstructure exhibits two glass transition temperatures: one from its rubbery PTFE phase and another from its ionic sulfonic acid clusters. In our previous work, we suggested that Nafion® may hold promise as a membrane material for CO_2 removal from *dehydrated* NG [38]. In this earlier study, solubility measurements revealed CO_2 uptake in Nafion® of about 8 cm^3(STP)/cm^3 at 10 atm – 3-fold lower than CA [39] and almost 2-fold lower than perfluorinated Cytop® [21]. Moreover, C_3H_8 uptake in Nafion® was about 1 cm^3(STP)/cm^3 at 2 atm – 25-fold lower than polyimide 6FDA-6FpDA [40] and 5-fold lower than Cytop® [21]. These

results motivated further research to determine Nafion's® permeation properties under high-pressure mixed-gas conditions.

In this work we report pure-gas permeation properties of Nafion® for H_2, O_2, N_2, CH_4, CO_2, C_2H_6, and C_3H_8 as a function of pressure at 35 °C. The coupling effects of penetrant sorption and diffusion in mixed-gas experiments often result in reduced selectivity. Accordingly, binary (50:50) CO_2/CH_4 mixed-gas permeation experiments were conducted to evaluate the potential effectiveness of Nafion® in separating CO_2/CH_4 mixtures.

6.3. Results and discussion

6.3.1. Pressure-dependent pure-gas permeability

Fig. 6.1 shows permeability of low sorbing gases: (a) N_2, CH_4 and (b) H_2, O_2, in Nafion® as a function of pressure at 35 °C. In all cases, permeability decreased slightly with increasing pressure. Gas permeabilities at 2 atm, tabulated in [38], were in reasonably good agreement with those reported by Chiou and Paul [41]. Solubilities of H_2, O_2, N_2, and CH_4 in Nafion® reported in our previous study were constant up to 20 atm and followed Henry's law, indicating rubber-like behavior [38]. Because permeability is the product of diffusivity and solubility, the constant solubility values indicate that the decrease in permeability was caused by a decrease in gas diffusivity. If polymer chain compression narrows gas transport pathways, larger penetrant molecules should display greater permeability decreases. Subsequently, as pressure increased from 2 to 20 atm, permeability of the largest gas CH_4 decreased by 13%, N_2 and O_2 decreased by 8%, and the much smaller H_2 by only 1%. Permeability reduction resulting from

compression has been reported for several gases in rubbery polymers where the decrease in permeability was associated with a compression-induced decrease in diffusivity with increase in pressure [42-44]. For example, in poly(dimethylsiloxane) (PDMS) non-interacting gases such as He and N_2 showed permeability decreases of 27 and 24%, respectively, between 3 and 30 atm [42]. Similarly, in poly(octylmethylsiloxane) (POMS), CH_4 and *n*-butane permeability dropped by 75 and 77%, respectively, between 2 and 10 atm [44]. Nafion® shows rubber-like behavior similar to PDMS and POMS with low Young's modulus and ~250% elongation at break at 35 °C (see **Fig. 5.3**).

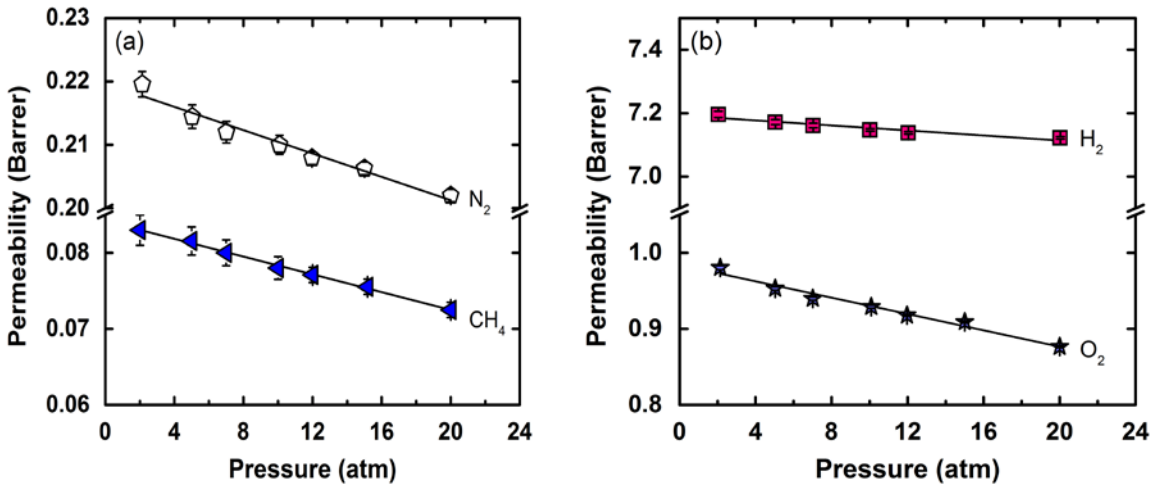

Fig. 6.1. Permeabilities of low sorbing penetrants in Nafion® for (a) N_2, CH_4; and (b) H_2, O_2, as a function of pressure at 35 °C.

Permeabilities of more condensable gases CO_2 and C_2H_6 increased with pressure, as shown in **Figs. 6.2(a)** and **(b)**. Permeabilities are plotted with their pressure-dependent diffusivities derived from $D=P/S$, using solubility values obtained from our previous study [38]. CO_2 and C_2H_6 permeabilities increased by 18 and 46%, respectively, as

pressure increased from 2 to 20 atm. Also, the permeability of CO_2 was considerably higher than that of C_2H_6 across the investigated pressure range. The increase in permeability with pressure can be explained as follows: the solubility coefficients of CO_2 and C_2H_6 measured in our previous study were essentially constant between 1 and 20 atm, so the observed permeability increase can be attributed solely to increases in diffusivities. Presumably, plasticization enhances polymer chain mobility and thereby increases the gas diffusivity in the polymer. The higher permeability of CO_2 relative to C_2H_6 results from its smaller molecular diameter combined with enhanced solubility due to its quadrupolar nature that enables strong specific (polar-quadrupolar) interaction with the polar sulfonate groups in Nafion® [45].

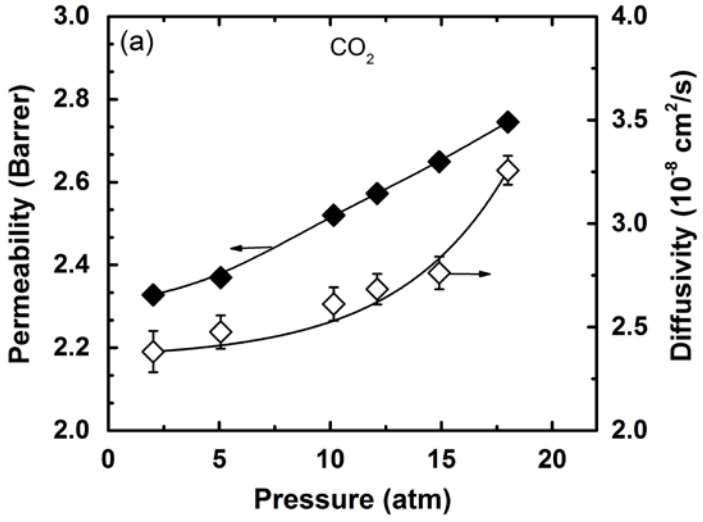

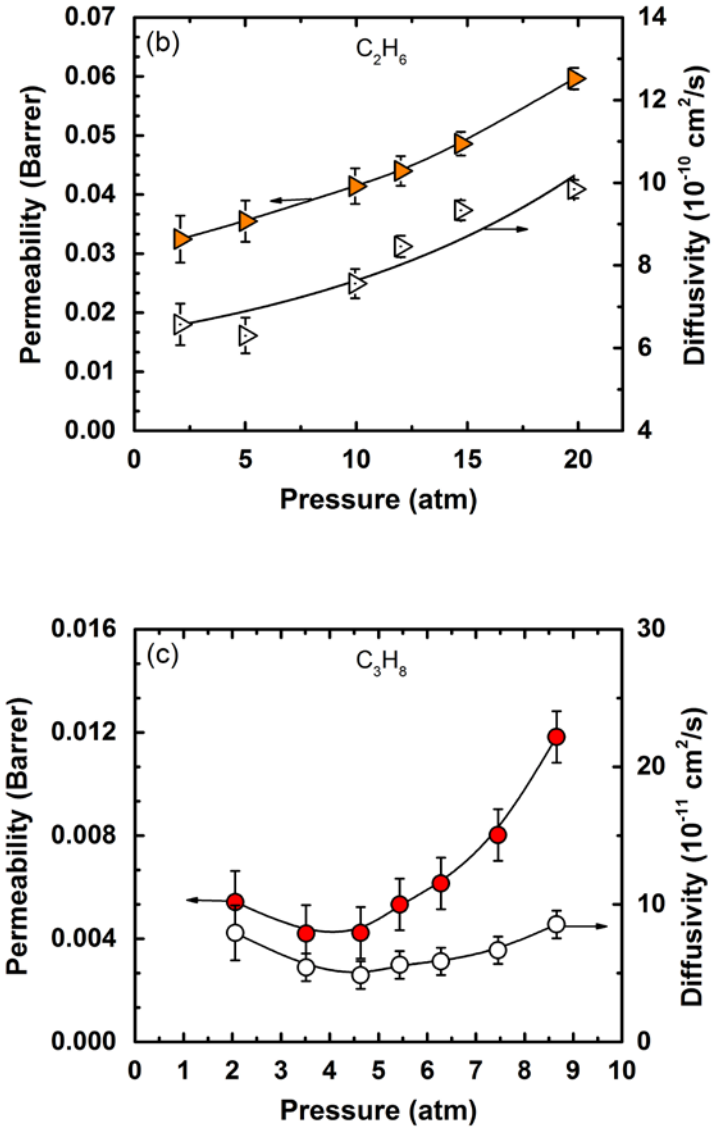

Fig. 6.2. Pressure dependence of pure-gas permeability (*P*) and diffusivity (*D*) for high sorbing penetrants (a) CO_2; (b) C_2H_6; and (c) C_3H_8 in Nafion® at 35 °C. Solubility (*S*) data were extracted from [38] and diffusivities were obtained from $D = P/S$. Open points: pure-gas diffusivity. Closed points: pure-gas permeability.

Fig. 6.2(c) shows C_3H_8 permeability as a function of pressure combined with diffusivities obtained as described above. Permeability decreased slightly as pressure increased from 2 to 4.6 atm, and then increased dramatically. The slight permeability decrease can be explained by analyzing individual contributions from solubility and diffusivity to the overall gas permeability. Solubility increased by 25% between 2 and 4.6 atm. As $P = DS$, the observed 22% decrease in permeability results from comparatively larger (~40%) decrease in diffusivity due to pressure-induced chain compression. As dissolved C_3H_8 concentration increases, the polymer matrix of Nafion® becomes softer which enhances chain mobility. As a result, a ~64% increase in C_3H_8 permeability was observed between 4.6 and 9 atm due to a dominant ~59% increase in solubility combined with ~43% increase in diffusivity. Plots of C_3H_8 permeability versus time are included in **Fig. 6.3** to show that sufficient time was provided to reach steady state.

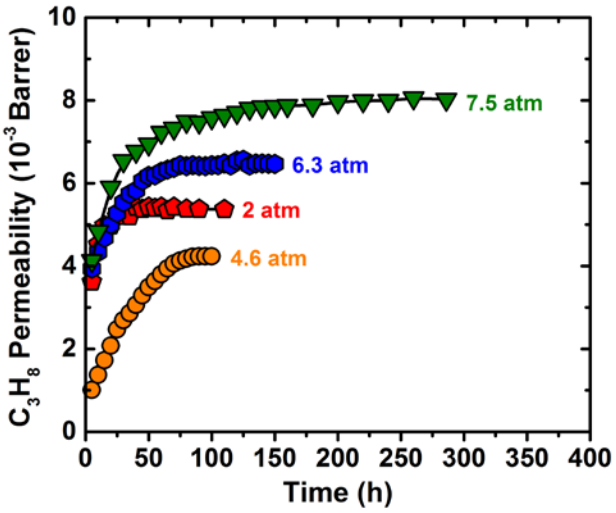

Fig. 6.3. Time-dependent pure-gas C_3H_8 permeability in Nafion® at various pressures and 35 °C.

6.3.2. Mixed-gas CO_2/CH_4 (50:50) permeation properties

Fig. 6.4 compares permeabilities of pure CH_4 (also shown in **Fig. 6.1(a)**) and CO_2 (**Fig. 6.2(a)**) with those of a 50:50 feed mixture as a function of pressure at 35 °C. It is well known that mixtures containing CO_2 tend to introduce non-ideal effects such as plasticization and competitive sorption, often resulting in different permeation behavior compared to pure-gas measurements. Thus, we conducted mixture experiments over a range of CO_2 partial pressures between 2 and 18 atm to assess the effect of plasticization on membrane separation performance.

Fig. 6.4(a) plots pure- and mixed-gas CO_2 permeabilities with respect to both pressure and fugacity. Fugacity values were calculated for each pressure point using the Soave-Redlich-Kwong (SRK) equation of state [46]. Across the entire pressure range investigated, mixed-gas CO_2 permeability was lower than pure-gas. For example, at 18 atm CO_2 partial pressure, CO_2 permeability was about 35% lower than its pure-gas value. Competitive sorption explains the difference: when CH_4 is added to the feed, it competes with CO_2 for sorption sites in the polymer, reducing CO_2 solubility. When plotted with respect to fugacity, mixed-gas CO_2 permeability increases with increasing pressure, but less steeply than in the pure-gas case. Under mixed-gas conditions, the permeability increase caused by plasticization is partially offset by the decrease caused by additional compression from CH_4. These offsetting effects of plasticization and compression were first highlighted by Jordan and Koros for rubbery PDMS in their mixed-gas study of CO_2/CH_4 and CO_2/N_2 [42].

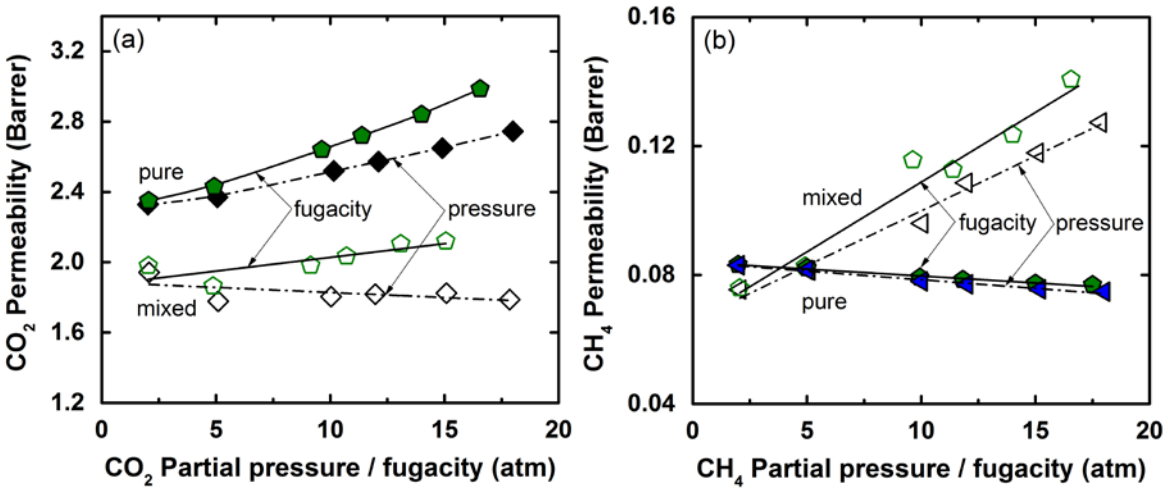

Fig. 6.4. Pure- and mixed-gas (50:50) permeability of (a) CO_2 and (b) CH_4 in Nafion® as a function of partial pressure or fugacity at 35 °C. Open points: mixed-gas permeability. Closed points: pure-gas permeability. The error was attributed to instrument leak rate that accounted for errors in permeabilities ranging between ±0.1-0.25%.

As shown in **Fig. 6.4(b)**, at lower pressures (up to 5 atm), mixed-gas CH_4 permeability was slightly lower than its pure-gas value. As discussed above, competitive sorption and compression can explain this decrease. At pressures above 5 atm, permeability increased linearly and markedly. CH_4 mixed-gas permeability with respect to fugacity was slightly higher; however, the general trend was the same. At 18 atm CO_2 partial pressure, mixed-gas CH_4 permeability was almost 70% higher than its pure-gas value. The polar sulfonate group in Nafion® allows specific interaction with CO_2 molecules, which increases segmental mobility. Thus, the significant increase in CH_4 permeability is a direct consequence of CO_2-induced plasticization that facilitates the diffusion of CH_4 molecules under mixed-gas conditions.

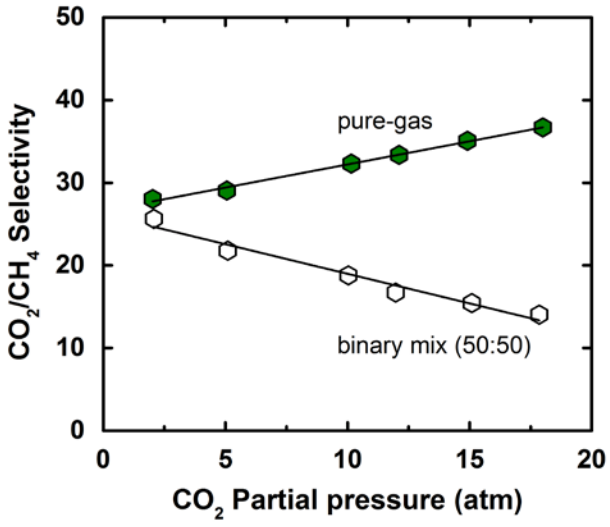

Fig. 6.5. Pure- and mixed-gas (50:50) CO_2/CH_4 selectivity in Nafion® as a function of CO_2 partial pressure at 35 °C. Open points: mixed-gas selectivity. Closed points: pure-gas selectivity. The error was attributed to instrument leak rate that accounted for errors in selectivities ranging between ±0.1-0.25%.

Given the decrease in mixed-gas CO_2 permeability coupled with comparatively larger increase in CH_4 permeability, overall mixed-gas CO_2/CH_4 selectivities were lower than pure-gas ideal selectivities over the entire pressure range investigated, as illustrated in **Fig. 6.5**. At CO_2 partial pressure of 10 atm, typical in natural gas applications [5, 7], Nafion® mixed-gas selectivity dropped by ~42% relative to its pure-gas value, from 32 to 19.

6.4. Conclusions

In summary, the pressure-dependent permeability results obtained for Nafion® highlighted two divergent phenomena: gas compression and plasticization. In pure-gas experiments, permeability of permanent gases H_2, O_2, N_2 and CH_4 decreased due to polymer compression, whereas the permeability of more condensable gases CO_2, C_2H_6 and C_3H_8 increased due to solubility-induced plasticization. Mixed-gas CO_2/CH_4 experiments showed reduced performance as a result of dominant CO_2 plasticization effects. At typical NG partial CO_2 pressure of 10 atm, Nafion® exhibited CO_2/CH_4 selectivity of 19, similar to standard industrial CA membranes.

The market for using Nafion® membranes as the primary separation unit in NG processing may not look promising owing to its low CO_2 permeability, moderate mixed-gas CO_2/CH_4 selectivity (see **Fig. 6.6**) and high cost. However, its unique ability to preferentially permeate CO_2 *and* N_2 while retaining CH_4 and C_{2+} hydrocarbons in the product stream may offer significant advantages compared to glassy polymeric membranes such as CA. Nafion® offers high N_2/CH_4 selectivity of 2.9, in contrast to commercially available polymers like CA (0.8), polysulfone (0.6), and polycarbonate (0.8) [47]. Considering that 14% of U.S. gas wells are contaminated with unacceptably high concentrations of N_2 [48], removing N_2 and CO_2 simultaneously is commercially valuable. In addition, NG is the world's major source of helium, typically containing 0.4-0.5%, which is usually recovered alongside N_2 [4, 49]. Nafion® could be a candidate membrane material for this application as it exhibits He/CH_4 selectivity of 440 owing

largely to its extraordinarily high diffusivity selectivity, and He permeability of 37 Barrer – 3-fold higher than CA.

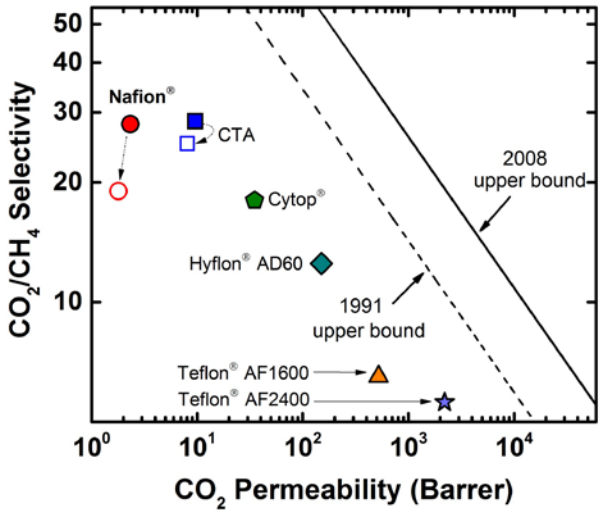

Fig. 6.6. Robeson upper bound curve for CO_2/CH_4 separation [36, 50]. All data points are reported at 35 °C. Open points are 50:50 mixed-gas data at 10 atm. Closed points are pure-gas data at 2 atm. Nafion® [this work], cellulose triacetate (CTA) (CA-436-80S) [51], Cytop® [21], Hyflon® AD60 [21], Hyflon® AD 80, Teflon®AF 2400 [52], Teflon® AF 1600 [53].

6.5. References

[1] Global natural gas consumption doubled from 1980 to 2010, EIA, (2012).

[2] R.W. Baker, K. Lokhandwala, Natural gas processing with membranes: an overview, Ind. Eng. Chem. Res. 47 (2008) 2109-2121.

[3] P. Bernardo, E. Drioli, Membrane gas separation progresses for process intensification strategy in the petrochemical industry, Petroleum Chemistry 50 (2010) 271-282.

[4] C.A. Scholes, G.W. Stevens, S.E. Kentish, Membrane gas separation applications in natural gas processing, Fuel 96 (2012) 15-28.

[5] R.W. Baker, Future directions of membrane gas separation technology, Ind. Eng. Chem. Res. 41 (2002) 1393-1411.

[6] J.D. Wind, D.R. Paul, W.J. Koros, Natural gas permeation in polyimide membranes, J. Membr. Sci. 228 (2004) 227-236.

[7] B.D. Bhide, S.A. Stern, Membrane processes for the removal of acid gases from natural gas. II. effects of operating conditions, economic parameters, and membrane properties, J. Membr. Sci. 81 (1993) 239-252.

[8] J.S. Chiou, D.R. Paul, Effects of CO_2 exposure on gas transport properties of glassy polymers, J. Membr. Sci. 32 (1987) 195-205.

[9] E.S. Sanders, Penetrant-induced plasticization and gas permeation in glassy polymers, J. Membr. Sci. 37 (1988) 63-80.

[10] M. Wessling, S. Schoeman, T. van der Boomgard, C.A. Smolders, Plasticization of gas separation membranes, Gas Sep. Purif. 5 (1991) 222-228.

[11] A. Bos, I.G.M. Pünt, M. Wessling, H. Strathmann, CO_2-induced plasticization phenomena in glassy polymers, J. Membr. Sci. 155 (1999) 67-78.

[12] J.S. Chiou, J.W. Barlow, D.R. Paul, Plasticization of glassy polymers by CO_2, J. Appl. Polym. Sci. 30 (1985) 2633-2642.

[13] J.R. Fried, H.C. Liu, C. Zhang, Effect of sorbed carbon dioxide on the dynamic mechanical properties of glassy polymers, J. Polym. Sci., Polym. Lett. 27 (1989) 385-392.

[14] H. Hachisuka, T. Sato, T. Imai, Y. Tsujita, A. Takizawa, T. Kinoshita, Glass transition temperature of glassy polymers plasticized by CO_2 gas, Polym. J. 22 (1990) 77-79.

[15] D.R. Paul, Gas sorption and transport in glassy polymers, Ber. Bunsen Ges. Phys. Chem. 83 (1979) 294-302.

[16] E.S. Sanders, S.M. Jordan, R. Subramanian, Penetrant-plasticized permeation in polymethylmethacrylate, J. Membr. Sci. 74 (1992) 29-36.

[17] A. Bos, I.G.M. Pünt, M. Wessling, H. Strathmann, Plasticization-resistant glassy polyimide membranes for CO_2/CO_4 separations, Sep. Purif. Technol. 14 (1998) 27-39.

[18] J.D. Wind, C. Staudt-Bickel, D.R. Paul, W.J. Koros, Solid-state covalent cross-linking of polyimide membranes for carbon dioxide plasticization reduction, Macromolecules 36 (2003) 1882-1888.

[19] C. Staudt-Bickel, W. J. Koros, Improvement of CO_2/CH_4 separation characteristics of polyimides by chemical crosslinking, J. Membr. Sci. 155 (1999) 145-154.

[20] R.S. Prabhakar, B.D. Freeman, I. Roman, Gas and vapor sorption and permeation in poly(2,2,4-trifluoro-5-trifluoromethoxy-1,3-dioxole-co-tetrafluoroethylene), Macromolecules 37 (2004) 7688-7697.

[21] T.C. Merkel, I. Pinnau, R. Prabhakar, B.D. Freeman, Gas and vapor transport properties of perfluoropolymers, in: Materials Science of Membranes for Gas and Vapor Separation, John Wiley & Sons, Ltd., Chichester, UK, 2006, pp. 251-270.

[22] B.C.H. Steele, A. Heinzel, Materials for fuel-cell technologies, Nature 414 (2001) 345-352.

[23] V. Arcella, A. Ghielmi, G. Tommasi, High performance perfluoropolymer films and membranes, Ann. N.Y. Acad. Sci. 984 (2003) 226-244.

[24] K.A. Mauritz, R.B. Moore, State of understanding of Nafion, Chem. Rev. 104 (2004) 4535-4586.

[25] Y.P. Yampolskii, Amorphous perfluorinated membrane materials: structure, properties and application, Russ. J. Gen. Chem. 79 (2009) 657-665.

[26] H. Teng, Overview of the development of the fluoropolymer industry, Appl. Sci. 2 (2012) 496-512.

[27] R.A. Pasternak, M.V. Christensen, J. Heller, Diffusion and permeation of oxygen, nitrogen, carbon dioxide, and nitrogen dioxide through polytetrafluoroethylene, Macromolecules 3 (1970) 366-371.

[28] V. Arcella, P. Colaianna, P. Maccone, A. Sanguineti, A. Gordano, G. Clarizia, E. Drioli, A study on a perfluoropolymer purification and its application to membrane formation, J. Membr. Sci. 163 (1999) 203-209.

[29] I. Pinnau, Z. He, A.R. Da Costa, K.D. Amo, R. Daniels, Gas separation using C_{3+} hydrocarbon-resistant membranes, US Patent 6361582, 2002.

[30] Z. He, T.C. Merkel, Y. Okamoto, Y. Koike, Gas separation membranes based on perfluorinated polymers, US Patent 8828121, 2014.

[31] Y. Okamoto, H. Zhang, F. Mikes, Y. Koike, Z. He, T.C. Merkel, New perfluoro-dioxolane-based membranes for gas separations, J. Membr. Sci. 471 (2014) 412-419.

[32] Y. Okamoto, Q. Du, K. Koike, F. Mikes, T.C. Merkel, Z. He, H. Zhang, Y. Koike, New amorphous perfluoro polymers: perfluorodioxolane polymers for use as plastic optical fibers and gas separation membranes, Polym. Adv. Technol. 27 (2016) 33-41.

[33] M. Macchione, J.C. Jansen, G. De Luca, E. Tocci, M. Longeri, E. Drioli, Experimental analysis and simulation of the gas transport in dense Hyflon® AD60X membranes: influence of residual solvent, Polymer 48 (2007) 2619-2635.

[34] N.A. Belov, A.A. Zharov, A.V. Shashkin, M.Q. Shaikh, K. Raetzke, Y.P. Yampolskii, Gas transport and free volume in hexafluoropropylene polymers, J. Membr. Sci. 383 (2011) 70-77.

[35] N. Belov, Y. Nizhegorodova, A. Zharov, I. Konovalova, V. Shantarovich, Y. Yampolskii, A new polymer, poly(perfluoropropylvinyl ether) and its comparison with other perfluorinated membrane materials, J. Membr. Sci. 495 (2015) 431-438.

[36] L.M. Robeson, The upper bound revisited, J. Membr. Sci. 320 (2008) 390-400.

[37] Z.P. Smith, R.R. Tiwari, M.E. Dose, K.L. Gleason, T.M. Murphy, D.F. Sanders, G. Gunawan, L.M. Robeson, D.R. Paul, B.D. Freeman, Influence of diffusivity and sorption on helium and hydrogen separations in hydrocarbon, silicon, and fluorocarbon-based polymers, Macromolecules 47 (2014) 3170-3184.

[38] M. Mukaddam, E. Litwiller, I. Pinnau, Gas sorption, diffusion, and permeation in Nafion, Macromolecules 49 (2016) 280-286.

[39] A.C. Puleo, D.R. Paul, S.S. Kelley, The effect of degree of acetylation on gas sorption and transport behavior in cellulose acetate, J. Membr. Sci. 47 (1989) 301-332.

[40] C. Staudt-Bickel, W.J. Koros, Olefin/paraffin gas separations with 6FDA-based polyimide membranes, J. Membr. Sci. 170 (2000) 205-214.

[41] J.S. Chiou, D.R. Paul, Gas permeation in a dry Nafion membrane, Ind. Eng. Chem. Res. 27 (1988) 2161-2164.

[42] S.M. Jordan, W.J. Koros, Permeability of pure and mixed gases in silicone rubber at elevated pressures, J. Polym. Sci., Part B: Polym. Phys. 28 (1990) 795-809.

[43] L.D. Miranda, R.J. Bell, R.T. Short, F.H.W. van Amerom, R.H. Byrne, The influence of hydrostatic pressure on gas diffusion in polymer and nano-composite membranes: application to membrane inlet mass spectrometry, J. Membr. Sci. 385–386 (2011) 49-56.

[44] J. Schultz, K.V. Peinemann, Membranes for separation of higher hydrocarbons from methane, J. Membr. Sci. 110 (1996) 37-45.

[45] S.G. Kazarian, M.F. Vincent, F.V. Bright, C.L. Liotta, C.A. Eckert, Specific intermolecular interaction of carbon dioxide with polymers, J. Am. Chem. Soc. 118 (1996) 1729-1736.

[46] G. Soave, Equilibrium constants from a modified Redlich-Kwong equation of state, Chem. Eng. Sci. 27 (1972) 1197-1203.

[47] R.W. Baker, Membrane Technology and Applications, 2nd ed., John Wiley & Sons, Ltd., Chichester, UK, 2004.

[48] K.A. Lokhandwala, I. Pinnau, Z. He, K.D. Amo, A.R. DaCosta, J.G. Wijmans, R.W. Baker, Membrane separation of nitrogen from natural gas: a case study from membrane synthesis to commercial deployment, J. Membr. Sci. 346 (2010) 270-279.

[49] Y. Yampolskii, Polymeric gas separation membranes, Macromolecules 45 (2012) 3298-3311.

[50] L.M. Robeson, Correlation of separation factor versus permeability for polymeric membranes, J. Membr. Sci. 62 (1991) 165-185.

[51] R. Swaidan, B. Ghanem, M. Al-Saeedi, E. Litwiller, I. Pinnau, Role of intrachain rigidity in the plasticization of intrinsically microporous triptycene-based polyimide membranes in mixed-gas CO_2/CH_4 separations, Macromolecules 47 (2014) 7453-7462.

[52] T.C. Merkel, V. Bondar, K. Nagai, B.D. Freeman, Y.P. Yampolskii, Gas Sorption, Diffusion, and Permeation in Poly(2,2-bis(trifluoromethyl)-4,5-difluoro-1,3-dioxole-co-tetrafluoroethylene), Macromolecules 32 (1999) 8427-8440.

[53] A.Y. Alentiev, V.P. Shantarovich, T.C. Merkel, V.I. Bondar, B.D. Freeman, Y.P. Yampolskii, Gas and Vapor Sorption, Permeation, and Diffusion in Glassy Amorphous Teflon AF1600, Macromolecules 35 (2002) 9513-9522.

Chapter 7. CO_2/CH_4 Separation in Iron (III)-Neutralized Nafion® Membranes

7.1. Abstract

This chapter describes an effective and convenient approach to mitigate the detrimental effect of CO_2 plasticization in Nafion® for CO_2/CH_4 separation. Fe^{3+} crosslinked Nafion® membranes were prepared and their physical and gas transport properties were examined. Raman and FT-IR techniques qualitatively measured the strength of the ionic bond between the Fe^{3+} cations and sulfonate anions. TGA data indicated that the incorporation of Fe^{3+} adversely affected the thermal stability of Nafion® due to the catalytic decomposition of perfluoroalkylether side-chains. Gas sorption isotherms were determined gravimetrically as a function of pressure up to 20 atm. Nafion® Fe^{3+} exhibited linear sorption uptake for O_2, N_2 and CH_4 following Henry's law, and concave behavior for CO_2, indicating glassy-like behavior at 35 °C. Pure-gas permeation results indicated reduced gas permeability but high permselectivities: N_2/CH_4 = 4.0 and CO_2/CH_4 = 35, attributable to the strong physical crosslinking effect of Fe^{3+} that caused chain tightening and therefore enhanced size-sieving behavior. XRD results did not reveal any significant changes in the average chain spacing upon cation exchange; however a high crystallinity value of 23% was measured for Nafion® Fe^{3+}. Binary CO_2/CH_4 (50:50) mixed-gas experiments at total feed pressures up to 30 atm quantified the effect of CO_2 plasticization on the CO_2/CH_4 separation performance. At 10 atm CO_2 partial pressure, CO_2/CH_4 selectivity in Nafion® Fe^{3+} decreased by 28% to 28 from its pure-gas value of 39, which was a significant improvement compared to that of a Nafion® H^+ membrane that showed a 42% decrease to 19 from its pure-gas value of 32.

7.2. Introduction

Polymeric membranes are of particular interest and importance for industrial gas separation applications such as nitrogen production from air, olefin/paraffin separation, hydrogen recovery in petrochemical plants, and carbon dioxide removal from natural gas [1-6]. The preferred membrane material of choice should combine high permeability, high selectivity, and good thermal and mechanical integrity at the operating conditions [7, 8]. Robeson's pure gas permeability/selectivity ‘upper-bound’ curves identified a crucial tradeoff: membranes with high selectivity show low permeability and vice versa [9, 10]. This relationship often limits the separation performance of membranes for a particular gas pair. In the area of CO_2/CH_4 separation, removal of CO_2 from natural gas (NG) is of particular commercial interest [1, 4, 11-13]. The strong interaction and resulting high sorption uptake of CO_2 in polymer membranes often results in swelling and plasticization. As a result, CO_2/CH_4 mixed-gas selectivity is often significantly reduced due to dilation of the polymer matrix, which leads to high CH_4 process losses and thus making membrane-based separation less attractive [14-19]. Therefore, considerable research has been devoted to tailoring the structure/composition of the polymer to achieve improved performance. Ionomers, such as sulfonated polymers comprising strong acidic sulfonate groups, potentially provide a convenient and advantageous approach for tailoring material properties via metal complexations that can cause substantial improvements in gas separation properties [20-26].

Ionomers are known for their complex morphology, in which chain-grafted sulfonic groups together with counterions form aggregates that enable physical crosslinking [27,

28]. Consequently, cation-exchange in ionomers can induce significant changes in their physical properties including enhancement in glass transition temperature [28-35], increase in Young's modulus [32, 34, 35] and reduced chain mobility [27, 28, 32, 33, 36] that play a crucial role in determining the intrinsic gas separation performance of the material. For example, Park et al. studied pure-gas transport properties of sulfonated polysulfone (SPS) membranes neutralized with several metal cations and showed that the cation-exchanged membranes improved the CO_2/N_2 selectivity moderately due to strong ionic crosslinking [20]. A SPS membrane in its Al^{3+} neutralized form exhibited 11% increase in CO_2/N_2 selectivity to 29 relative to the value of 25 in the unneutralized form. However, CO_2 permeability was reduced by 63% from 5.4 to 2.0 Barrers due to a reduction in diffusion coefficient. Chen et al. reported permeabilities for a series of gases including CO_2 and CH_4 in sulfonated polystyrene (PSS) membranes neutralized with Na^+ and Mg^{2+} cations. PSS-Mg^{2+} and PSS-Na^+ exhibited CO_2/CH_4 permselectivities of 65 and 49, respectively, which was substantially higher than the value of 18 in the unneutralized H^+ form. Additionally, it was shown that the CO_2 permeability in PSS-Mg^{2+} increased by only 9% between 1 and 7 atm indicating that the membrane was less prone to CO_2 plasticization [21]. Rhim et al. investigated CO_2/CH_4 separation properties in sulfonated poly(phenylene oxide) (SPPO) membranes cation-exchanged with several mono-, di- and trivalent cations. The trivalent Al^{3+} cation-exchanged membrane demonstrated the highest enhancement in CO_2/CH_4 selectivity by 75% to 20 compared to the value of 11 in the protonated form [25]. Khan et al. reported mixed-gas CO_2/CH_4 selectivity in Al^{3+} neutralized sulfonated poly(ether ether ketone) (S-PEEK) membrane that showed an increase by approximately 62% to 19 compared to 11 in the protonated

form [22]. The enhanced selectivity was attributed to the strong crosslinking effect of trivalent cations that hindered the diffusivity of the larger sized CH_4 molecule more effectively that CO_2.

Interestingly, only a few studies have reported the gas separation performance of cation-exchanged Nafion® membranes. For example, Sakai et al. investigated gas transport properties of Nafion® K^+ cation-exchanged membrane and showed that O_2/N_2 selectivity increased from 2.2 to 7.4 [37]. Mohammad et al. investigated the free volume and gas permeation properties of Nafion® Na^+ and K^+ cation-exchanged membranes [34]. Their study demonstrated approximately 26% increase in free volume, and 45 and 72% reduction of O_2 permeability in the Nafion® Na^+ and K^+ forms, respectively, compared to the H^+ form. This behavior was contradictory to the concept of free volume, which states that a polymer with high free volume typically exhibits higher permeability [38, 39]. Recently, Fan et al. studied Nafion® neutralized with monovalent (Li^+, Na^+, K^+) and divalent (Ca^{2+}) cations to investigate the effect of ionic interaction on the gas transport properties [40]. Their study showed higher gas permeability for cation-exchanged membranes compared to Nafion® H^+ and suggested that high gas solubility of Nafion® in metal-cation form dominated gas permeation. However, no significant correlation between the cation type and its observed gas permeabilities could be concluded. Our previous study of Nafion® H^+ quantified the effect of CO_2 plasticization on CO_2/CH_4 separation performance [41]. Despite low solubility of CO_2 in Nafion® H^+ compared to the conventional hydrocarbon polymers [42], binary mixed-gas experiments revealed that the strong affinity of CO_2 with the sulfonate groups caused large increase in segmental

mobility resulting in 40% reduction in CO_2/CH_4 selectivity from 26 to 15 with increasing CO_2 partial pressure from 2 to 15 atm.

This study investigated the physical modification of Nafion® for improving its CO_2/CH_4 separation performance by exchanging the H^+ ions with trivalent Fe^{3+} cations. It was expected that the crosslinking effect of Fe^{3+} could reduce the segmental mobility caused by favorable dipolar-polar interaction of CO_2 with the sulfonate groups. The Fe^{3+} cation-exchanged membrane was characterized by inductively coupled plasma optical emission spectrometry (ICP-OES), wide-angle X-ray diffraction (WAXD), thermogravimetric analysis (TGA), Raman and Fourier transform infrared spectroscopy (FT-IR). Pure-gas permeation properties of Nafion® Fe^{3+} for N_2, O_2, CH_4, and CO_2 as a function of pressure were measured at 35 °C using the constant-volume/variable-pressure technique. Additionally, extensive high-pressure gravimetric gas sorption studies were performed at 35 °C. Finally, binary (50:50) CO_2/CH_4 mixed-gas permeation experiments were conducted as a function of pressure at 35 °C.

7.3. Results and Discussion

7.3.1. Elemental Analysis

Nafion® Fe^{3+} cation-exchanged membrane was digested in a mixture of 6 mL nitric acid (HNO_3) and 1 mL H_2O_2 using a microwave digestion system (1000 W), diluted to 25 mL, and analyzed with an ICP-OES. The Fe^{3+} loading measured was 1.9 wt %.

7.3.2. X-Ray Diffraction

The effect of cation exchange on the microstructure of Nafion® was qualitatively assessed using wide-angle X-ray diffraction (WAXD) as illustrated in **Fig 7.1**. The spectra showed semi-crystalline behavior for Nafion® H^+ and Fe^{3+} membranes represented by: (i) a crystalline peak at $2\theta = 17.7°$ and (ii) two amorphous halo peaks: Nafion® H^+ at $2\theta = 16.8$ and 39.3° and Nafion® Fe^{3+} at $2\theta = 16.4$ and 40.4°. The average inter-chain spacings (d) were determined from Bragg's equation, ($d = \lambda/2sin\theta$) and are summarized in **Table 7.1**. The diffraction pattern for Nafion® H^+ reported in this study are in reasonably good agreement with those reported by Fan et al [40]. Apparently, the inter-chain spacing in Nafion® was not significantly affected by cation exchange, consistent with previously reported XRD results for other cation-exchanged ionomers [40, 43]. The only noticeable difference was the relative increase in crystallinity from 9% in Nafion® H^+ to 23% in Nafion® Fe^{3+}. The crystallinity was calculated by applying the Pearson VII distribution function. Such increases in crystallinity upon cation-exchange have been previously reported [23]. The increase in crystallinity may influence the gas transport, as the crystallites act as impermeable regions in the polymer and the gas transport is assumed to occur only through the amorphous regions [44].

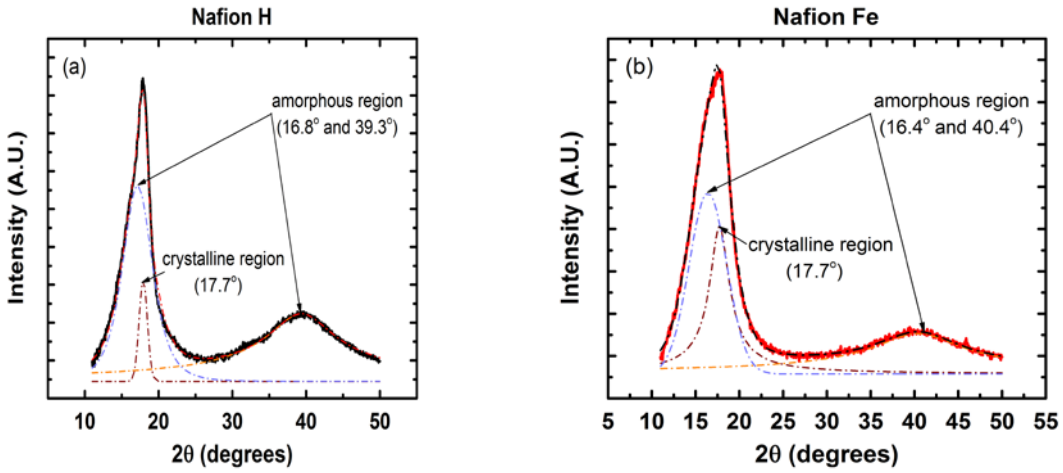

Fig. 7.1. Microstructure of Nafion® H^+ (black) and Nafion® Fe^{3+} (red) thermally treated at 80 °C. under vacuum for 2 days. The diffraction spectra were corrected for background scattering and the crystalline and amorphous peaks were obtained by applying the Pearson VII distribution function.

Table 7.1. Inter-chain spacing and percentage of crystallinity for Nafion® H^+ and Fe^{3+} membranes obtained from WAXD.

Cation	d_c (Å)	d_{a1} (Å)	d_{a2} (Å)	Crystallinity (%)
H^+	5.0	5.3	2.3	9
Fe^{3+}	5.0	5.4	2.2	23

7.3.3. Thermal Degradation

The effect of cation-exchange on the physical and chemical properties of Nafion® can be qualitatively analyzed by measuring the thermal stability of membranes using thermogravimetric analysis (TGA). The TGA profiles of Nafion® H^+ and Fe^{3+} membranes are presented in **Fig. 7.2(a)** and (**b)** as percentage weight loss and first order derivatives, respectively. The thermal decomposition temperatures are shown in **Table 7.2**.

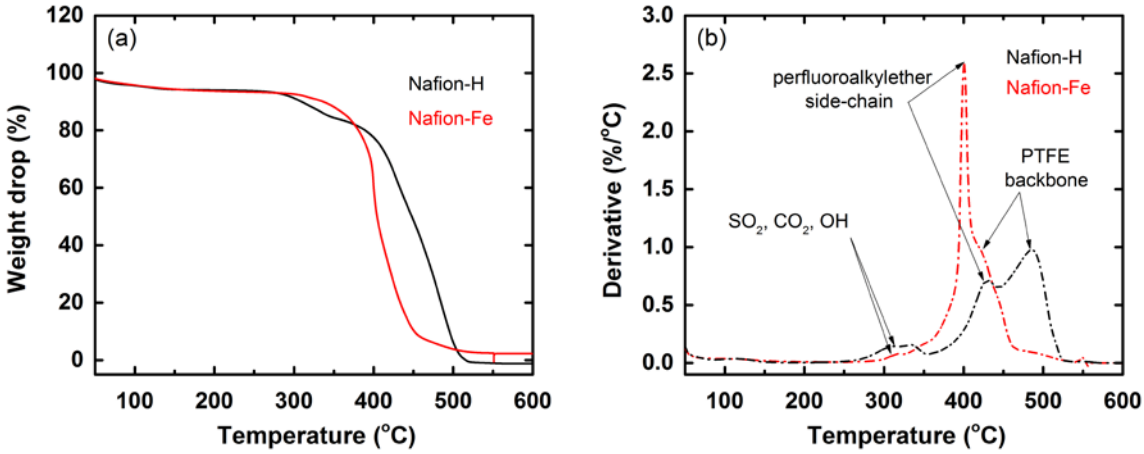

Fig. 7.2. TGA profile presented as: (a) percentage weight loss; and (b) first order derivative of Nafion® H^+ (black) and Nafion® Fe^{3+} (red) operated under N_2 atmosphere at a heating rate of 3 °C/min.

Both Nafion® types exhibited *four* stages of decomposition between 100 and 600 °C. The *first* stage weight loss occurred between T_1= 50 and 280 °C. The gases evolved during this temperature range were mostly water with trace amounts of SO_2 and CO_2 as

identified using FT-IR [45]. TGA was also used to quantify the amount of water lost from each membrane type by measuring the kinetics of the dehydration process at 80 °C as illustrated in **Fig. 7.3**. A period of ~300 mins was required to reach essentially dry state in both membrane types.

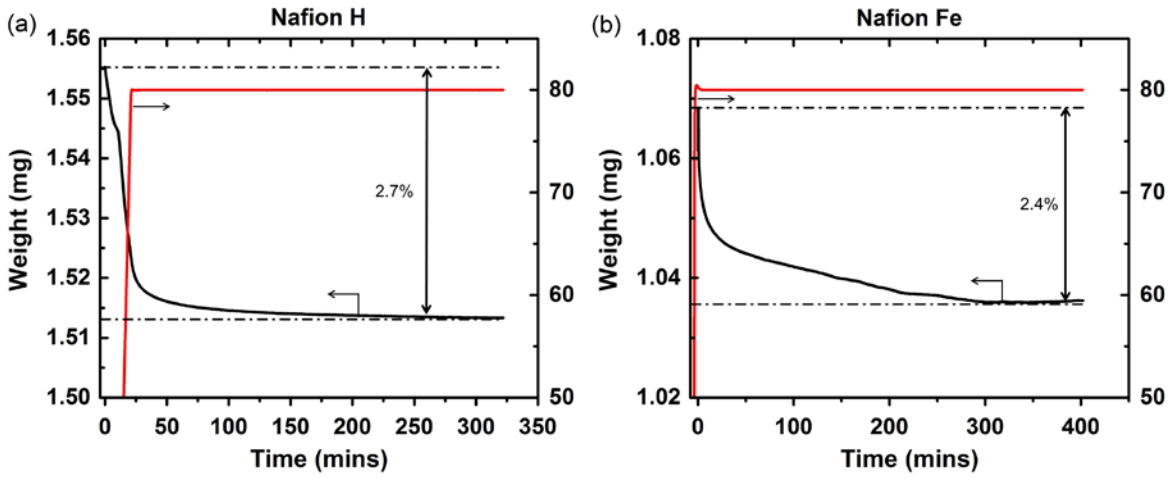

Fig. 7.3. Thermogravimetric analysis (TGA) profile for (a) Nafion® H^+; and (b) Nafion® Fe^{3+} membranes comparing the amount of water lost as a function of time upon drying at 80 °C under inert N_2 gas.

The *second* stage weight loss occurred between 280 and 350 °C and according to Wilkie et al. was primarily due to the release of SO_2 and CO_2 gases with minimal amount of water [45]. SO_2 evolved due to the cleavage of C-S bonds, forming CF_2, SO_2 and OH radicals [45]. Interestingly, the weight drop (excluding water loss) observed in Nafion® H^+ was 7% while the weight loss in Nafion® Fe^{3+} was only 1%, indicating that the stronger interaction between Fe^{3+} cations and the sulfonate anions prevented the cleavage

of C-S bonds. The absence of the desulfonation process for Nafion® cation-exchanged membranes has been previously reported [40, 45-48].

The *third* stage weight loss occurred between 350 and 410 °C in Nafion® Fe^{3+} with a sharp decomposition temperature peak at 400 °C, whereas in Nafion® H^+, the weight loss occurred between 350 and 450 °C with the peak maxima at 423 °C. This weight loss has been attributed to the degradation of perfluoroalkylether side-chain groups of Nafion® [46, 48]. The shift towards lower degradation temperature in the Fe^{3+} ion-exchanged membrane corresponded to a decrease in thermal stability. A similar trend was observed for an Al^{3+} ion-exchanged Nafion® membrane where the decrease in thermal stability was attributed to the breaking of perfluoroalkylether bonds catalyzed by aluminum oxides that act as Lewis acids [46, 48].

Above ~400 °C, the *final* decomposition of the poly(tetrafluoroethylene) (PTFE) backbone began and continued until the polymer mass decomposed to 100% in Nafion® H^+ and 97.9% in Nafion® Fe^{3+} at 600 °C. The remaining 2.1% in Nafion® Fe^{3+} corresponded to the weight percent of Fe^{3+} in the polymer whose value was recorded at 800 °C, corroborating the information obtained by ICP.

Table 7.2. Thermal decomposition temperatures of Nafion® H^+ and Fe^{3+} membranes obtained from TGA. The temperatures are reported for the maximum weight loss measured indicated by the peak in the derivate weight loss (**Fig. 7.2(b)**).

Cation	**$T_{5\%}$ (°C)**	**T1 (°C)**	**T2 (°C)**	**T3 (°C)**

H^+	117	335	423	473
Fe^{3+}	123	315	400	422

7.3.4. Raman and FTIR

The Raman and FT-IR spectra in Nafion® H^+ and Fe^{3+} membranes are presented in **Fig. 7.4** and their relative peak maxima values are tabulated in **Table 7.3**. The spectra provide qualitative and quantitative information on the changes in the membrane microstructure (chain packing, ordering, bond strength) by measuring the shift and broadening of the spectra maxima [49]. The maxima observed at 1058 (FT-IR) and 1062 (Raman) for Nafion® H^+ correspond to the symmetric S-O stretching vibrations of the sulfonate group. The assignment of this band has been reported in previous work [50-52]. As shown, the maxima shifted towards higher frequency when the protons were exchanged with Fe^{3+} cations. The shift in frequency is proportional to the bond strength between the cation and the sulfonate anion. The ion pairs are strongly attached to the polymer chains. Therefore, the strength of the ionic interactions influences the flexibility of the polymer chain molecules [27], which may alter the gas transport properties.

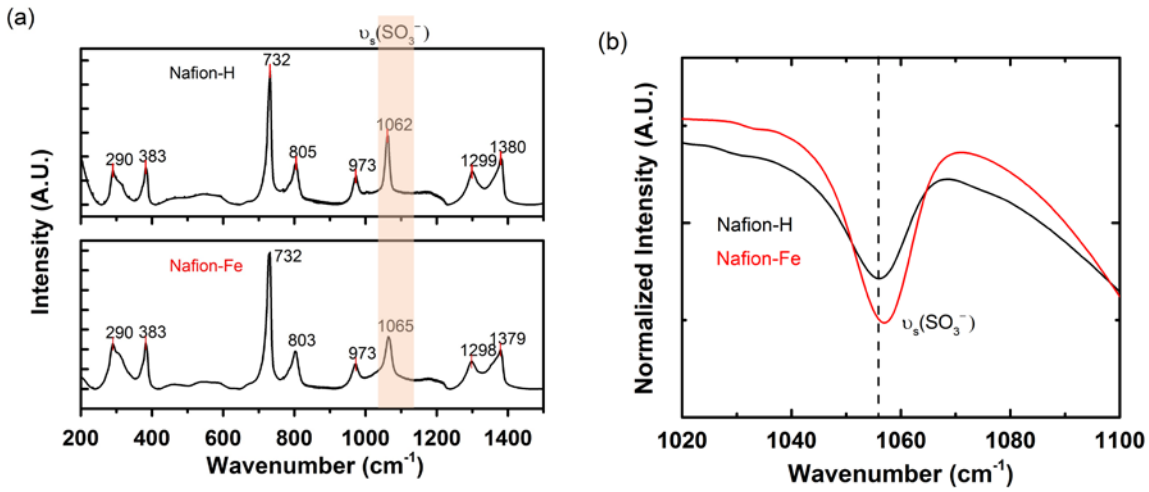

Fig. 7.4. (a) Raman; and (b) FT-IR spectra of Nafion® H^+ and Fe^{3+} membranes thermally treated at 80 °C under vacuum for 2 days. The black dotted line is drawn through the center of Nafion® H^+ maxima for visualizing the relative frequency shift.

Table 7.3. Raman and FT-IR spectra maxima in Nafion® H^+ and Fe^{3+} membranes thermally treated at 80 °C under vacuum for 2 days.

Cation	Raman υ_s (cm^{-1})	FT-IR υ_s (cm^{-1})
H^+	1062	1056
Fe^{3+}	1065	1057

7.3.5. Pure-Gas Permeation Properties

The pure-gas permeation properties of He, H_2, N_2, O_2, CH_4, and CO_2 in Nafion® H^+ and Fe^{3+} membranes are presented in **Table 7.4**. The permeabilities of Nafion® H^+

membranes were measured in our previous study under the same conditions and are reported here for comparison [42]. The permeabilities of the Fe^{3+} ion-exchanged membrane followed the order of increasing gas kinetic diameter (d_k): He > H_2 > CO_2 > O_2 > N_2 > CH_4, indicative of its strong size-dependent permeation mechanism, qualitatively similar to the permeability behavior of a Nafion® H^+ membrane.

Table 7.4. Pure-gas permeability and ideal selectivity in Nafion® H^+ and Fe^{3+} membranes at 2 atm and 35 °C.

	Permeability (Barrers)						**Ideal Selectivity**	
Cation	He	H_2	O_2	N_2	CH_4	CO_2	N_2/CH_4	CO_2/CH_4
[a]H^+	37	7.2	1.0	0.24	0.083	2.3	2.9	28
Fe^{3+}	33	6.2	0.78	0.18	0.045	1.6	4.0	35

[a]Previous work [42].

The Fe^{3+} ion-exchanged membrane demonstrated reduced permeability for all gases compared to the H^+ form. For example, He and H_2 permeability was reduced by 10 and 13%, respectively; O_2 and N_2 permeability decreased by 23 and 24% respectively, while CO_2 and CH_4 permeability was lower by 32 and 45%, respectively. The high crystallinity determined by WAXD and tight chain packing could be a plausible cause to explain the reduced permeability in the Fe^{3+} ion-exchanged membrane. The significant drop in CH_4 permeability enhanced N_2/CH_4 selectivity by 39% from 2.9 to 4.0 and CO_2/CH_4 selectivity by 25% from 28 to 35. The higher selectivity can be attributed to the strong

crosslinking effect of trivalent Fe^{3+}cations that hindered the diffusivity of the larger sized CH_4 molecule more effectively than N_2 and CO_2.

7.3.6. Pure-Gas Solubility and Diffusivity Coefficients

To better understand the effect of cation-exchange on the gas transport mechanism in Nafion®, individual contributions from diffusivity and solubility to the overall permeability were analyzed. **Table 7.5** compares the diffusivity and solubility data of the Nafion® Fe^{3+} cation-exchanged membrane with previously measured values of the Nafion® H^+ membrane [42]. The gas solubility coefficients in the Nafion® Fe^{3+} membrane were measured using the gravimetric technique and the diffusivity coefficients were then deduced from the relationship $D = P/S$.

Table 7.5. Summary of gas diffusivity and solubility coefficients in Nafion® H^+ (2.0 g/cc) and Fe^{3+} (2.1 g/cc) membranes determined by barometric and gravimetric techniques at 2 atm and 35 °C.

	Diffusivity (10^{-8} cm^2/s)				**Solubility (10^{-2} cm^3 (STP)/cm^3 cmHg)**			
Cation	O_2	N_2	CH_4	CO_2	O_2	N_2	CH_4	CO_2
H^{+a}	5.9	1.8	0.45	2.7	0.17	0.13	0.19	0.87
Fe^{3+}	3.1	0.88	0.10	0.64	0.39	0.32	0.57	2.3

[a]Solubility (*S*) values were obtained from a previous study [42] and were measured by barometric gas sorption. The corresponding diffusivity (*D*) values were determined using *D=P/S*.

The gas solubilities followed the order of increasing condensability: $CO_2 > CH_4 > O_2 > N_2$. The Nafion® Fe^{3+} cation-exchanged membrane demonstrated almost 3-fold higher gas solubility values compared to the Nafion® H^+ membrane. Similar solubility enhancements have been reported for Nafion® [37, 40] and other ionomers upon cation exchange [20, 21]. Fan et al. suggested that the high gas sorption in cation-exchanged membranes resulted from the large cation size that acted as a spacer causing polymer chain expansion [40]. However, the reported low diffusion coefficients of cation-exchanged membranes compared to H^+ membrane do not support this argument, as an increase in chain spacing should facilitate gas diffusion [40]. To elucidate the conundrum of higher gas sorption in the Fe^{3+} membrane, high-pressure gravimetric gas sorption experiments were conducted at 35 °C.

As shown in **Fig. 7.5 (a), (b) and (c)**, the sorption isotherms in Nafion® Fe^{3+} were linear up to 20 atm, following Henry's law. Both Nafion® types showed similar qualitative solubility trends; however, the solubilities in Nafion® Fe^{3+} were significantly higher than in Nafion® H^+ across the entire pressure range. Interestingly, the isotherm for CO_2 in Nafion® Fe^{3+} as shown in **Fig. 7.5 (d)**, was concave to the pressure axis contrary to the linear solubility isotherm for Nafion® H^+. Crosslinking in Nafion® induced by trivalent Fe^{3+} ions effectively reduced the segmental mobility and caused tighter chain packing in the vicinity of ionic aggregations. The rigid chains probably created regions consisting of fixed holes similar to glassy polymers that provided additional sites for gas sorption. The observed increase in glass transition temperature reported in Nafion® [28-30, 34, 35] and other ionomers [32, 33] upon cation-exchange supports this hypothesis.

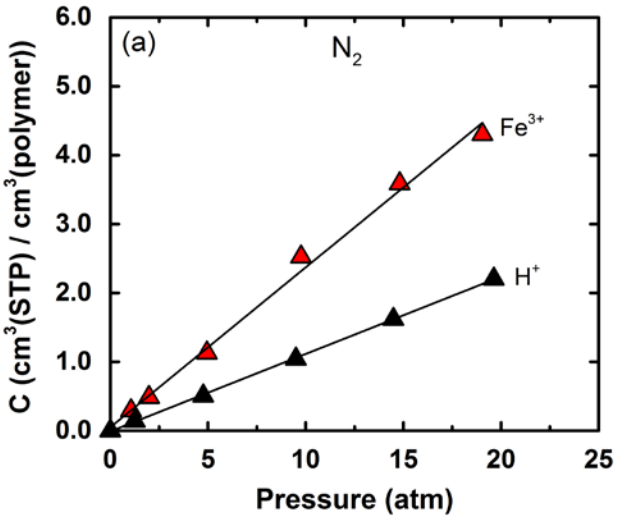
(a)
N2
Fe3+
H+
C (cm3(STP) / cm3(polymer))
Pressure (atm)
0.0
1.0
2.0
3.0
4.0
5.0
6.0
0
5
10
15
20
25

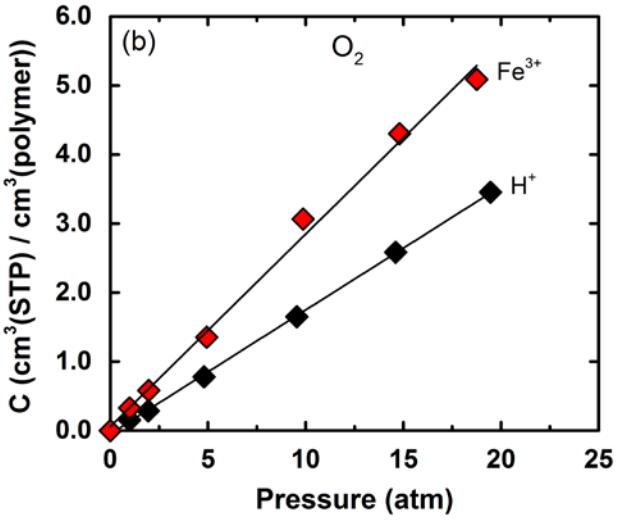
(b)
O2
Fe3+
H+
C (cm3(STP) / cm3(polymer))
Pressure (atm)
0.0
1.0
2.0
3.0
4.0
5.0
6.0
0
5
10
15
20
25

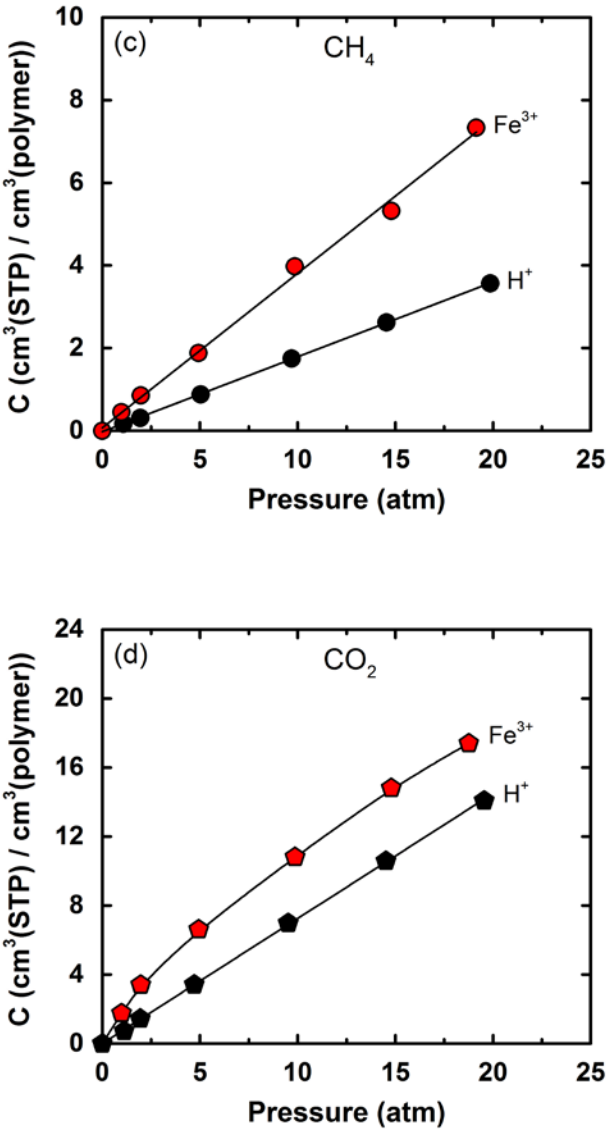

Fig. 7.5. Sorption isotherms in Nafion® Fe^{3+} (red) measured gravimetrically and Nafion® H^+ (black) measured barometrically [42] at 35 °C: (a) N_2; (b) O_2; (c) CH_4; and (d) CO_2.

Pure-gas diffusion (D) coefficients in Nafion® Fe^{3+} calculated from the ratio of permeabilities and directly measured gravimetric sorption data at 2 atm and 35 °C are shown in **Table 7.5**. The diffusivities decreased with increasing penetrant size: $O_2 > CO_2 > N_2 > CH_4$ (except for CO_2). As expected, the Nafion® Fe^{3+} ion-exchanged membrane

showed lower diffusivities compared to the Nafion® H^+ membrane. The extent of these differences is significant: the diffusivity of CH_4 in Fe^{3+} is ~6 times lower than that in H^+. This result highlights the exceptional molecular sieving properties of Nafion® Fe^{3+} cation-exchanged membrane. Multivalent cations are known to physically crosslink the Nafion® matrix by coordinating with two and three sulfonate anions, depending on the cation charge, resulting in tighter chain packing and, therefore, improved size-sieving properties [21, 22]. The larger N_2/CH_4 and CO_2/CH_4 selectivity in Nafion® Fe^{3+} was primarily due to its enhanced diffusivity selectivity, as shown in **Table 7.6**.

Table 7.6. Gas diffusivity and solubility selectivity in Nafion® H^+ and Fe^{3+} membranes at 2 atm and 35 °C.

	Diffusivity Selectivity		**Solubility Selectivity**	
Cation	N_2/CH_4	CO_2/CH_4	N_2/CH_4	CO_2/CH_4
H^+	4.1	6.0	0.7	5
Fe^{3+}	7.2	8.6	0.6	4.1

7.3.7. Pressure-Dependant Pure- and Mixed-Gas CO_2/CH_4 (50:50) Permeation Properties

Pure-gas permeabilities of CO_2 and CH_4 in Nafion® H^+ and Fe^{3+} membranes are compared in **Fig. 7.6** as a function of pressure at 35 °C. Across the entire pressure range investigated, Nafion® Fe^{3+} demonstrated lower CO_2 and CH_4 permeabilities compared to Nafion® H^+. For example, at 15 atm, CO_2 and CH_4 permeability in Nafion® Fe^{3+} was

approximately 34 and 44% lower than in Nafion® H^+. The strong crosslinking effect of Fe^{3+} and the higher crystallinity content probably caused this difference. As pressure increased from 2 to 15 atm, CH_4 permeability was reduced by 7% compared to 9% in Nafion® H^+, whereas CO_2 permeability in Nafion® Fe^{3+} increased by 9% compared to 14% in Nafion® H^+. The decrease in CH_4 permeability was caused by a decrease in gas diffusivity most likely due to chain compression [41]. On the other hand, increase in CO_2 permeability with pressure can solely be attributed to increased diffusivity. Presumably, quadrupolar CO_2 molecules interacted favorably with the polar metal-sulfonate groups of Nafion® to increase its segmental mobility causing membrane plasticization [27, 53, 54]. The Fe^{3+} cation-exchanged membrane was less affected by CO_2 plasticization as indicated by the smaller increase in CO_2 permeability compared to the Nafion® H^+ membrane.

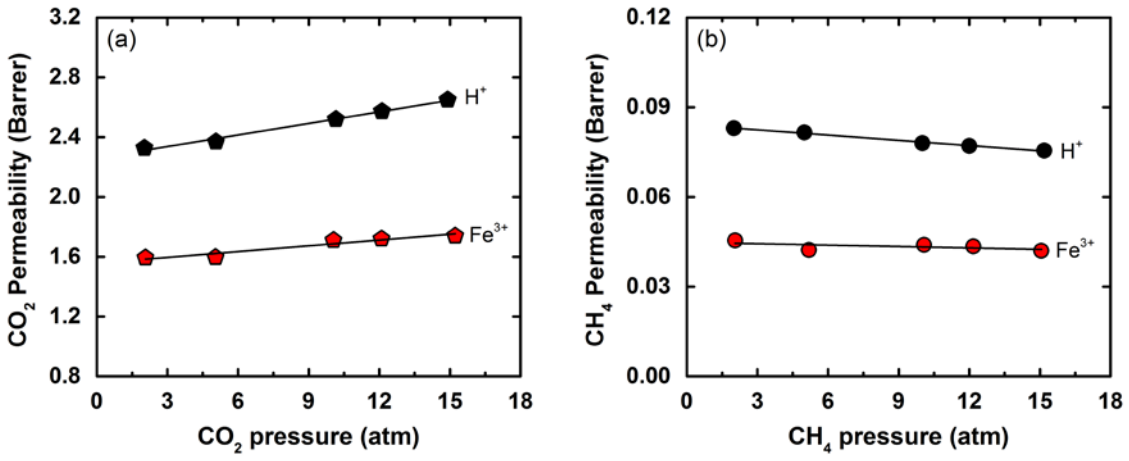

Fig. 7.6. Pure-gas permeability of (a) CO_2; and (b) CH_4 in Nafion® H^+ (black) and Fe^{3+} (red) as a function of pressure at 35 °C.

Fig. 7.7 compares permeabilities of CO_2 and CH_4 in Nafion® H^+ and Fe^{3+} membranes tested with a 50:50 feed gas mixture, as a function of pressure at 35 °C. These mixture experiments are important to assess the membrane material performance as CO_2 tends to introduce non-ideal effects such as plasticization and competitive sorption, typically resulting in different permeation behavior compared to pure-gas permeabilities.

Across the entire pressure range investigated, mixed-gas CO_2 permeabilities in Nafion® Fe^{3+} were lower than their pure-gas values. For example, at 15 atm CO_2 partial pressure, mixed-gas CO_2 permeability in Nafion® Fe^{3+} was about 36% lower than its pure-gas permeability. It is suggested that competition between CO_2 and CH_4 for the available sorption sites in the polymer effectively reduced CO_2 solubility. In comparison to Nafion® H^+, CO_2 permeabilities in Nafion® Fe^{3+} were lower at all pressure points, as shown in **Fig. 7.7(a)**. For example, at 15 atm CO_2 partial pressure, mixed-gas CO_2 permeability in Nafion® Fe^{3+} was about 34% lower than in Nafion® H^+ due to the strong crosslinking effect of the trivalent cation. As pressure increased from 2 to 15 atm, mixed-gas CO_2 permeability of Nafion® Fe^{3+} increased slightly by 6% because of CO_2 plasticization.

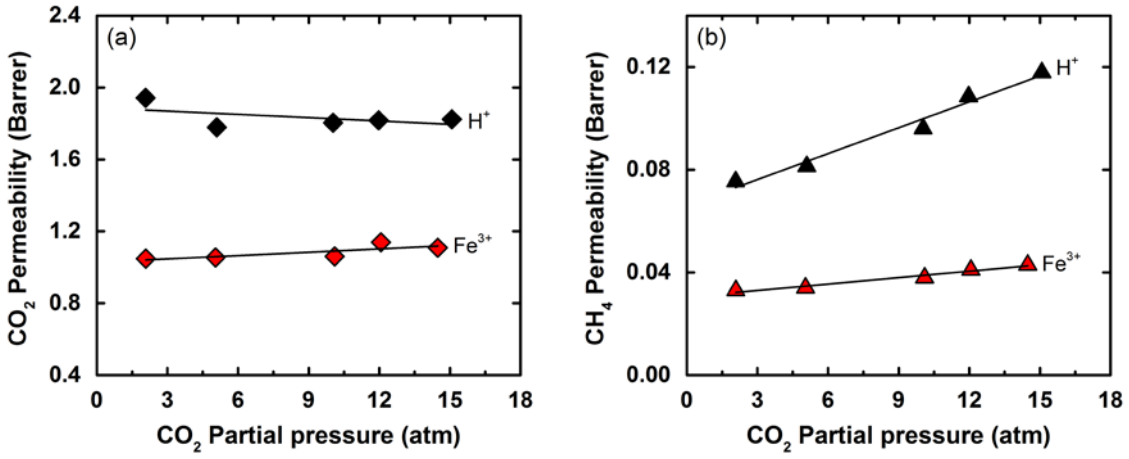

Fig. 7.7. Mixed-gas permeabilities of (a) CO_2; and (b) CH_4 in Nafion® H^+ (black) and Fe^{3+} (red) as a function of CO_2 partial pressure at 35 °C.

Mixed-gas CH_4 permeabilities in Nafion® Fe^{3+} were lower than their pure-gas values across the investigated pressure range. As discussed above, competitive sorption and polymer chain compression can explain this decrease. In comparison to Nafion® H^+, CH_4 permeabilities in Nafion® Fe^{3+} were lower at all pressure points, as shown in **Fig. 7.7(b).** As pressure increased from 2 to 15 atm, mixed-gas CH_4 permeability in Nafion® Fe^{3+} increased by 30%, whereas in Nafion® H^+, the CH_4 permeability increased by almost 56%. The strong crosslinking in Nafion® Fe^{3+} suppressed CO_2-induced increase in segmental mobility more effectively compared to Nafion® H^+, and consequently reduced plasticization.

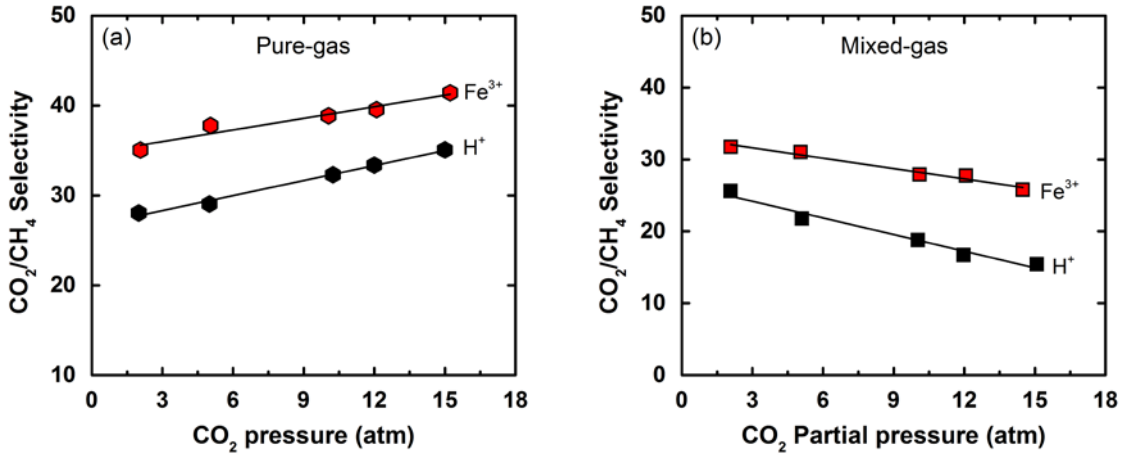

Fig. 7.8. (a) Pure-gas and (b) mixed-gas (50:50) CO_2/CH_4 selectivity in Nafion® H^+ (black) and Fe^{3+} (red) membranes as a function of CO_2 partial pressure at 35 °C.

Fig. 7.8 compares pure- and mixed gas (50:50) CO_2/CH_4 selectivities in Nafion® H^+ and Fe^{3+} membranes. In the pure-gas experiment, Nafion® Fe^{3+} demonstrated higher CO_2/CH_4 selectivities compared to Nafion® H^+ across the entire pressure range due to physical crosslinking by Fe^{3+} ions enabling enhanced diffusivity selectivity. Between 2 and 15 atm, pure-gas CO_2/CH_4 selectivity in Nafion® Fe^{3+} increased by 18% from 35 to 41. In the mixed-gas experiment, the dominant increase in CH_4 permeability caused mixed-gas CO_2/CH_4 selectivities in Nafion® Fe^{3+} to drop by 19% from 32 at 2 atm to 26 at 15 atm CO_2 partial pressure. At typical NG operating conditions (~10 atm CO_2 partial pressure) [55, 56], Nafion® Fe^{3+} exhibited mixed-gas CO_2/CH_4 selectivity of 28, which was 48% higher than the value obtained in Nafion® H^+. The considerable improvement in CO_2/CH_4 selectivity for the Nafion® Fe^{3+} cation-exchanged membrane offers significant cost savings in NG applications due to reduced CH_4 loss.

7.4. Conclusions

In summary, the physical and gas transport properties of Nafion® neutralized with trivalent Fe^{3+} cations were investigated. WAXD results revealed a high crystallinity value of ~23% for the Nafion® Fe^{3+} cation-exchanged membrane. The magnitude of physical crosslinking in Nafion® Fe^{3+} was quantified by the high N_2/CH_4 and CO_2/CH_4 permselectivity of 4.0 and 35, respectively, compared to values of 2.9 and 28 in Nafion® H^+. This was attributed to the strong ionic interactions between Fe^{3+} cations and sulfonate anions that caused chain tightening leading to enhanced diffusivity selectivities. High-pressure gas solubility measurements showed linear solubility isotherms for N_2, O_2 and CH_4, and a concave isotherm for CO_2, indicative of the existence of Langmuir-type holes that created additional sorption sites. Consequently, the gas solubilities in Nafion® Fe^{3+} were almost three times higher than in Nafion® H^+. Binary mixed-gas experiments demonstrated that physical crosslinking via trivalent Fe^{3+} cations was an effective approach to reduce high solubility CO_2-induced plasticization of Nafion®. At typical natural gas feed CO_2 partial pressure of 10 atm, Nafion® Fe^{3+} exhibited a CO_2/CH_4 selectivity of 28 compared to 15 in Nafion® H^+.

7.5. References

[1] R.W. Baker, K. Lokhandwala, Natural gas processing with membranes: an overview, Ind. Eng. Chem. Res. 47 (2008) 2109-2121.

[2] P. Bernardo, E. Drioli, Membrane gas separation progresses for process intensification strategy in the petrochemical industry, Petroleum Chemistry 50 (2010) 271-282.

[3] Y. Yampolskii, Polymeric gas separation membranes, Macromolecules 45 (2012) 3298-3311.

[4] R.W. Baker, B.T. Low, Gas separation membrane materials: a perspective, Macromolecules 47 (2014) 6999-7013.

[5] Z.P. Smith, R.R. Tiwari, T.M. Murphy, D.F. Sanders, K.L. Gleason, D.R. Paul, B.D. Freeman, Hydrogen sorption in polymers for membrane applications, Polymer 54 (2013) 3026-3037.

[6] I. Pinnau, Z. He, A.R. Da Costa, K.D. Amo, R. Daniels, Gas separation using C_{3+} hydrocarbon-resistant membranes, US Patent 6361582, 2002.

[7] W.J. Koros, R. Mahajan, Pushing the limits on possibilities for large scale gas separation: which strategies?, J. Membr. Sci. 175 (2000) 181-196.

[8] I. Pinnau, Recent advances in the formation of ultrathin polymeric membranes for gas separations, Polym. Adv. Technol. 5 (1994) 733-744.

[9] L.M. Robeson, Correlation of separation factor versus permeability for polymeric membranes, J. Membr. Sci. 62 (1991) 165-185.

[10] L.M. Robeson, The upper bound revisited, J. Membr. Sci. 320 (2008) 390-400.

[11] P. Bernardo, E. Drioli, G. Golemme, Membrane gas separation: a review/state of the art, Ind. Eng. Chem. Res. 48 (2009) 4638-4663.

[12] C.A. Scholes, G.W. Stevens, S.E. Kentish, Membrane gas separation applications in natural gas processing, Fuel 96 (2012) 15-28.

[13] A.L. Lee, H.L. Feldkirchner, S.A. Stern, A.Y. Houde, J.P. Gamez, H.S. Meyer, Field tests of membrane modules for the separation of carbon dioxide from low-quality natural gas, Gas Sep. Purif. 9 (1995) 35-43.

[14] A.Y. Houde, B. Krishnakumar, S.G. Charati, S.A. Stern, Permeability of dense (homogeneous) cellulose acetate membranes to methane, carbon dioxide, and their mixtures at elevated pressures, J. Appl. Polym. Sci. 62 (1996) 2181-2192.

[15] A. Bos, I.G.M. Pünt, M. Wessling, H. Strathmann, CO_2-induced plasticization phenomena in glassy polymers, J. Membr. Sci. 155 (1999) 67-78.

[16] A.F. Ismail, W. Lorna, Penetrant-induced plasticization phenomenon in glassy polymers for gas separation membrane, Sep. Purif. Technol. 27 (2002) 173-194.

[17] A.C. Puleo, D.R. Paul, S.S. Kelley, The effect of degree of acetylation on gas sorption and transport behavior in cellulose acetate, J. Membr. Sci. 47 (1989) 301-332.

[18] A. Bos, I.G.M. Pünt, M. Wessling, H. Strathmann, Plasticization-resistant glassy polyimide membranes for CO_2/CO_4 separations, Sep. Purif. Technol. 14 (1998) 27-39.

[19] C. Staudt-Bickel, W. J. Koros, Improvement of CO_2/CH_4 separation characteristics of polyimides by chemical crosslinking, J. Membr. Sci. 155 (1999) 145-154.

[20] H.B. Park, S.Y. Nam, J.W. Rhim, J.M. Lee, S.E. Kim, J.R. Kim, Y.M. Lee, Gas-transport properties through cation-exchanged sulfonated polysulfone membranes, J. Appl. Polym. Sci. 86 (2002) 2611-2617.

[21] W.J. Chen, C.R. Martin, Gas-transport properties of sulfonated polystyrenes, J. Membr. Sci. 95 (1994) 51-61.

[22] A.L. Khan, X. Li, I.F.J. Vankelecom, Mixed-gas CO_2/CH_4 and CO_2/N_2 separation with sulfonated PEEK membranes, J. Membr. Sci. 372 (2011) 87-96.

[23] J.-Y. Lai, S.-J. Huang, S.-H. Chen, Poly(methyl methacrylate)/(DMF/metal salt) complex membrane for gas separation, J. Membr. Sci. 74 (1992) 71-82.

[24] A. Taubert, J.D. Wind, D.R. Paul, W.J. Koros, K.I. Winey, Novel polyimide ionomers: CO_2 plasticization, morphology, and ion distribution, Polymer 44 (2003) 1881-1892.

[25] J.-W. Rhim, G. Chowdhury, T. Matsuura, Development of thin-film composite membranes for carbon dioxide and methane separation using sulfonated poly(phenylene oxide), J. Appl. Polym. Sci. 76 (2000) 735-742.

[26] Y. Li, T.S. Chung, Highly selective sulfonated polyethersulfone (SPES)-based membranes with transition metal counterions for hydrogen recovery and natural gas separation, J. Membr. Sci. 308 (2008) 128-135.

[27] A. Eisenberg, B. Hird, R.B. Moore, A new multiplet-cluster model for the morphology of random ionomers, Macromolecules 23 (1990) 4098-4107.

[28] K.A. Page, K.M. Cable, R.B. Moore, Molecular origins of the thermal transitions and dynamic mechanical relaxations in perfluorosulfonate ionomers, Macromolecules 38 (2005) 6472-6484.

[29] T. Kyu, M. Hashiyama, A. Eisenberg, Dynamic mechanical studies of partially ionized and neutralized Nafion polymers, Can. J. Chem. 61 (1983) 680-687.

[30] S.J. Osborn, M.K. Hassan, G.M. Divoux, D.W. Rhoades, K.A. Mauritz, R.B. Moore, Glass transition temperature of perfluorosulfonic acid ionomers, Macromolecules 40 (2007) 3886-3890.

[31] S.C. Yeo, A. Eisenberg, Physical properties and supermolecular structure of perfluorinated ion-containing (Nafion) polymers, J. Appl. Polym. Sci. 21 (1977) 875-898.

[32] K. Wakabayashi, R.A. Register, Morphological origin of the multistep relaxation behavior in semicrystalline ethylene/methacrylic acid ionomers, Macromolecules 39 (2006) 1079-1086.

[33] R.A. Weiss, W.C. Yu, Viscoelastic behavior of very lightly sulfonated polystyrene ionomers, Macromolecules 40 (2007) 3640-3643.

[34] H.F.M. Mohamed, Y. Kobayashi, C.S. Kuroda, A. Ohira, Effects of ion exchange on the free volume and oxygen permeation in Nafion for fuel cells, J. Phys. Chem. B 113 (2009) 2247-2252.

[35] F.M.M. Hamdy, Y. Kobayashi, C.S. Kuroda, A. Ohira, Free volume and gas permeation in ion-exchanged forms of the Nafion® membrane, J. Phys. Conf. Ser. 225 (2010) 012038.

[36] D. Ruan, D.S. Simmons, Roles of chain stiffness and segmental rattling in ionomer glass formation, J. Polym. Sci., Part B: Polym. Phys. 53 (2015) 1458-1469.

[37] T. Sakai, H. Takenaka, N. Wakabayashi, Y. Kawami, E. Torikai, Gas permeation properties of solid polymer electrolyte (SPE) membranes, J. Electrochem. Soc. 132 (1985) 1328-1332.

[38] S. Matteucci, Y. Yampolskii, B.D. Freeman, I. Pinnau, Transport of gases and vapors in glassy and rubbery polymers, in: Materials Science of Membranes for Gas and Vapor Separation, John Wiley & Sons, Ltd, 2006, pp. 1-47.

[39] K. Ghosal, B.D. Freeman, Gas separation using polymer membranes: an overview, Polym. Adv. Technol. 5 (1994) 673-697.

[40] Y. Fan, D. Tongren, C.J. Cornelius, The role of a metal ion within Nafion upon its physical and gas transport properties, Eur. Polym. J. 50 (2014) 271-278.

[41] M. Mukaddam, E. Litwiller, I. Pinnau, Pressure-dependent pure- and mixed-gas permeation properties of Nafion®, J. Membr. Sci.

[42] M. Mukaddam, E. Litwiller, I. Pinnau, Gas sorption, diffusion, and permeation in Nafion, Macromolecules 49 (2016) 280-286.

[43] D.G. Peiffer, R.A. Weiss, R.D. Lundberg, Microphase separation in sulfonated polystyrene ionomers, J. Polym. Sci.: Polym. Phys. Ed. 20 (1982) 1503-1509.

[44] A.S. Michaels, H.J. Bixler, Solubility of gases in polyethylene, J. Polym. Sci. 50 (1961) 393-412.

[45] C.A. Wilkie, J.R. Thomsen, M.L. Mittleman, Interaction of poly(methyl methacrylate) and Nafions, J. Appl. Polym. Sci. 42 (1991) 901-909.

[46] Y. Iwai;, T. Yamanishi, Thermal stability of ion-exchange Nafion N117CS membranes, Polym. Degrad. Stab. 94 (2009) 679-687.

[47] S.H. de Almeida, Y. Kawano, Thermal behavior of Nafion membranes, J. Therm. Anal. Calorim. 58 (1999) 569-577.

[48] L. Sun, J.S. Thrasher, Studies of the thermal behavior of Nafion® membranes treated with aluminum(III), Polym. Degrad. Stab. 89 (2005) 43-49.

[49] M. Reichenbächer, J. Popp, Vibrational spectroscopy, in: Challenges in Molecular Structure Determination, Springer Berlin Heidelberg, Berlin, Heidelberg, 2012, pp. 63-143.

[50] C. Heitner-Wirguin, Infra-red spectra of perfluorinated cation-exchanged membranes, Polymer 20 (1979) 371-374.

[51] A. Gruger, A. Régis, T. Schmatko, P. Colomban, Nanostructure of Nafion® membranes at different states of hydration: an IR and Raman study, Vib. Spectrosc 26 (2001) 215-225.

[52] M. Laporta, M. Pegoraro, L. Zanderighi, Perfluorosulfonated membrane (Nafion): FT-IR study of the state of water with increasing humidity, PCCP 1 (1999) 4619-4628.

[53] J.D. Wind, C. Staudt-Bickel, D.R. Paul, W.J. Koros, The effects of crosslinking chemistry on CO_2 plasticization of polyimide gas separation membranes, Ind. Eng. Chem. Res. 41 (2002) 6139-6148.

[54] S.G. Kazarian, M.F. Vincent, F.V. Bright, C.L. Liotta, C.A. Eckert, Specific intermolecular interaction of carbon dioxide with polymers, J. Am. Chem. Soc. 118 (1996) 1729-1736.

[55] B.D. Bhide, S.A. Stern, Membrane processes for the removal of acid gases from natural gas. II. effects of operating conditions, economic parameters, and membrane properties, J. Membr. Sci. 81 (1993) 239-252.

[56] R.W. Baker, Future directions of membrane gas separation technology, Ind. Eng. Chem. Res. 41 (2002) 1393-1411.

Chapter 8. Conclusions and Recommendations

8.1. Introduction

The objective of this research was to investigate the potential of using a perfluorosulfonic acid polymer, Nafion®, as a plasticization-resistant membrane material for natural gas applications specifically for CO_2 removal from natural gas. Chapter 5 through 7 rationalized the structure/gas property relationship in Nafion® through physical characterization and gas transport measurements. This chapter provides a brief overview of the outcomes discovered in this research in a unifying manner. In addition, some recommendations will be presented for further material assessment that can be built upon those presented herein.

8.2. Conclusions

High-pressure gas sorption experiments revealed linear sorption isotherms for He, H_2, N_2, O_2, CO_2 and CH_4, and convex sorption isotherms for highly sorbing propane and *n*-butane, indicative of rubber-like solubility behavior in Nafion® H^+ at 35 °C. The stress-strain profile demonstrated large elongation at break up to ~255% and a low Young's modulus value of 0.22 GPa at 35 °C, corroborating the rubber-like behavior obtained from gas solubility measurements. These results elucidated the common misconception of Nafion's® physical state as a glass or rubber. Interestingly, Nafion® exhibited tightly packed amorphous chain domains with sharp size-sieving regions that allowed *extraordinarily* high permselectivities especially between small gases (He, H_2, CO_2) and large hydrocarbon gases (C_{1+}). Moreover, Nafion® exhibited low-hydrocarbon and CO_2 solubility compared to other hydrocarbon and perfluorocarbon polymers: CO_2 uptake in

Nafion® of about 8 cm^3(STP)/cm^3 at 10 atm was 3-fold lower than in CA [1] and almost 2-fold lower than in perfluorinated Cytop® [2]; C_3H_8 uptake in Nafion® of about 1 cm^3(STP)/cm^3 at 2 atm was 25-fold lower than in polyimide 6FDA-6FpDA [3] and 5-fold lower than in Cytop® [2]. These attributes highlighted Nafion's® potential to resist membrane plasticization that could potentially be harnessed for dry feed streams for: (i) helium recovery; (ii) CO_2 removal in natural gas applications and (iii) hydrogen recovery from refinery gas streams.

The above results motivated further research to determine Nafion's® permeation properties under high-pressure mixed-gas conditions. Thus, the permeabilities of CO_2 and CH_4 in Nafion® H^+ membranes were measured with a (50:50) binary feed gas mixture, as a function of pressure at 35 °C. At typical NG operating conditions (10 atm CO_2 partial pressure), CH_4 permeability increased by 23% to 0.096 Barrers from its pure-gas value of 0.078 Barrers, while CO_2 permeability decreased by 28% to 1.80 Barrers from its pure-gas value of 2.52 Barrers. Consequently, CO_2/CH_4 selectivity decreased to 19, i.e., 42% below its pure-gas value of 32. This was attributed to CO_2-solubility-induced swelling and plasticization that enhanced CH_4 diffusion and consequently reduced selectivity.

To counter the effect of CO_2-plasticization, Fe^{3+} crosslinked Nafion® membranes were prepared and their physical and gas transport properties were examined. The strong ionic interactions between Fe^{3+} cations and sulfonate anions caused chain tightening leading to enhanced diffusivity selectivities. Consequently, Nafion® Fe^{3+} exhibited CO_2/CH_4 permselectivity of 35 compared to the value of 28 in Nafion® H^+. Surprisingly,

gas solubility measurements showed concave isotherm for CO_2, indicative of the existence of Langmuir-type holes that created additional sorption sites. Consequently, the gas solubilities in Nafion® Fe^{3+} were almost three times higher than in Nafion® H^+. Overall, binary mixed-gas experiments revealed that the strong physical crosslinking in Nafion Fe^{3+}-exchanged membrane was an effective approach to reduce CO_2-induced plasticization of Nafion®. At CO_2 partial pressure of 10 atm, Nafion® Fe^{3+} exhibited a CO_2/CH_4 selectivity of 28 compared to 15 in Nafion® H^+.

8.3. Recommendations for Future Work

Field conditions in natural gas processing are quite different compared to those typically observed in laboratories. The present study has demonstrated the potential of Nafion® as plasticization-resistant membranes for CO_2 removal under dry feed conditions. However, natural gas contains water and because Nafion® is highly hygroscopic, the presence of water can significantly affect its separation performance. Therefore, it is of utmost importance to perform future CO_2/CH_4 mixed-gas experiments under humid conditions. Sarti et al. investigated pure-gas permeabilities of He, O_2, N_2 and CO_2 in Nafion® H^+ between 0 and 80% relative humidity conditions [4, 5]. Their study indicated up to *two orders* of magnitude higher permeabilities compared to the values obtained under dried conditions due to water-induced swelling and plasticization. To date, very few studies have addressed water sorption in Nafion® Fe^{3+} cation-exchanged membranes. It would be of interest to examine the effect of water on the physical crosslinking in Nafion® Fe^{3+} and consequently its separation properties.

This work focused on a detailed characterization study of thick (25 μm) Nafion® H^+ and Nafion® Fe^{3+} films. Future work should also be directed at the formation of thin-film composite membranes (< 1 μm thickness) and their gas permeation properties. Finally, the effect of counter ions other than Fe^{3+} may shed more light on the role of the ion size and crosslinking mechanism on the permeation properties of cation-exchanged Nafion® membranes.

8.4. References

[1] A.C. Puleo, D.R. Paul, S.S. Kelley, The effect of degree of acetylation on gas sorption and transport behavior in cellulose acetate, J. Membr. Sci. 47 (1989) 301-332.

[2] T.C. Merkel, I. Pinnau, R. Prabhakar, B.D. Freeman, Gas and vapor transport properties of perfluoropolymers, in: Materials Science of Membranes for Gas and Vapor Separation, John Wiley & Sons, Ltd., Chichester, UK, 2006, pp. 251-270.

[3] C. Staudt-Bickel, W.J. Koros, Olefin/paraffin gas separations with 6FDA-based polyimide membranes, J. Membr. Sci. 170 (2000) 205-214.

[4] M. Giacinti Baschetti, M. Minelli, J. Catalano, G.C. Sarti, Gas permeation in perflurosulfonated membranes: influence of temperature and relative humidity, Int. J. Hydrogen Energy 38 (2013) 11973-11982.

[5] J. Catalano, T. Myezwa, M.G. De Angelis, M.G. Baschetti, G.C. Sarti, The effect of relative humidity on the gas permeability and swelling in PFSI membranes, Int. J. Hydrogen Energy 37 (2012) 6308-6316.